SEVENTH FRAMEWORK PROGRAMME
Capacities Specific Programme
Research Infrastructures

Project No.: 227887

SERIES

SEISMIC ENGINEERING RESEARCH INFRASTRUCTURES FOR EUROPEAN SYNERGIES

Work package [WP8 – TA4 EQUALS]

MAID

Seismic behaviour of L- and T-shaped unreinforced Masonry shear walls including Acoustic Insulation Devices

Preliminary test report

User Group Leader: Hervé Degée

H.Degee@ulg.ac.be

University of Liège

July, 2013

ABSTRACT

This report presents the two phases of the SERIES project TA5 EQUALS MAID.

The purpose of the first phase is to elaborate a better understanding of the seismic behaviour of masonry walls in dynamic conditions and to investigate the consequences of the use of rubber elements aiming at improving the acoustic performance of buildings. The tested specimens are four simple unreinforced clay masonry walls, two of them including rubber soundproofing devices at the bottom and top of the wall. Results demonstrate a significant rocking behaviour and comparisons between the four specimens provide useful information about the influence of the aspect ratio of the walls and of the presence of rubber devices.

The second phase has a double purpose. The first objective is to characterize the frame effects in masonry shear walls coupled by horizontal elements (concrete lintel and slab). The second objective is to study the influence of the presence of walls perpendicular to the earthquake action. The second test series consists thus in two specimens made of two walls with horizontal cross-section respectively in T and L shape coupled at their top by a lintel and a slab. Different loading conditions are also considered, with a slab resting on entire walls or only on part of them.

Keywords: Unreinforced Masonry Buildings, Soundproofing Devices, Flanged walls, Frame behaviour

ACKNOWLEDGMENTS

The research leading to these results has received funding from the European Community's Seventh Framework Programme [FP7/2007-2013] for access to EQUALS shake table under grant agreement n° 227887

REPORT CONTRIBUTORS

University of Liege	Hervé Degée
	Christophe Mordant
Univerisity of Bristol	Matt Dietz
	Colin Taylor
Wienerberger nv	Luc Vasseur

Contents

1 Introduction

Contemporary architecture is currently in a very fast evolution process aiming at improving the comfort of dwellings and at reducing their ecological footprint. On the other hand, it is also expected that building may resist actions such as earthquakes or other exceptional actions, which may lead to contradictory technical requirements compared to environmental and comfort demands. As a matter of example, a correct acoustical comfort requires significant mechanical disconnection between the structural elements to avoid vibration propagation while earthquake stability requires oppositely adequate connection.

Coming to the North-Western European context (i.e. Belgium, the Netherlands, Germany), the problem can be better specified in relation with masonry structures. In these regions, the common way to build masonry structures is a generalized use of unreinforced masonry (without any confining or reinforcing elements) with rather thin bearing walls (10 to 19 cm). This is in particular the case when using clay units. Clay products have been developed for many years for use in single-family dwellings but their evolution in terms of resistance and implementation is such that they are nowadays more and more efficient for moderate-height building up to 5-6 storeys. These buildings are particularly suitable for apartments. It means also that specific devices have to be developed for improving the acoustic comfort of inhabitants by limiting the noise transfer between apartments. One possible solution, proposed by a good cooperation between two partners of the current project (Wienerberger and CDM), consists in combining appropriate disconnection of walls and/or slabs with the use of rubber mats.

On the other hand, regarding the seismic aspect, these regions were classically considered as non-seismic, while the new seismic zonations associated with Eurocode 8 (return period of 475 years) lead to reconsider the situation and to classify important part of the above-mentioned countries as low-to-moderately seismic (with PGA from 0.05g to 0.1g at the bedrock). This acceleration level combined to the important mass of masonry structure, to the slenderness of

walls, to the architectural wish of wide openings and to the conservative rules of Eurocode 6 regarding shear and in-plane bending resistance of walls often leads to difficulties in justifying the seismic stability of the structure if only shear walls parallel to the seismic action are considered. Moreover, even if recent studies have been improving the knowledge about masonry shear walls under seismic action, very few is still known about the global structural behaviour. Furthermore, the mechanical consequences of the thermal and acoustical insulation systems such as described above are highly uncertain.

The main experimental results currently available and dedicated to the relevant type of masonry structures are those developed during the ESECMaSE3 research project (FP6). However these tests are mainly dealing with single walls or entire houses (and not on sub-structures) and do not include any insulation device.

The present proposal takes place in a global research strategy dealing with seismic behaviour of modern unreinforced masonry structures in low-to-moderate seismic area. The final goal of this research strategy is to define integrated constructive solutions that match the strongest requirements in terms of thermal and acoustical performances and that ensure resistance and stability when subjected to horizontal dynamic loading (earthquake, but also strong winds).

In this wide context, the MAID project focuses on two main aspects:

1. Obtain accurate information about the behaviour of T and L-shape shear walls under seismic action.

It has been shown on design examples that considering only shear walls parallel to the direction of earthquake action was often not sufficient to justify the seismic stability of unreinforced masonry building, even for situations of low-to-moderate seismicity such as defined for some regions in Belgium, Germany and South-Netherlands. As allowed by the design codes (and even strongly suggested in case of wind loading), an alternative solution is to consider resisting elements including flanges. This is particularly necessary in the North-Western Europe context due to the quite limited thickness of walls and the absence of any confining elements. Flanges allow increasing the inertia and resistance of the global resisting system. Moreover, a very common way of realizing floors is to use prefabricated concrete slabs spanning in one direction. It means that walls in one direction are significantly more loaded than in the other one and exhibits thus a much higher resistance to horizontal load. It is therefore felt very valuable to account for walls in both directions in a single resisting element, so that at least a part of the resisting element is under compression. Flanges are then made of a part of the walls in the

direction transverse to earthquake action. Eurocode 6 gives rules to estimate the participating width of such transverse walls. However this implies of course to account carefully for the longitudinal shear at the junction between the shear wall and its flange(s). In the recent years, theoretical and experimental research has been carried out on the shear and in-plane bending behaviour of shear walls without flanges under seismic action (FP6 ESECMaSE project for example). On the other hand, some tests have also been carried out (and are still planned to be carried out) on entire structures. However, nothing is available yet to validate specifically numerical and design models of unreinforced masonry walls under dynamic earthquake excitation considering the presence of flanges. The first objective of the MAID project is to contribute to this lack of knowledge.

2. Complement the available results of static tests regarding the behaviour of clay block walls including acoustic rubber mats in a dynamic context.

When used in the more and more commercially and socially attractive context of low-to-moderate buildings for apartments, it is more or less mandatory (according to the national codes) to provide efficient soundproofing. An efficient and validated solution has been introduced here above and consists in placing rubber mats at appropriate locations in the structure. However, nothing is known up to now on the dynamic earthquake behaviour of such acoustically modified walls. It is pretty clear that it is changing the dynamic properties of the wall (stiffness, period, damping) but also that it creates a possible weakness in the mechanical system (or at least a point obviously less under control than the main part of the wall). The objective of the MAID project is thus to complement results obtained recently in University of Liège under static cyclic loading conditions by dynamic test results.

2 First test series – single walls – Specimens and instrumentation

2.1 GEOMETRY OF THE SPECIMENS

In the first phase, four walls are tested. Two of them have an aspect ratio close to 1.0, while the other two have an aspect ratio close to 0.4. These dimensions are chosen to trigger different failure modes. The strength of the wall with aspect ratio close to 1.0 is theoretically limited by shear, while the bending behaviour limits the strength of the walls with aspect ratio close to 0.4. Exact dimensions of the specimens are as follows:

- Length x Height x Width = *2.1m x 1.8m x 0.14m*
- Length x Height x Width = *0.72m x 1.8m x 0.14m*

Two walls (one for each aspect ratio) are including soundproofing elements at the bottom and top. The other two are built without such devices. This choice is aiming at a possible comparative study of the dynamic behaviour of similar geometrical configurations with and without soundproofing rubber elements. The four configurations are illustrated in Figure 1 to Figure 3.

Figure 1 – Starting of the wall construction

Figure 2 – Top (left side) and bottom (right side) view of walls with aspect ratio equal to 0.4

Figure 3 – View of the walls with aspect ratio equal to 1.0 with acoustic devices (left side) or without (right side)

2.2 LOADING

To emulate the structural floor load, a mass is placed on the top of the wall. To fulfil the technical requirements of the shaking table of the laboratory, the additional mass should be limited to 5 tons. The loading device (in steel) is shown on Figure 4.

Even if the value of the added mass is limited by the table capacity, a minimum compression level is compulsory in order to model realistic loading conditions of load-bearing masonry. With a 5-tons dead load, the average compressive stress is about 0.5 MPa for the 0.72 m long wall and about 0.15 MPa for the 2.1m long wall. These values are in the usual range of the compression level in clay masonry.

Figure 4 – Loading device – additional 5 tons mass

2.3 PRELIMINARY ASSESSMENT OF THE WALLS

2.3.1 Mechanical and geometrical characteristics

The units used to realize the walls are clay blocks. The walls are built in thin bed masonry. Vertical joints are empty and horizontal ones are glued. The block size is:

$$(Length\ x\ Width\ x\ Height) = (300.0\,mm\ x\ 138.0\,mm\ x\ 188.0\,mm)$$

Mechanical characteristics of the units and masonry are the following ones:

- Normalised compressive strength of units (EN 772-1 Annex A)

$$f_b = 13.0\,N/mm^2$$

- Measured characteristic masonry compressive strength (EN 1052-1)

$$f_k = 5.6\,N/mm^2$$

- Characteristic compressive strength (EN 1996-1-1)

$$f_k = 4.2\,N/mm^2$$

- Characteristic compressive strength (NBN-EN 1996-1-1)

$$f_k = 3.9\,N/mm^2$$

No specific characterization has been carried out for shear behaviour. Usual standard values are considered for further assessment:

- Initial shear strength (NBN-EN 1996-1-1)

$$f_{vk0} = 0.3\,N/mm^2$$

- Characteristic shear strength (NBN-EN 1996-1-1)

$$f_{vk} = 0.5 f_{vk0} + 0.4\sigma_d \le 0.045 f_b \ (= 0.585 N/mm^2)$$

2.3.2 Estimation of the maximum sustainable acceleration

This preliminary assessment aims at estimating a value of the maximum acceleration which can be sustained by the wall. The model uses an equivalent static analysis and the verification is done according to Eurocode 6 procedure, based on the concept of compressive length and considering three limit states (overturning, crushing of the units, shear resistance). Eurocode proposals are followed for the determination of the E and G moduli, as well as for the characteristic shear and compression strengths. Stiffness and first natural periods are also calculated. Data and results of the preliminary assessment are summarized in Table 1. This leads to conventional main natural frequencies of respectively 4.5 and 17.2 Hz.

Table 1 - Data and results of the preliminary assessment

Tested wall	*Length [m]*	*Compressive load [kg]*	*Compression Level [MPa]*	$V_{Sd,max}$ *[N]*	$a_{g,max}$ *[m/s²]*	*Stiffness K [N/m]*	*Period T [s]*
Long wall	2.10	5000	0.2	26200	2.0	58.69×10^6	0.058
Short wall	0.72	5000	0.5	9000	0.7	3.92×10^6	0.224

2.4 REFERENCE SYSTEM

The axis origin conventionally considered at EQUALS is the centre of the shaking table. For the axis convention, the following is applicable:

- X-axis is positive from the near to the far end of the table ;
- Y- axis is positive from left to right ;
- Z-axis is positive upward

The reference for “near end”, “far end”, “left” and “right” of the shaking table is the control mezzanine located as shown in Figure 5.

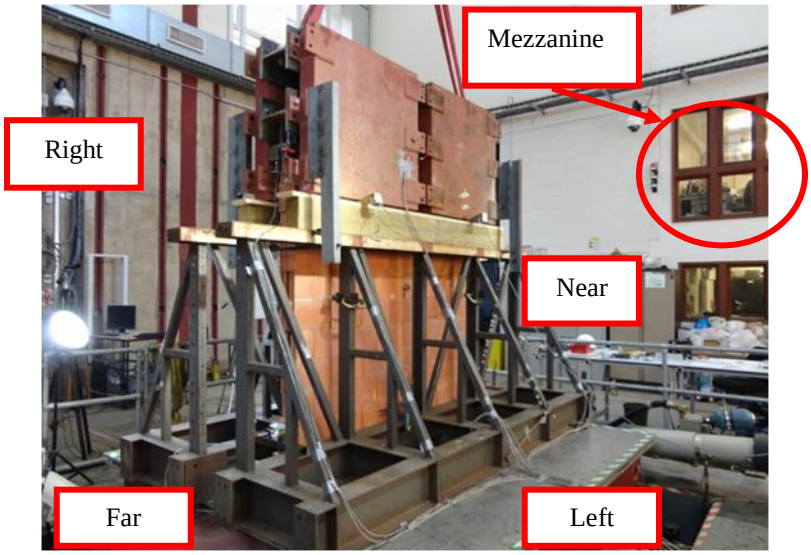

Figure 5 – View of the control mezzanine

2.5 INSTRUMENTATION

Monitoring of the test specimens is classically carried out with two different types of measurements, i.e. accelerations and displacements.

The very details of the measuring devices are not given in this report but the interested readers can refer to "*TA5/TMS – Seismic Behaviour of L- and T-shaped Unreinforced Masonry Shear Walls Including Acoustic Insulation Devices*" available at the "*Earthquake Engineering Centre*" of the University à Bristol (Department of Civil Engineering).

The instrumentation layout is illustrated in Figure 6 to Figure 10.

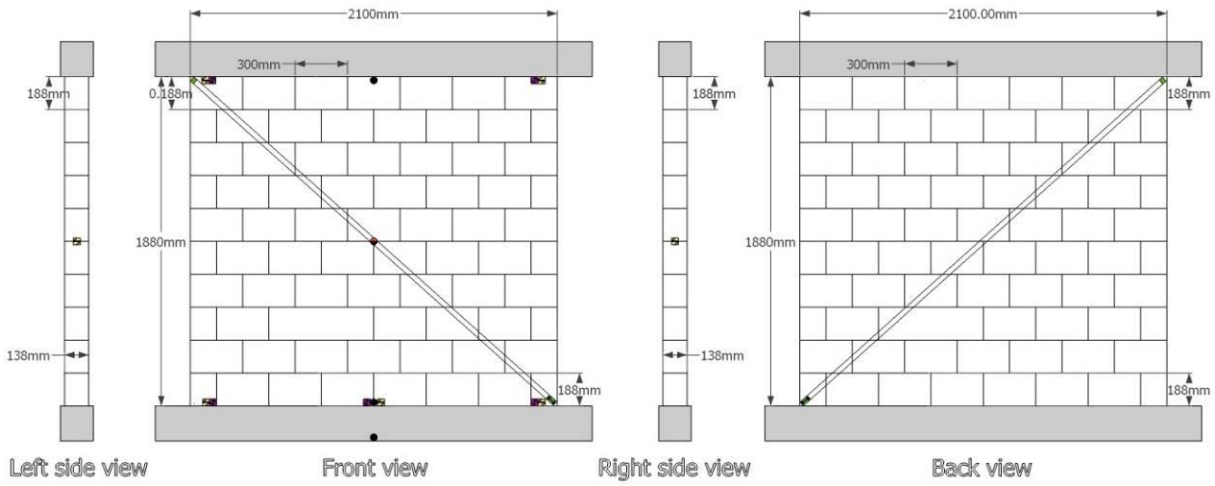

Figure 6 – Instrumentation layout for Specimen 1

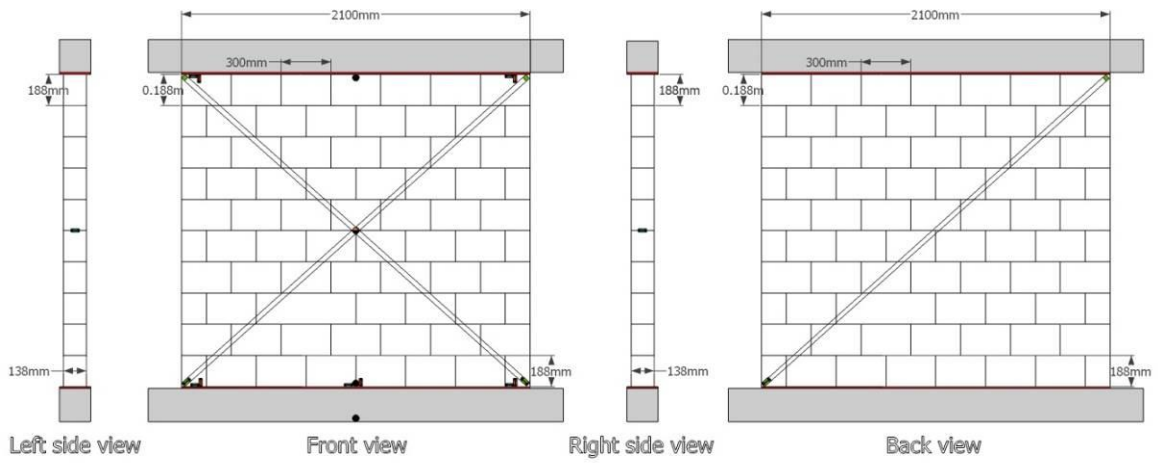

Figure 7 – Instrumentation layout for Specimen 2

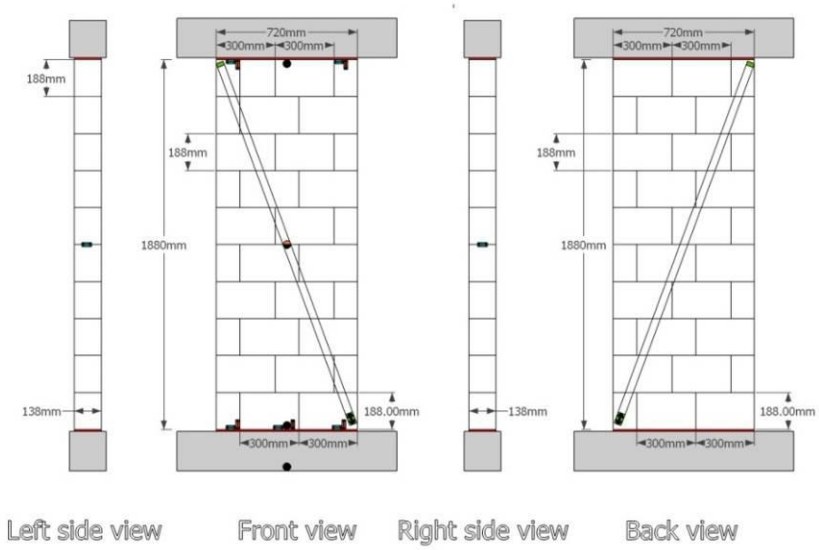

Figure 8 – Instrumentation layout for Specimen 3

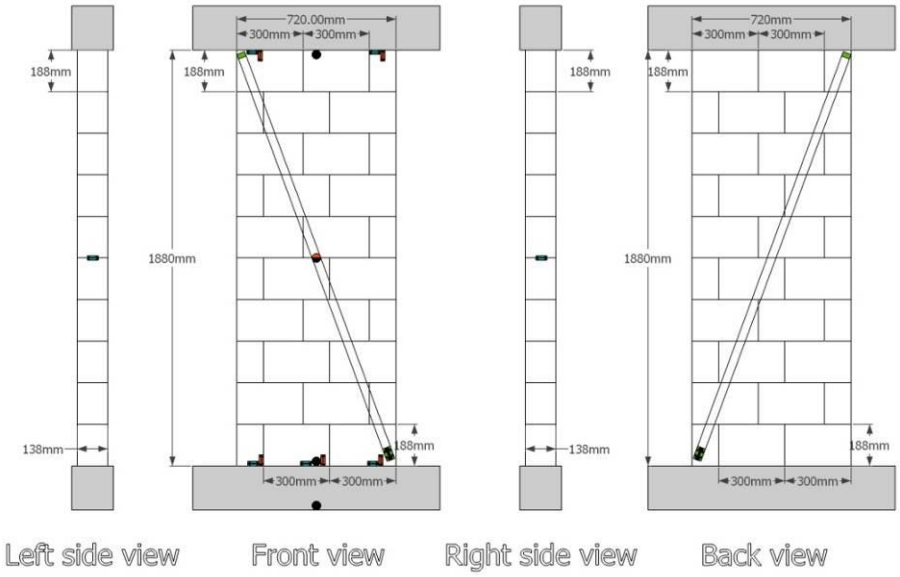

Figure 9 – Instrumentation layout for Specimen 4

Figure 10 – Legend of the instrumentation layout

Some devices are also directly connected with the table (one X-direction accelerometer) and with the added mass (one X-direction accelerometer and eight targets for the optical tracking of global displacements in X- and Z-directions).

As a whole, a total of 31 devices are located on the table, the wall and the mass. Table 2 summarizes the information on these devices for the long walls:

- Location of the device (including coordinates and axis convention);
- Channel and type of device;
- Calibration factors.

Instrumentation is similar for long and short walls with the only exception of the X-coordinate of the position of the LVDT.

Table 2 – Information for instrumentation devices (long walls)

Reference	*No chan.*	*Type of Device*	*Position*	*Measurement*	*Calibration factor*	*Note*[1]
On table	1	SETRA 141A	(-1.30 ; 0.00 ; 0.00)	X-acceleration	1	
	2	SETRA 141A	(-1.10 ; -0.05 ; 0.05)	- X-acceleration	1	
On wall	3	SETRA 141A	(0.00 ; 0.07 ; 0.20)	X-acceleration	1	
	4	SETRA 141A	(0.00 ; 0.07 ; 1.20)	X-acceleration	1	
	5	SETRA 141A	(0.00 ; 0.07 ; 1.20)	Y-acceleration	1	
	6	SETRA 141A	(0.00 ; 0.07 ; 2.00)	X-acceleration	1	
On mass	7	SETRA 141A	(0.10 ; 0.07 ; 2.10)	X-acceleration	1	
On wall	8	LVDT	(-1.10 ; -0.01 ; 0.25)	Z-displacement	2.178	R.T.
	9	LVDT	(-1.10 ; -0.07 ; 1.90)	- Z-displacement	2.1654	R.M.
	10	LVDT	(1.10 ; 0.02 ; 0.25)	Z-displacement	1.4673	R.T.
	11	LVDT	(1.10 ; -0.06 ; 1.90)	- Z-displacement	1.4831	R.M.
	12	LVDT	(0.15 ; 0.07 ; 0.25)	Z-displacement	1.369	R.T.
	13	LVDT	(-0.80 ; 0.07 ; 1.15)	- Y-displacement	1.3835	R.T.
	14	LVDT	(0.80 ; 0.07 ; 1.15)	- Y-displacement	2.1728	R.T.
	15	LVDT	(-1.10 ; 0.03 ; 0.30)	X-displacement	2.8562	R.T.
	16	LVDT	(0.00 ; 0.07 ; 0.35)	- X-displacement	5.4193	R.T.
	17	LVDT	(1.10 ; -0.03 ; 0.35)	- X-displacement	5.5649	R.T.
	18	LVDT	(-0.95 ; 0.07 ; 1.90)	X-displacement	10.7215	R.M.
	19	LVDT	(1.00 ; 0.07 ; 2.00)	- X-displacement	2.735	R.M.
	20	Celesco	(0.95 ; -0.07; 0.30)	Diag. displac.	21.338	
	21	Celesco	(0.95 ; 0.07; 0.30)	Diag. displac.	21.546	
Table sensors	22	Instron	/	X-displacement	10	
	23	Instron	/	Y-displacement	10	
	24	Instron	/	Z-displacement	10	
	25	Instron	/	ρ-angle	0.1	
	26	Instron	/	Ø-angle	0.1	
	27	Instron	/	X-acceleration	1	
	28	Instron	/	Y-acceleration	1	
	29	Instron	/	Z-acceleration	1	
	30	Instron	/	ρ-acceleration	1	
	31	Instron	/	Ø-acceleration	1	

[1] R.M. means that the measurement is relative to the mass
R.T. means that the measurement is relative to the table

The instrumentation also includes a vision system data (Imetrum Video-Gauge Vision System). Four targets are placed on the steel frame connected to the table and four targets are placed on the additional mass (see Figure 11). Horizontal and vertical displacements are recorded. Coordinates of the targets are given in the Table 3.

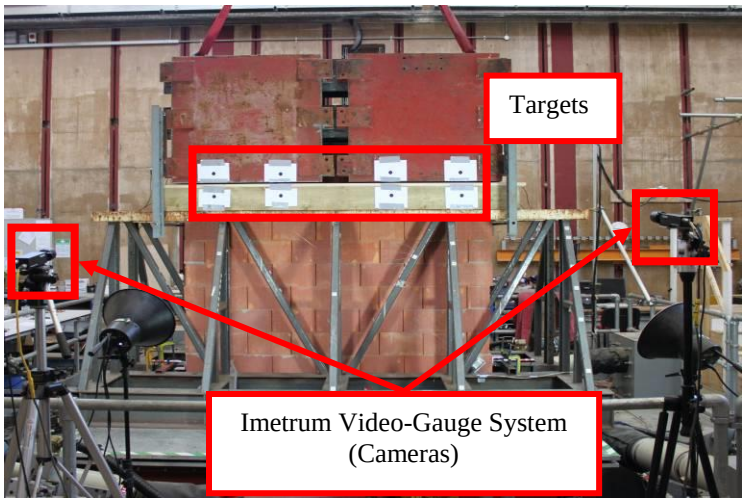

Figure 11 - Targets for the Imetrum Video-Gauge Vision System (VS).

Table 3 - Position of the targets for the Imetrum Video-Gauge Vision System (VS).

Location	*Coordinates (x [m],z [m])*			
	Left	*Middle left*	*Middle right*	*Right*
On the mass	(-0.9 ; 2)	(-0.4 ; 2)	(0.4 ; 2)	(0.9 ; 2)
On the frame	(-0.9 ; 1.8)	(-0.4 ; 1.8)	(0.4 ; 1.8)	(0.9 ; 1.8)

2.6 EXCITATION WAVEFORMS

All walls are designed according to Eurocode 6 and 8. The excitation waveform is thus chosen compatible with a Eurocode 8 type spectrum. The excitation waveform used for the tests is shown in Figure 12.

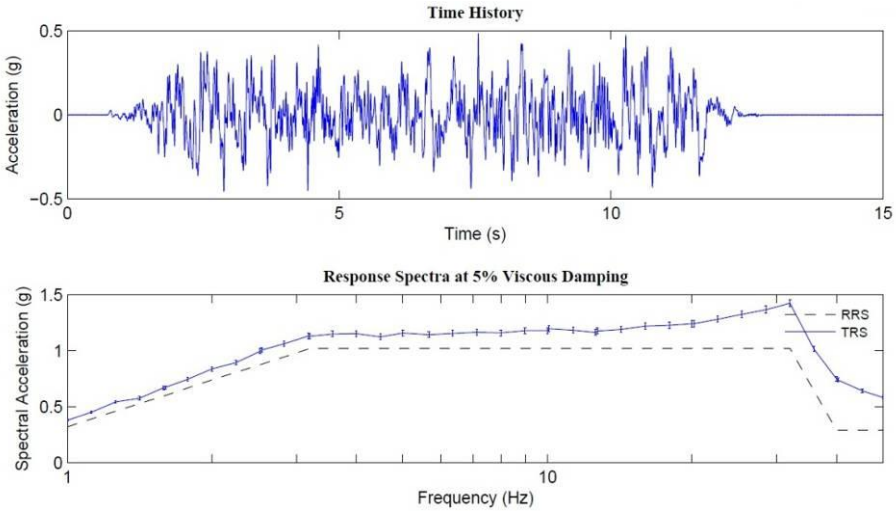

Figure 12 – Excitation waveform

Figure 12 shows two graphs. The top one plots the time-history of the acceleration imposed to the table. The time history is divided in different parts. At the beginning, the acceleration is zero. Between the first second and the third second, it increases and the maximum is reached after 3 seconds. The maximum intensity is kept for 8 seconds. Between second 11 and second 13, the acceleration decreases and comes back to zero after 13 seconds. The bottom part of Figure 12 shows the associated spectral acceleration (TRS) compared to the theoretical Eurocode 8 spectral acceleration (RRS). Extreme accelerations of the reference signal (later referred as "100 %") are equal to 0.485g and -0.455g.

3 First test series – Results

3.1 LOAD SEQUENCE

Measurements are first taken during the static loading (i.e. differential displacements before and after positioning the additional mass). Data provided during this initial stage allow the assessment of an estimate of the elastic modulus of the masonry and of the rubber device under pure compression.

The wall is then subjected to an alternated sequence of seismic loading and white noise excitation. Each seismic loading is characterized by a specific maximum acceleration level. The first acceleration level imposed to the specimen corresponds to 10% of the reference acceleration defined in section 2.6. Low level white noise excitation phases are aiming at the evaluation of the dynamic characteristics of the walls (natural modes and frequencies, damping) and of their evolution after increasing intensity seismic loadings.

The detailed load sequence is provided in Table 4, Table 5 and Table 6 respectively for the long walls (same load sequence with and without soundproofing devices), for the short wall with soundproofing devices and for the short wall without soundproofing devices. Values of the targeted seismic acceleration levels are given in percentage of the reference signal (see section 2.6) and in *g*. It is also reminded that the estimated values of the maximum sustainable acceleration according to a normative approach are:

- For the long walls : $a_g = 0.2g$
- For the short walls : $a_g = 0.07g$

Test acceleration values closest to these code-estimated maximum sustainable accelerations are highlighted in bold in the corresponding tables. The tables also show that some tests are doubled at a same acceleration level in order to estimate the progressive degradation of the system.

Table 4 – Earthquake Simulator test log for long walls

Test No.	*Type of test*	*%*	*PGA [g]*
1	Static load (SL1)	/	/
2	Noise (N1)	/	/
3	Noise (N2)	/	/
4	Noise (N3)	/	/
5	Seismic (S1)	10	≈ 0.05 g
6	Noise (N4)	/	
7	Seismic (S2)	20	≈ 0.1 g
8	Noise (N5)	/	
9	Seismic (S3)	20	≈ 0.1 g
10	Noise (N6)	/	
11	**Seismic (S4)**	**40**	**≈ 0.2 g**
12	Noise (N7)	/	
13	Seismic (S5)	60	≈ 0.3 g
14	Noise (N8)	/	
15	Seismic (S6)	80	≈ 0.4 g
16	Noise (N9)	/	
17	Seismic (S7)	100	≈ 0.5 g
18	Noise (N10)	/	
19	Seismic (S8)	120	≈ 0.6 g
20	Noise (N11)	/	
21	Seismic (S9)	140	≈ 0.7 g
22	Noise (N12)	/	

Table 5 – Earthquake Simulator test log for short wall with rubber

Test No.	*Type of test*	*%*	*PGA [g]*
1	Static load (SL1)	/	/
2	Static load (SL2)	/	/
3	Noise (N1)	/	/
4	Noise (N2)	/	/
5	Noise (N3)	/	/
6	Seismic (S1)	10	≈ 0.05 g
7	Noise (N4)	/	/
8	**Seismic (S2)**	**15**	**≈ 0.075 g**
9	Noise (N5)	/	/

10	**Seismic (S3)**	**15**	**≈ 0.075 g**
11	Noise (N6)	/	/
12	Seismic (S4)	20	≈ 0.1 g
13	Noise (N7)	/	/
14	Seismic (S5)	30	≈ 0.15 g
15	Noise (N8)	/	/
16	Seismic (S6)	30	≈ 0.15 g
17	Noise (N9)	/	/
18	Seismic (S7)	40	≈ 0.2 g
19	Noise (N10)	/	/

Table 6 – Earthquake Simulator test log for short wall without rubber

Test No.	*Type of test*	*%*	*PGA [g]*
1	Static load (SL1)	/	/
2	Static load (SL2)	/	/
3	Static load (SL3)	/	/
4	Noise (N1)	/	/
5	Noise (N2)	/	/
6	Seismic (S1)	10	≈ 0.05 g
7	Noise (N3)	/	/
8	**Seismic (S2)**	**15**	**≈ 0.075 g**
9	Noise (N4)	/	/
10	**Seismic (S3)**	**15**	**≈ 0.075 g**
11	Noise (N5)	/	/
12	Seismic (S4)	20	≈ 0.1 g
13	Noise (N6)	/	/
14	Seismic (S5)	30	≈ 0.15 g
15	Noise (N7)	/	/
16	Seismic (S6)	30	≈ 0.15 g
17	Noise (N8)	/	/
18	Seismic (S7)	40	≈ 0.20 g
19	Noise (N9)	/	/
20	Seismic (S8)	40	≈ 0.20 g
21	Noise (N10)	/	/
22	Seismic (S9)	50	≈ 0.25 g
23	Noise (N11)	/	/

Remarks:

- Tests at 30% for both short walls and at 40% for the short wall without rubber devices had to be repeated because the safety equipment disturbed the test conditions (steels bars collide on side frames). Measurements obtained during the first shake at each of these levels are thus to be considered with care;
- Tests of the long walls were stopped because of excessive degradation of the specimens (in particular for the case without rubber);
- Tests of the short walls were stopped because the guiding system was about to come out of safe position, possibly leading to destabilizing the mass. The amplitude of motion observed for the last recorded acceleration level was however felt as large enough to derive useful conclusions.

3.2 ACCELERATION EFFECTIVELY MEASURED AT THE TABLE

The values of the PGA reported in Table 4, Table 5 and Table 6 are those theoretically sent to the table. Because of the high inertia of the specimens, the real PGA's are slightly lower than these theoretical values. Measured values are given in Table 7. They are obtained as the maximum value recorded by channel 1 corresponding to the accelerometer directly located on the table. Highlighted lines correspond to the test providing acceleration closest to the design value.

Table 7 – Comparison of targeted and measured PGA

Test	*Theoretical PGA [g]*				*Measured PGA [g]*			
	Wall 1	**Wall 2**	**Wall 3**	**Wall 4**	**Wall 1**	**Wall 2**	**Wall 3**	**Wall 4**
S1	0.049	0.049	0.049	0.049	0.039	0.043	0.042	0.041
S2	0.097	0.097	**0.073**	**0.073**	0.078	0.090	**0.060**	**0.065**
S3	0.097	0.097	**0.073**	**0.073**	0.078	0.088	**0.061**	**0.064**
S4	**0.194**	**0.194**	0.097	0.097	**0.158**	**0.187**	**0.080**	**0.087**
S5	0.291	0.291	0.145	0.145	**0.239**	**0.278**	0.124	0.136
S6	0.388	0.388	0.145	0.145	0.323	0.356	0.128	0.133
S7	0.485	0.485	0.194	0.194	0.450	0.457	0.171	0.178
S8	0.582	0.582	/	0.194	0.572	0.569	/	0.187
S9	0.679	0.679	/	0.243	0.688	0.639	/	0.234

- *Wall 1 - long wall without rubber;*
- *Wall 2 - long wall with rubber;*

- *Wall 3 - short wall with rubber;*
- *Wall 4 - short wall without rubber.*

3.3 MEASUREMENTS DURING THE STATIC LOADING

The idea of the measurements done during the "static loading" (i.e. differential displacements before and after the positioning of the additional mass) is to take advantage of the presence of the sensors on the wall to get an order of magnitude of the elastic compression modulus of the masonry and of the rubber devices.

Elastic properties of the wall will be derived from measurements given by channels 20 and 21 (diagonal displacements of the wall) and from additional channels 8 to 12 (local vertical compressive displacements of the rubber layers at the top – ch. 9 and 11 – and at the bottom – ch. 8, 10 and 12 – of the wall) in presence of acoustic devices.

Young's Modulus *E [MPa]* can be deduced from the displacement with the following basic formula:

$$E = \frac{N.H}{A\delta_v}$$

where $N\left[N\right]$ is the weight of the mass ;

$H\left[mm\right]$ is the height of the wall, resp. the thickness of acoustic insulation device ;

$A\left[mm^2\right]$ is the surface on which the mass is applied ;

$\delta_v\left[mm\right]$ is the directly or indirectly measured vertical displacement.

3.3.1 Elastic modulus of the masonry

If the application of the above formula will be straightforward for the rubber devices since the sensors corresponding to the channels 8 to 12 directly measure the relevant vertical displacements, the approach is not that easy for the determination of the modulus of the masonry wall. Indeed, channels 20 and 21 record diagonal displacements. Therefore, it is first necessary to derive the vertical displacement from the diagonal one.

The vertical displacement is obtained by projection of the diagonal displacement δ_d, as illustrated in Figure 13 and Figure 14. In the first figure, the diagonal displacement is measured by a wire between two points, A and B.

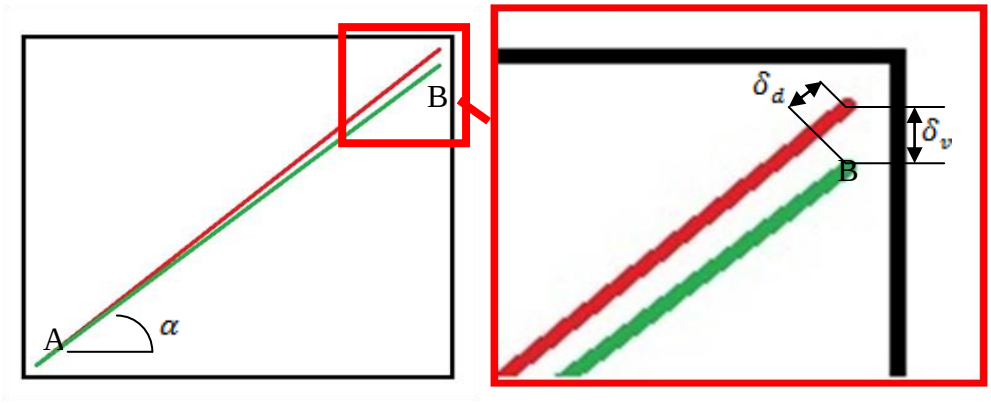

Figure 13 – View of diagonal and vertical displacements

In Figure 14, the vertical displacement is obtained by using the next relation :

$$\delta_v = \delta_d / \sin\alpha$$

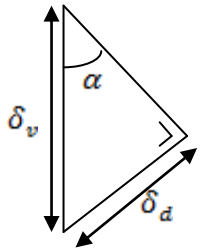

Figure 14 – Projection of diagonal displacement

Once the vertical displacement of both wires (one on each face, named 'back' and 'front' in table 8) is known, elastic modulus can be obtained according to the formula given above. This procedure relies on the assumption that the horizontal component of the displacement of points A and B is negligible (i.e. neglecting Poisson's effect). In this way, different values of the Young Modulus of masonry walls are obtained.

Outcomes are given in Table 8 and show a rather large dispersion of the values obtained. The order of magnitude is however in all cases of 10^4, which seems somehow stiffer than foreseen by Eurocode 6 ($1000 \times f_k \approx 5000$ MPa). This parameter will be further investigated later on based on the dynamic measurements.

Table 8 - Elastic modulus for masonry

	Type of measurement [Units]	Long wall without rubber devices Static load 1	Long wall with rubber devices Static load 1	Short wall without rubber devices Static load 1&2	Short wall without rubber devices Static load 3	Short wall with rubber devices Static load 2
"Front" side	**Vertical disp. [mm]**	/	-0.0401	0.0386	-0.0693	-0.4240
"Back" side	**Vertical disp. [mm]**	-0.0475	0.0237	-0.2130	-0.0115	-0.0833
Average	**Vertical disp. [mm]**	-0.0475	-0.0082	-0.0872	-0.0404	-0.2536
	E [MPa]	6409.2	37153	10190	22005	3503.2

3.3.2 Young modulus of soundproofing devices

Elastic modulus of rubber devices is more straightforward because the sensors directly measure the relevant relative vertical displacement. An average is made from the two sensors at the wall top and the three ones at the wall bottom. Outcomes are provided in Table 9.

Table 9 – Young Modulus for Rubber devices

	Type of measurement [Units]	Long wall with rubber devices Static load 1	Short wall with rubber devices Static loads 1 & 2
Top of the wall	**Near Vertical displacement [mm]**	/	-1.8459
	Far Vertical displacement [mm]	/	-2.2777
Mean	**Vertical displacement [mm]**	/	-2.0618
	Young Modulus [MPa]	/	2.3943
Bottom of the wall	**Near Vertical displacement [mm]**	-0.2850	-0.6197
	Middle Vertical displacement [mm]	0.0102	-1.8520
	Far Vertical displacement [mm]	-0.4321	-0.9779
Mean	**Vertical displacement [mm]**	-0.2356	-1.1499
	Young modulus [MPa]	7.183	4.2932

The measured modulus of the acoustic insulation devices ranges from 2.4 to 7.2 MPa. The variability is likely to come from two main sources:

- The uneven stress distribution;
- The intrinsic dispersion of the material properties (values announced by the producer between 3 and 12 MPa).

3.4 'WHITE NOISE' TESTS

The white noise tests are performed according to the following procedure (Dietz, 2012).

"A random (white noise) excitation with frequency content between 1Hz and 100Hz and at level of about 0.1g RMS is generated using an Advantest R9211C Spectrum Analyser. The random signal is used to drive the Earthquake Simulator (ES) in a single direction.

The 'input' and 'response' channels of the Spectrum Analyser are connected to appropriate instrumentation (e.g. ES Y acceleration and inclusion-head Y acceleration, respectively). The Spectrum Analyser acquires 32 segments of time data, convert to the frequency domain and average results to produce a transfer function. Natural frequency and damping values are determined for all coherent resonances using curve-fitting algorithm running on the Spectrum Analyser. Visual inspections are made after each test to ensure no damage has occurred**.**"

3.4.1 Direct post-processing by EQUALS

'White noise' tests are carried out when the mass is put on the wall fixed on the shaking table and after each seismic test. The full set of transfer functions has been derived. Two cases are illustrated in the present report, namely after the acceleration level $S3$ (*long walls*) in Figure 15 and $S4$ (*short walls*) in Figure 16.

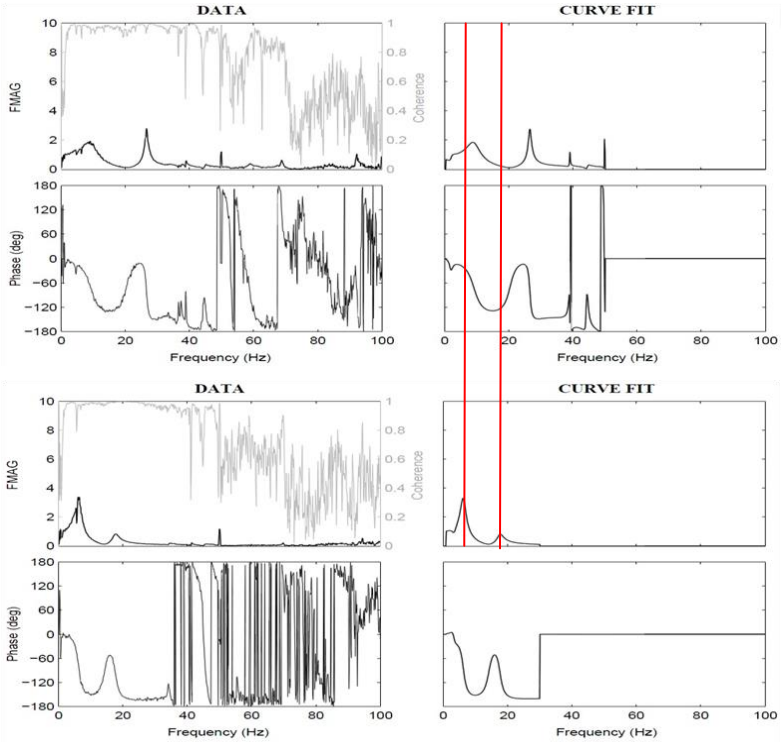

Figure 15 – Transfer Function of long walls without (above) and with (below) rubber devices

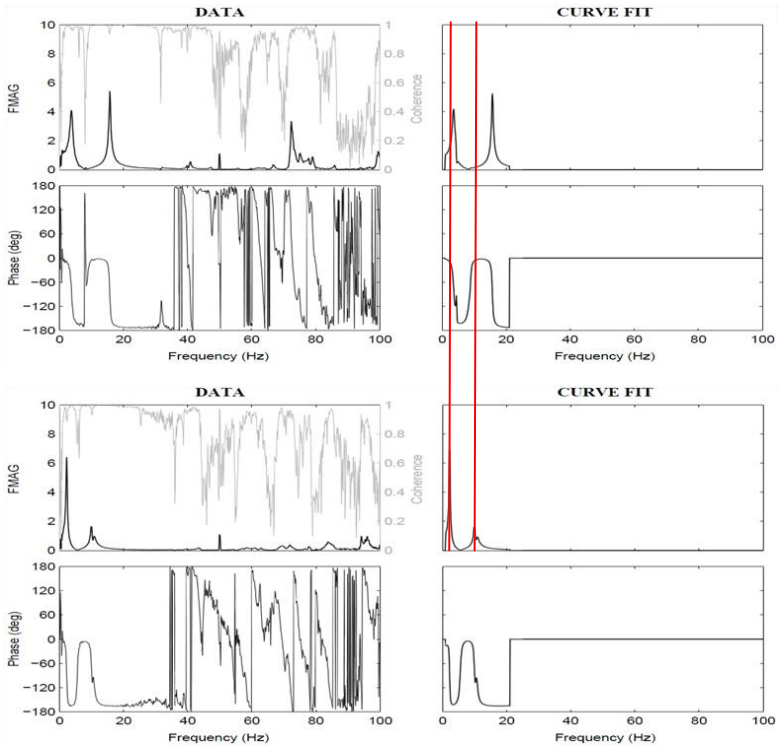

Figure 16 – Transfer Function of short walls without (above) and with (below) rubber devices

Figure 15 shows the transfer functions and the phases of the long walls without acoustic insulation devices in the top four graphs and with acoustic devices in the bottom four. Figure 16 shows the same elements for short walls, with acoustic insulation for the top four graphs and without acoustic devices for the bottom four.

Each group of four graphs comprises :

- Top left: transfer function calculated with recorded data ;
- Top right: curve fitting of the transfer function ;
- Bottom left: phase calculated with recorded data ;
- Bottom right: curve fitting of the phase.

For both figures, two red lines are drawn on the fitting curves to evidence frequency peaks of the wall with rubber devices illustrating the shift of natural frequency towards lower values induced by the presence of these rubber elements. Table 10 gives the full set of natural frequencies (first two peaks) obtained from the curve fitting procedure for all tests, together with the corresponding estimates of the damping ratio.

Table 10 confirms the lower natural frequencies of the wall with acoustic insulation devices in comparison with the wall of the same length without these devices. It can also be seen that the value of the first peak frequency decreases after each seismic test translating a progressive degradation of the system for increasing seismic acceleration.

The variation of the damping associated with the first peak is very important for the long walls (maximum between 40 and 162%). This remarks particularly stands for the long wall without rubber devices (161.90%). This translates again a high degradation of the wall. The frequency of the second peak is more stable and the associated damping is lower (max. 8.4%).

Table 10 – Frequencies and damping of the peaks of transfer functions (EQUALS Post-processing)

Long wall without rubber devices	1st peak frequency [Hz]	1st peak damping [%]	2nd peak frequency [Hz]	2nd peak damping [%]
N 4	9.23	8.94	26.94	1.56
N 5	9.19	23.71	26.61	1.74
N 6	9.17	28.46	26.62	1.82
N 7	10.41	93.77	26.21	2.21
N 8	7.67	82.94	25.97	2.42

N 9	5.93	126.33	25.69	2.50
N 10	6.29	132.20	25.45	2.50
N 11	5.02	161.90	25.52	2.65
N 12	5.26	95.75	26.11	2.41
Long wall with rubber devices				
N 4	6.45	8.33	17.86	5.88
N 5	6.29	14.30	17.65	5.78
N 6	6.16	13.90	17.62	5.93
N 7	5.91	28.16	17.30	6.23
N 8	5.53	40.43	17.05	6.59
N 9	4.75	26.29	16.62	7.18
N 10	4.87	42.54	16.29	6.81
N 11	4.68	36.83	16.08	7.80
N 12	4.31	31.93	15.70	8.37
Short wall without rubber devices				
N 3	3.99	3.86	15.88	1.30
N 4	3.86	7.27	15.81	1.45
N 5	3.77	14.97	15.81	1.45
N 6	3.63	10.87	15.71	1.56
N 7	3.67	15.06	15.44	1.91
N 8	3.54	15.54	15.38	1.74
N 9	3.50	17.44	15.00	2.05
N 10	3.45	19.60	14.87	2.00
N 11	3.30	17.84	14.38	2.32
Short wall with rubber devices				
N 4	2.38	9.14	11.37	4.01
N 5	2.30	6.53	10.83	3.76
N 6	2.26	6.70	10.54	3.87

N 7	2.24	6.52	10.79	3.99
N 8	2.17	9.41	10.61	2.74
N 9	2.21	8.45	10.49	4.29
N 10	2.22	9.19	10.16	5.22

3.4.2 Complementary post-processing

An alternative post-processing procedure has also been developed for the following reasons:
On one hand, the transfer functions of the walls present some rather wide peaks (
Figure 15). It follows that the curve fitting is less accurate and gives approximate values of peak frequencies and damping. Thus, the results are not reliable in particular regarding the damping estimate.
On the other hand, the alternative post-processing will additionally allow the identification of the shape of the vibration modes corresponding to the first two natural frequencies.

The alternative post-processing consists in starting from the direct acceleration measurements and in deriving their Power Spectral Densities (PSD) and Cross-Power Spectral Densities. This calculation yields a square frequency-dependant matrix whose dimensions are the number of accelerometers considered. 5 channels are taken into consideration (Ch. 2, 3, 4, 6 and 7, i.e. longitudinal acceleration at the table, at the bottom, mid-height and top of the wall and on the additional mass). Transfer function between the table and the additional mass are calculated as the ratio between their respective PSD and the associated damping is estimated based on the bandwidth of the frequency peaks according to the following formula:

$$\xi = \frac{\beta_2 - \beta_1}{\beta_2 + \beta_1}$$

Where $\beta_2 - \beta_1$ is the width of the peak at mid-height (see also Fig. 17).

Figure 18, Figure 19, Figure 20 and
Figure 21 depict the transfer functions obtained for each of the four tested walls in identification phases directly following the increasing acceleration levels used for seismic tests. Corresponding natural frequencies and damping are given in Table 11 and Table 12. In these two tables, some

damping ratios are not given, i.e. for cases where the peak is identified as too flat to consider the use of the bandwidth method as reliable.

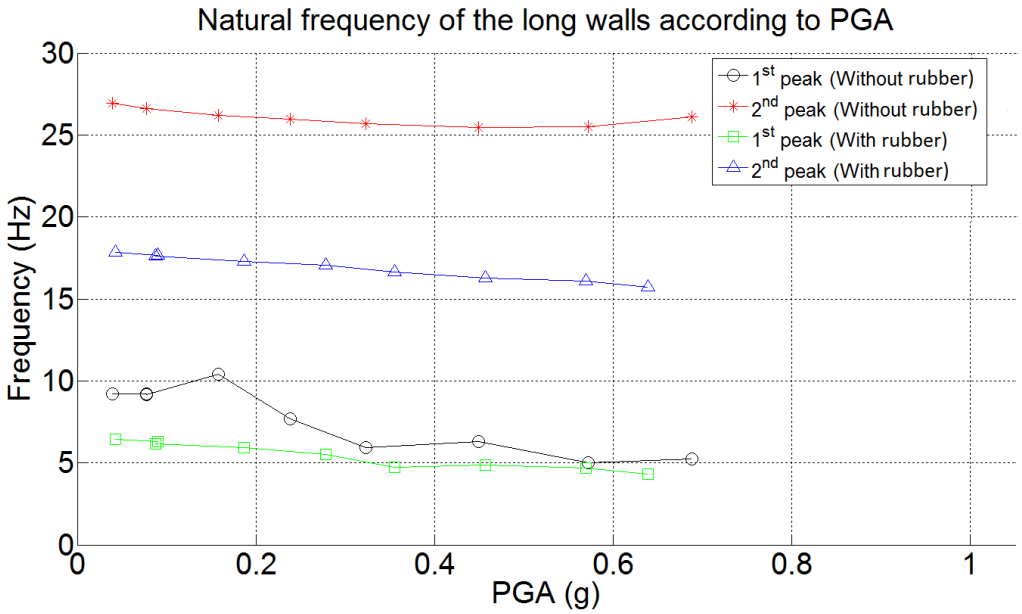

Figure 22 and Figure 23 summarize the evolution of the natural frequencies after increasing seismic shakes while Figure 24, Figure 25, Figure 26 and Figure 27 show the modal shapes respectively for each of the four tested walls. These vibration modes are determined by calculating the eigenmode associated with the largest eigenvalue of the 5 x 5 cross-DSP matrix with the frequency fixed at the value corresponding to the first resp. second peak frequency obtained from the DSP.

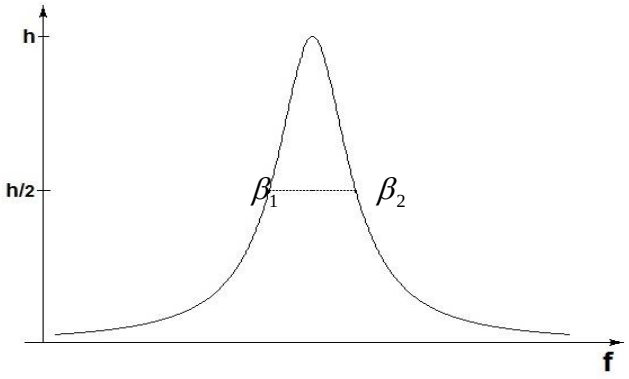

Figure 17 – Calculation of the damping

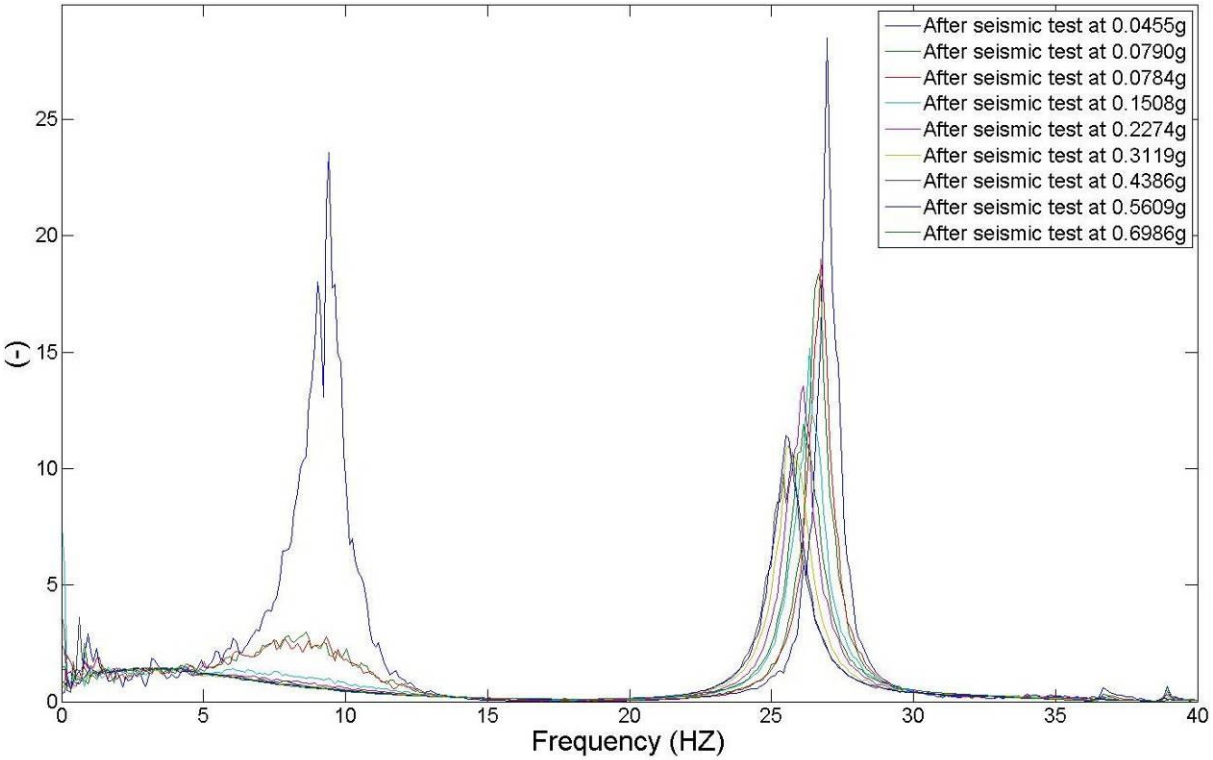

Figure 18 – Transfer functions of long wall without rubber devices

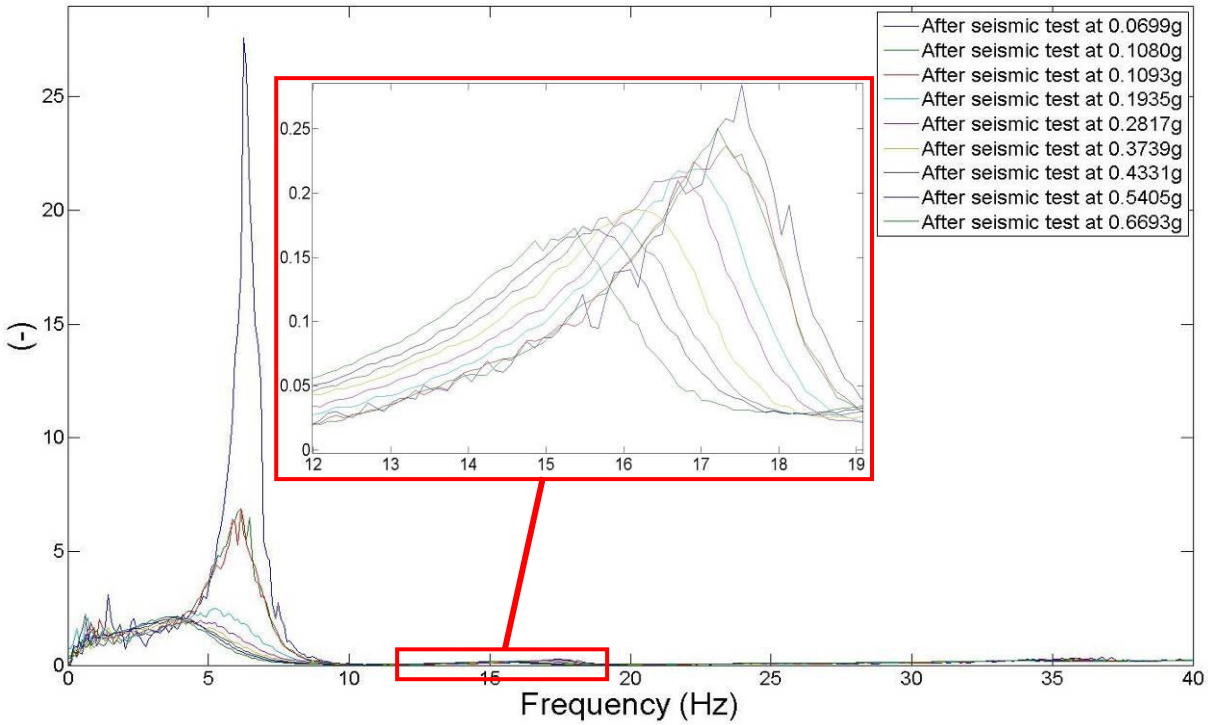

Figure 19 – Transfer functions of long wall with rubber devices

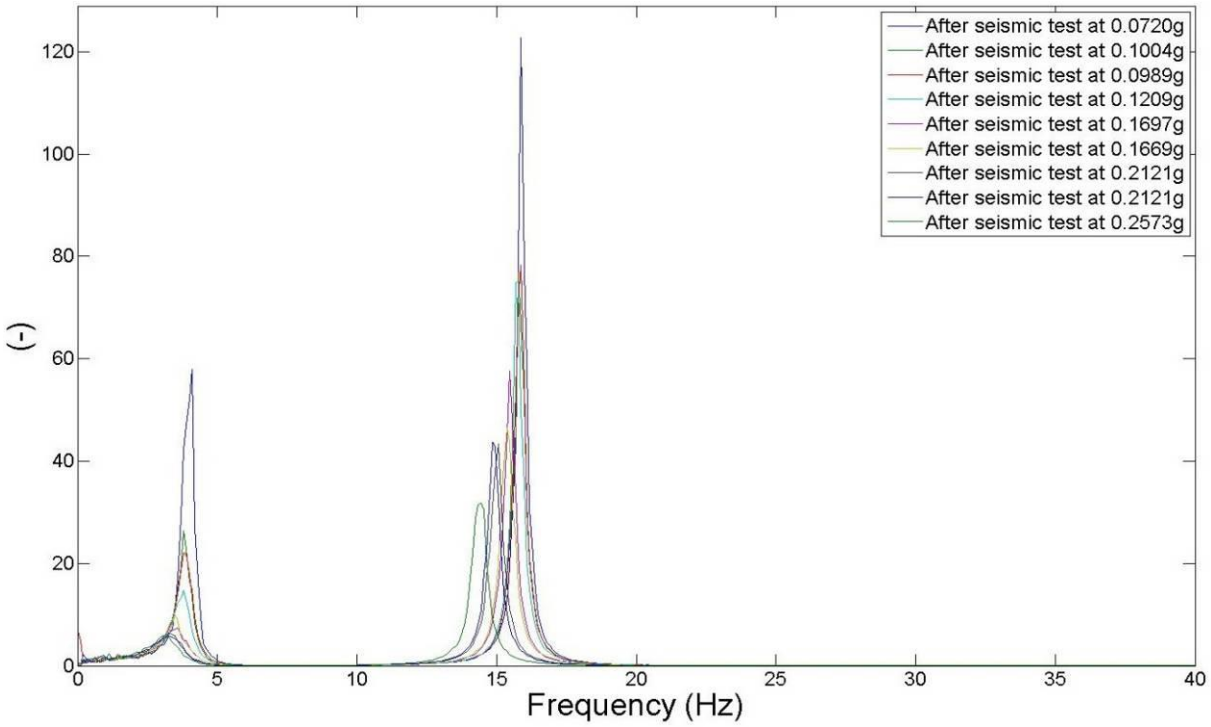

Figure 20 – Transfer functions of short wall without rubber devices

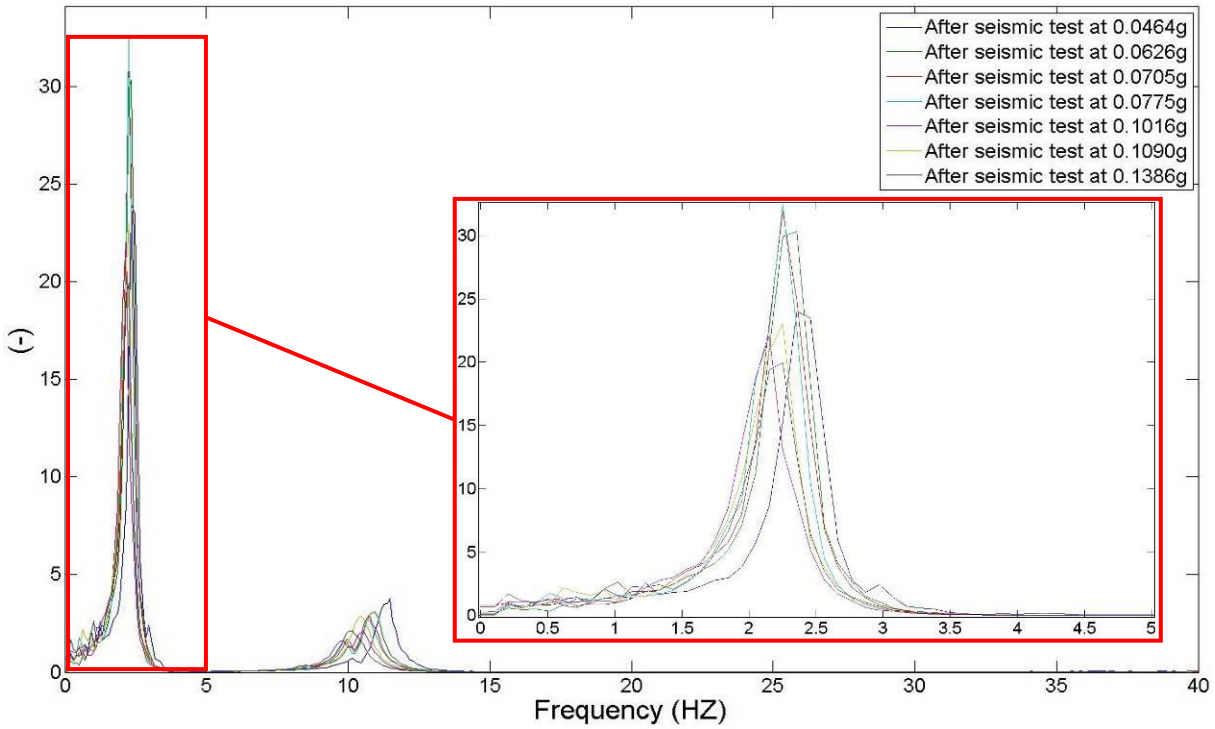

Figure 21 – Transfer functions of short wall with rubber devices

Table 11 – Frequencies and damping of the transfer functions peaks (Compl. post-processing – Long wall)

Long wall without rubber devices	*1e peak frequency [Hz]*	*1e peak damping [%]*	*2e peak frequency [Hz]*	*2e peak damping [%]*
N 4	9.43	6.73	26.95	1.28
N 5	8.61	31.4	26.74	1.6
N 6	9.23	38.69	26.64	1.68
N 7	6.05	/	26.33	2.01
N 8	3.40	/	26.13	1.94
N 9	3.68	/	25.62	2.74
N 10	3.38	/	25.72	2.76
N 11	3.18	/	25.51	2.56
N 12	3.18	/	26.13	2.46

Long wall with rubber devices	*1st peak frequency [Hz]*	*1st peak damping [%]*	*2nd peak frequency [Hz]*	*2nd peak damping [%]*
N 4	6.25	6.36	17.52	5.91
N 5	6.1	16.78	17.21	6.86
N 6	6.15	16.67	17.32	7.49
N 7	5.23	50.26	16.91	8.07
N 8	4.71	/	16.80	8.55
N 9	4.20	/	16.19	9.63
N 10	3.89	/	15.78	9.82
N 11	3.89	/	15.47	10.55
N 12	3.48	/	15.37	10.5

Table 12 – Frequencies and damping of the transfer functions peaks (Compl. post-processing – Short walls)

Short wall without rubber devices	*1st peak frequency [Hz]*	*1st peak damping [%]*	*2nd peak frequency [Hz]*	*2nd peak damping [%]*
N 3	4.10	6.43	15.88	0.98
N 4	3.79	7.82	15.78	1.39
N 5	3.79	8.79	15.88	1.42
N 6	3.79	10.51	15.78	1.36

N 7	3.58	17.94	15.47	1.55
N 8	3.48	11.4	15.37	1.95
N 9	3.28	20.01	15.06	1.83
N 10	3.18	23.07	14.86	1.78
N 11	3.07	22.75	14.45	2.23
Short wall with rubber devices				
N 4	2.36	8.06	11.48	3.49
N 5	2.36	8.71	10.96	4.05
N 6	2. 24	8.34	10.76	3.81
N 7	2.25	8.73	10.76	3.72
N 8	2.15	9.78	10.56	2.56
N 9	2.25	9.65	10.45	4.49
N 10	2.25	10.24	10.04	3.39

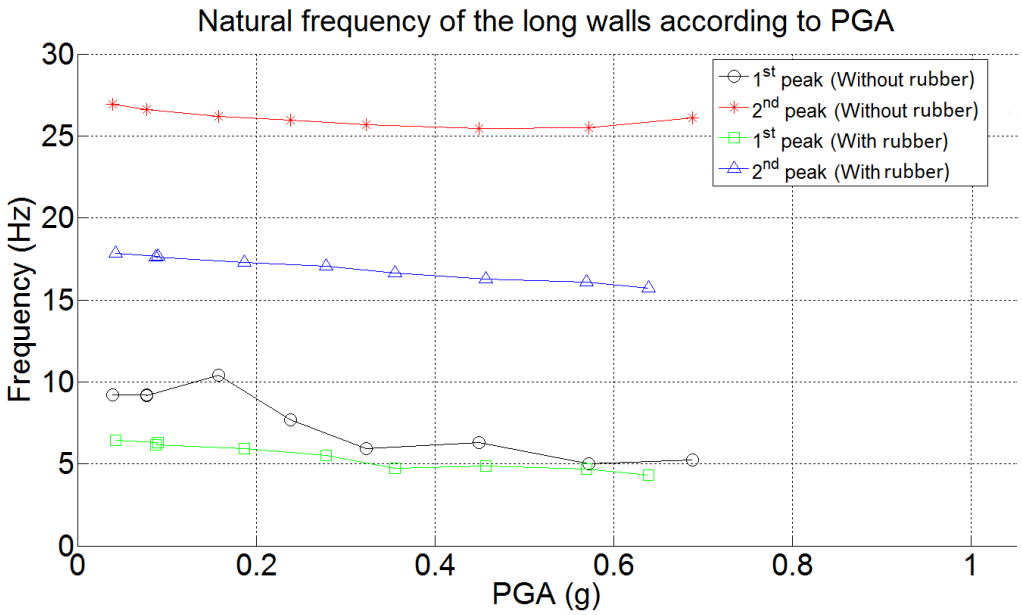

Figure 22 – Natural frequencies of the long walls according to PGA

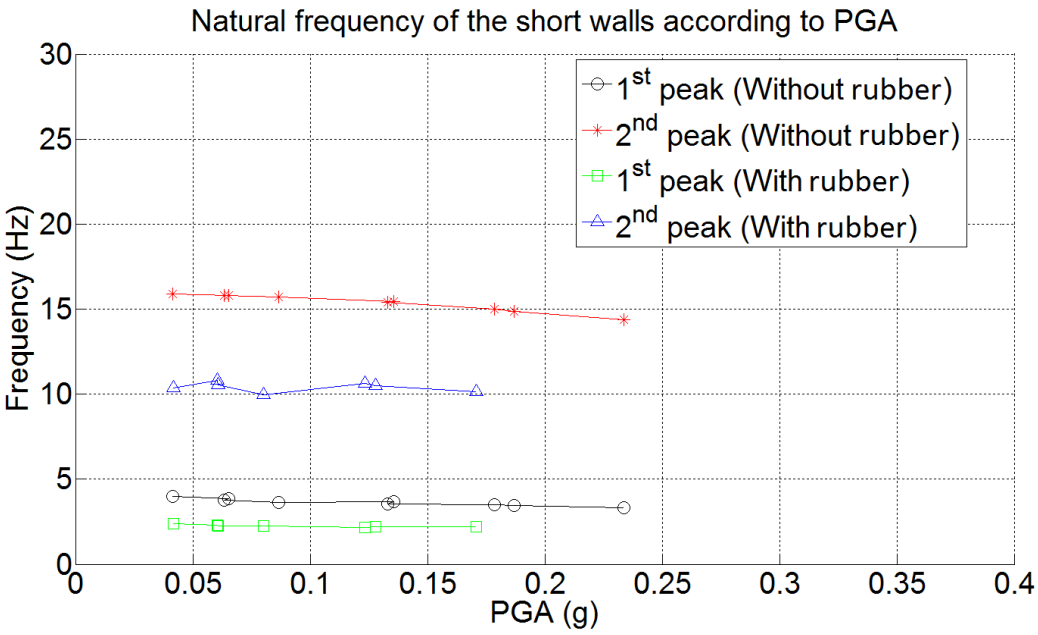

Figure 23 – Natural frequencies of the short walls according to PGA

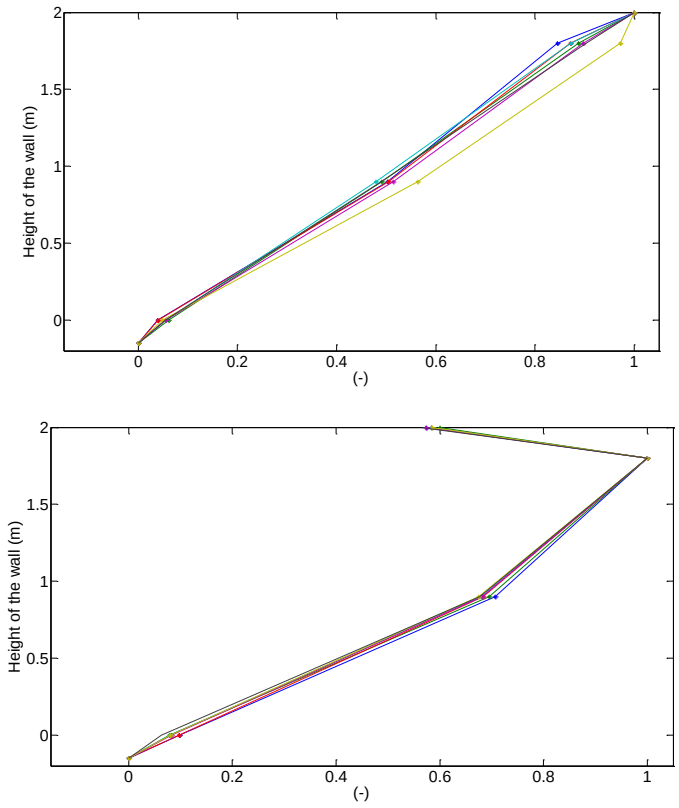

Figure 24 – 1st (above) and 2nd (below) modal shapes (Long wall without rubber)

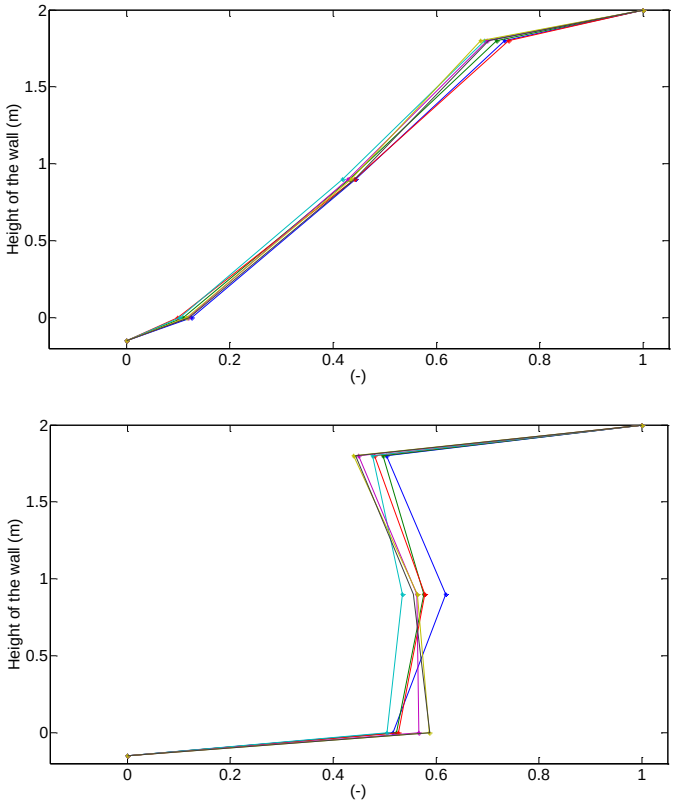

Figure 25 – 1st (above) and 2nd (below) modal shapes (Long wall with rubber)

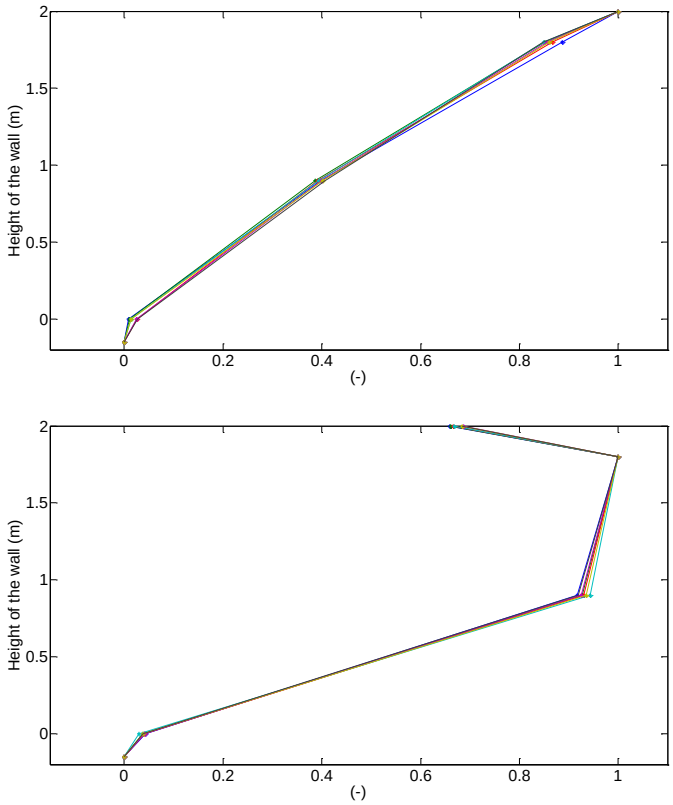

Figure 26 – 1st (above) and 2nd (below) modal shapes (Short wall without rubber)

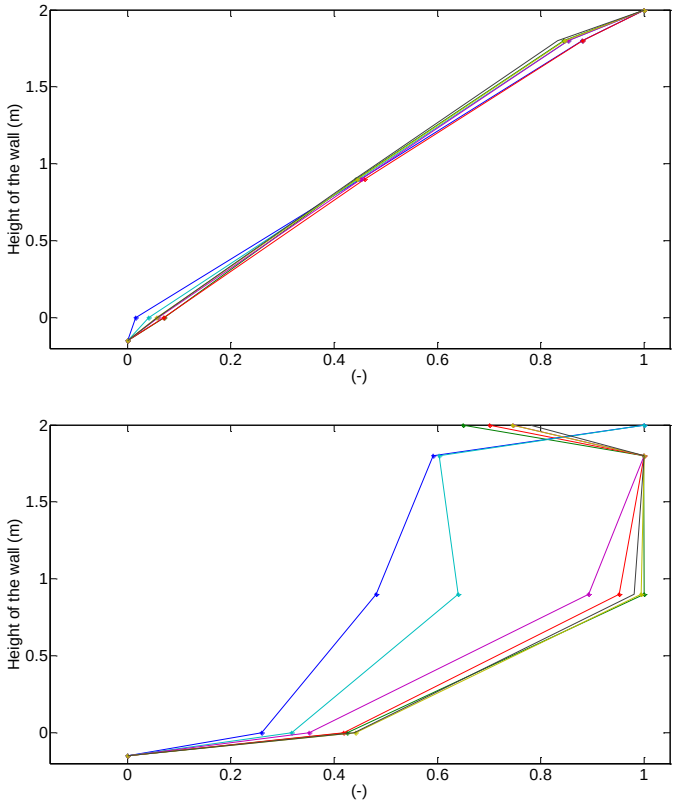

Figure 27 – 1st (above) and 2nd (below) modal shapes (Short wall with rubber)

3.4.3 Observations

For the long walls, the first peak frequency of the transfer function progressively decreases following increasing seismic accelerations. The peak also gets larger. The deterioration of the structure certainly explains this phenomenon, which involves also progressive increase of the damping ratio. The value of the first peak frequency starts around 9 Hz for the long wall without rubber devices and around 6 Hz for the one with acoustic insulation devices. The second peak remains more stable, although slightly decreasing. The second peak frequency is about 26.5 Hz for the long wall without rubber devices and about 16.5 Hz for the one with acoustic insulation devices.

Comparison of values in Table 11 and Table 10 (EQUALS and additional post-processing outcome) leads to the following observations. Frequencies of the 1st peak are close for the first three tests (N4, N5 and N6) but become then different from one post-processing to the other. The relative difference is about 0.1% to 6% for the tests N4, N5 & N6, and about 10 to 55 % for the others. The difference is more important in the case of the long wall without rubber devices in

relation with a flatter shape of the 'peak' in this latter case. Concerning the values of the frequency of the 2nd peak, the maximum relative difference between the two methods is about 4% at least. The damping values are very close. The relative difference is at most about 0.26% for the long wall without rubber devices and about 0.44% for the long wall with these devices. In conclusion for the long walls, the deterioration of the first frequency peak and its flattening make approximate the value of the peak frequency by a fitting algorithm. It results in a rather important variability of the value of the measured natural frequency once the wall starts degrading. Concerning the damping, it seems to be well assessed as the two post-processing give close values.

For the short walls, Figure 20 and
Figure 21 show that the first peak of transfer function also decreases when the acceleration level of seismic tests increases. However, the deterioration is less important than in the case of the long walls and the peak remains better identifiable. The same comments can be made for the second peak of short walls than the one of long walls. Both procedures results then in more consistent values (8 % maximum difference for the 1st peak and 2 % maximum for the 2nd peak). The damping values are also very close. The relative difference is at most about 0.41% for the short wall without rubber devices and about 0.35% for the short wall with these devices. In conclusion, some degradation also occurs in the short wall, but the peaks remains sharper even at the end of the full testing program.

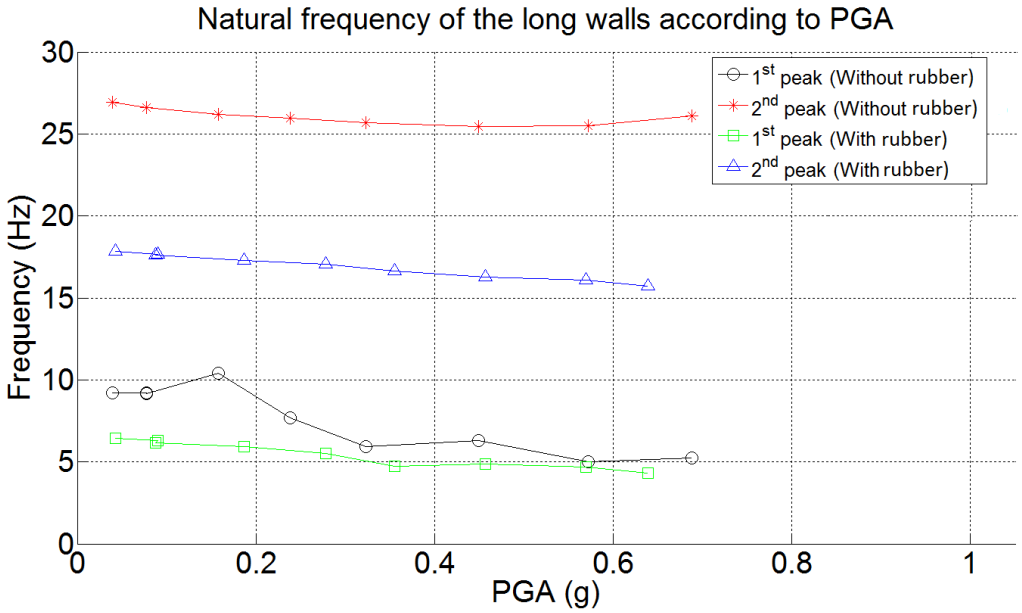

Figure 22 and Figure 23 summarize the natural frequencies of the four walls and illustrate the comments expressed right above. A difference is particularly visible in the case of the long wall

without acoustic insulation devices because the first peak of frequency of this wall is the most degraded after the tests. Moreover, the presence of the rubber elements reduces the frequency of the corresponding wall without rubber by about 30 %.

Regarding the modal shapes, it is observed that they remain fairly identical after increasing seismic accelerations. Mode 1 is a classical cantilever deformation shape while mode 2 is related to the additional mass vibrating in phase opposition with respect to the wall. In presence of rubber elements, concentration of deformation is observed as expected at the level of these rubber elements, particularly for the case of the first mode of the long wall.

3.4.4 Comparison with the reference theoretical assessment

Table 13 gives the experimental natural frequencies of the 'wall+mass' structures before any seismic test. These will be compared in this section with simple theoretical values.

Table 13 – Natural frequencies of the long wall obtained by the laboratory processing

		Wall without rubber		Wall with rubber	
		First peak	Second peak	First peak	Second peak
Long wall	N3	9.01 Hz	25.50 Hz	5.26 Hz	16.15 Hz
Short wall	N2/3	3.81 Hz	15.67 Hz	2.53 Hz	11.14 Hz

In the preliminary assessment (section 2.3.2), the period of the corresponding single-freedom degree structure and hence the natural frequency was calculated as follows:

$$T = \frac{1}{f} = 2\pi\sqrt{\frac{M}{K}}$$

Where M [kg] is the mass (5000 kg)

K [N/m] is the stiffness of the structure

The system flexibility is the sum of two contributions (see Tomazevic, 1999): the bending (1) and the shear (2) deformability respectively. In the case of a wall built-in at the bottom and free at the top, it yields:

$$\frac{H^3}{3EI}\ (1) \qquad \frac{H}{GA'}\ (2)$$

$$K = \frac{1}{\frac{H^3}{3EI} + \frac{H}{GA'}}$$

Where H [m] is the height of the wall;

I [m^4] is the inertia of the wall;

A' [m^2] is the shear area of the wall, taken to 5/6 of the wall area (Serge Cescotto & Charles Massonet, 2001);

E [N/m^2] is the elastic modulus of the masonry;

G [N/m^2] is the shear modulus of the masonry.

For use in seismic context, the value of the elastic modulus E should be divided by 2 (Eurocode 8, 2004), thus equal to 500 f_k, and the shear modulus should be taken as 40% of the elastic modulus (Eurocode 6, 2004).

These formulas are directly usable for the walls without acoustic insulation devices.

Table 14 – Natural frequency according to the Eurocodes & dynamic equations

Tested wall	Length [m]	M [kg]	Stiffness K [N/m]	Period T [s]	Frequency [Hz]
Long wall	2.10	5000	$52.76\ 10^6$	0.064	15.59
Short wall	0.72	5000	$3.84\ 10^6$	0.238	4.203

The comparison between the values of the frequency of the first peak given in Table 13 with the theoretical estimates of Table 14 shows a difference. The relative error is equal to:

- 45.69 % for the long wall
- 9.35 % for the short wall

The difference is more important for the long wall. Consequently, the shear contribution to the stiffness seems to be the problem. In this case, the shear contribution is actually of the same order of magnitude as the bending one, as showed in Table 15, while in the case of the short wall, the shear contribution is about 10% of the bending one. The assessment of the wall stiffness according to EC6 seems to suggest a wrong value of the shear stiffness estimate (this might be due to the fact that vertical joints are open in the specimens). A first trial and error procedure shows that the shear modulus should be closer to 0.1 E than 0.4 E. This preliminary conclusion will be further investigated in next stages of the research work by a consistent model updating procedure, together with a quantification of the effect of rubber layers on the global stiffness and hence on the resulting vibration periods.

Table 15 – Stiffness of the wall according to the EC

Tested wall	Bending contribution (flexibility) [m/N]	Shear Contribution (flexibility) [m/N]	Stiffness *K* [N/m]
Long wall	$9.38\ 10^{-9}$	$9.57\ 10^{-9}$	$52.76\ 10^{6}$
Short wall	$2.37\ 10^{-7}$	$2.79\ 10^{-8}$	$3.84\ 10^{6}$

3.5 SEISMIC TESTS

Measurements taken during the seismic tests allow studying the behaviour of the walls in dynamic conditions. The main aspects directly investigated from the test measurements are dealing with:

- the compressive length;
- the horizontal displacement of the wall;
- the shear strength;
- the behaviour of the additional mass.

A comparison is also directly possible between the long and the short walls without rubber devices, whereas the comparison between walls of same length, but with or without acoustic insulation devices, shows the influence of these devices.

3.5.1 Assessment of the compressive length

As it could be seen in the preliminary assessment, the compressive (or contact) length is a key parameter for evaluating the strength of the wall. It governs indeed the overturning, the compression and the shear failure.

In order to estimate the contact length from the experimental measurements, the LVDT devices 8, 10 and 12 are considered. They provide the relative vertical displacement between the wall and the bottom beam at three locations, approximately at the wall near end (8), at the mid-width wall (12) and at the wall far end (10).

From these three points, a linear interpolation is carried and a fitting of two parameters is derived (see Figure 28): the mean vertical displacement δ_m and the rotation θ of the wall base. In this

procedure, the wall is supposed to behave as a rigid body. The mean displacement is positive in case of an uplift of the wall and the slope is positive when the "far" side is uplifted.

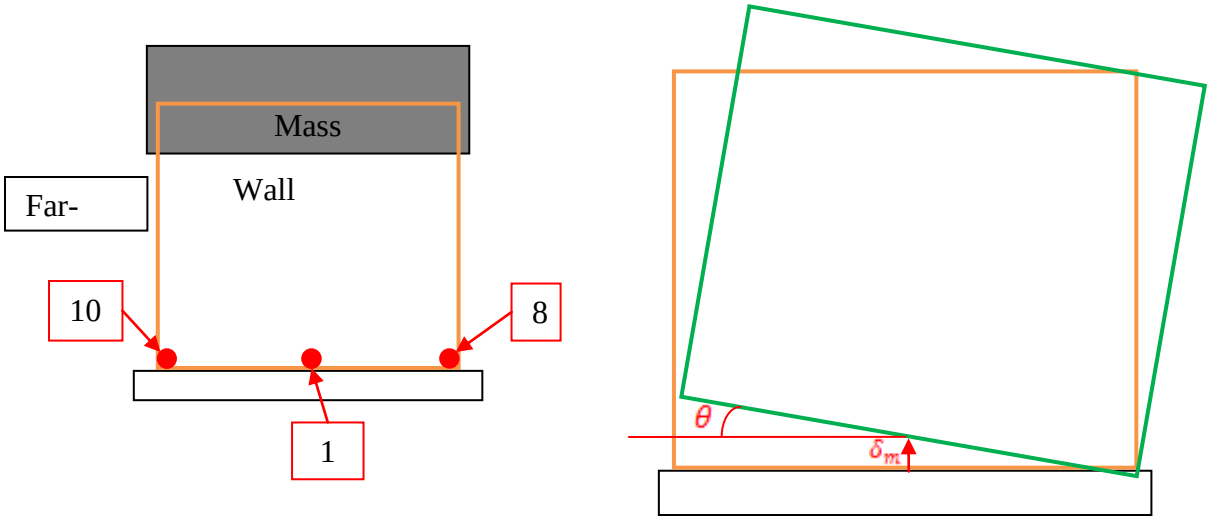

Figure 28 – Position of the used sensors (left) and derived parameters (right)

As an illustration, Figure 29 to Figure 34 show the time evolutions of these two parameters for three different acceleration levels for the long wall without rubber devices. The levels are chosen such as the first one below the theoretical estimated maximum acceleration, the second one is close to this level and the last is above.

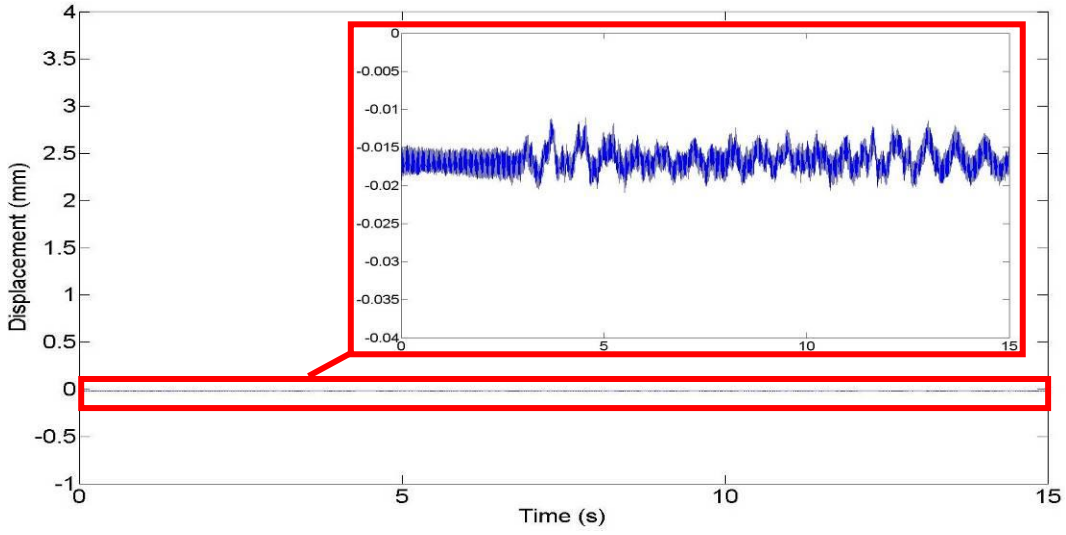

Figure 29 – Mean displacement during the seismic test at 0.0393g

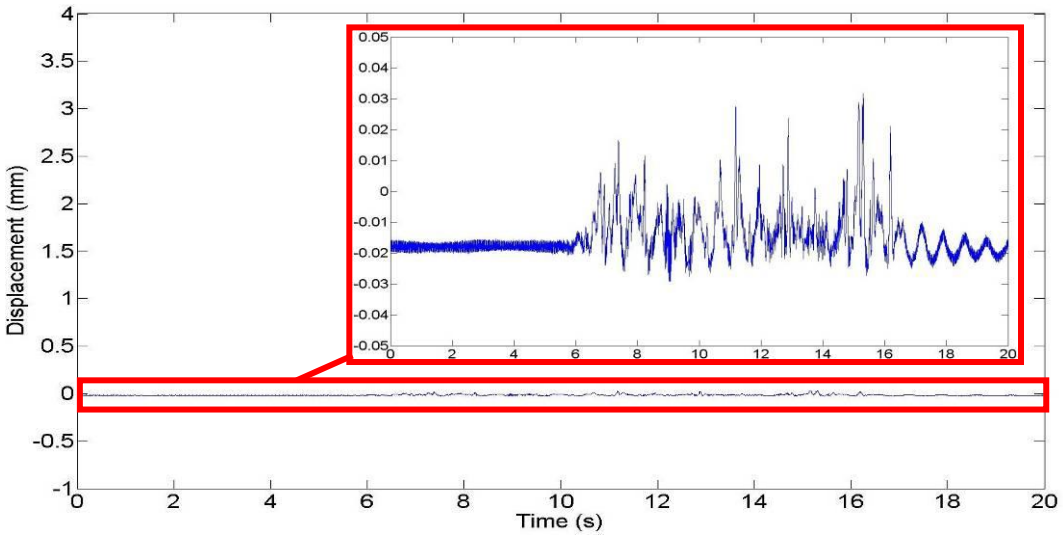

Figure 30 – Mean displacement during the seismic test at 0.2387g (Ref. acceleration = 0.2g)

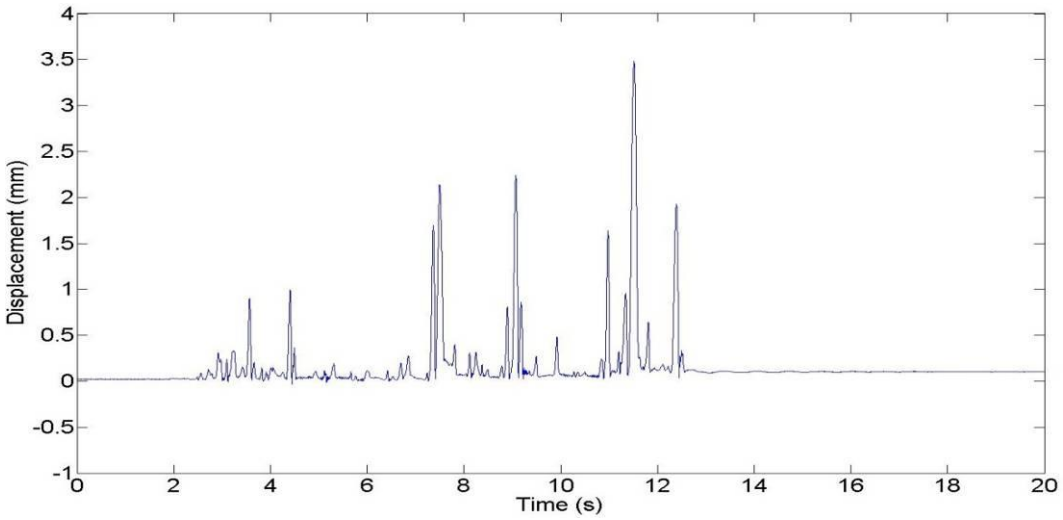

Figure 31– Mean displacement during the seismic test at 0.6878g

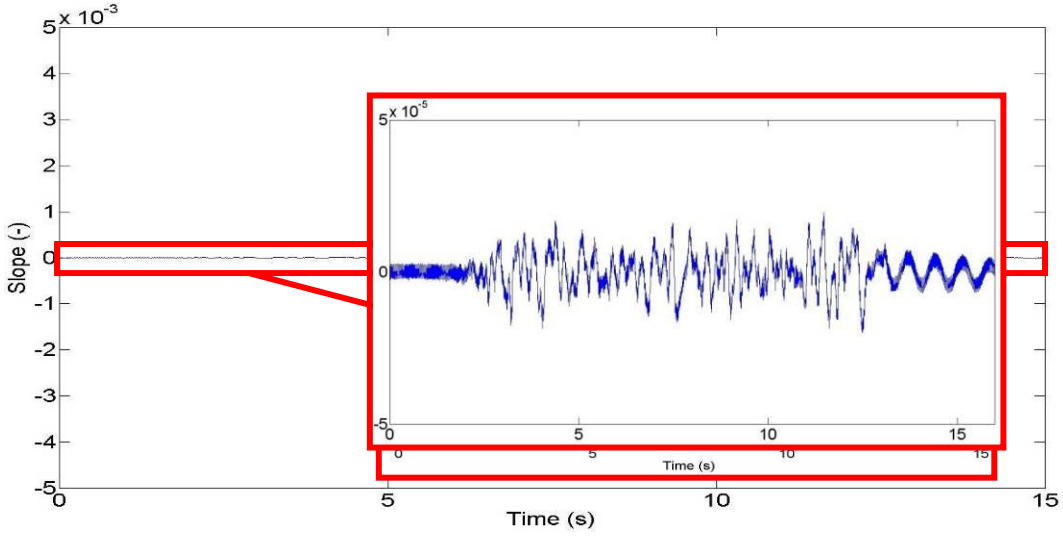

Figure 32 – Base rotation during the seismic test at 0.0393g

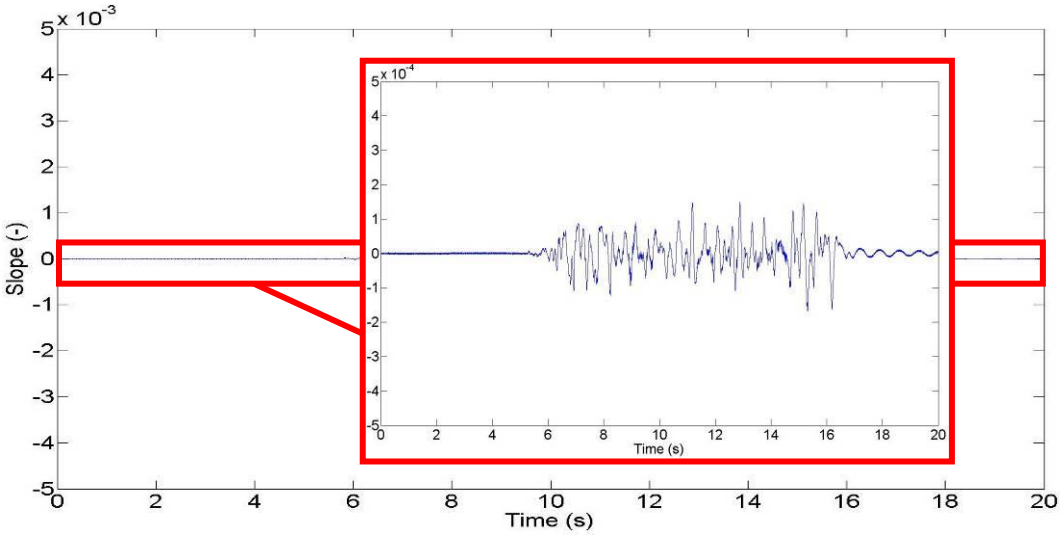

Figure 33 – Base rotation during the seismic test at 0.2387g (Ref. acceleration = 0.2g)

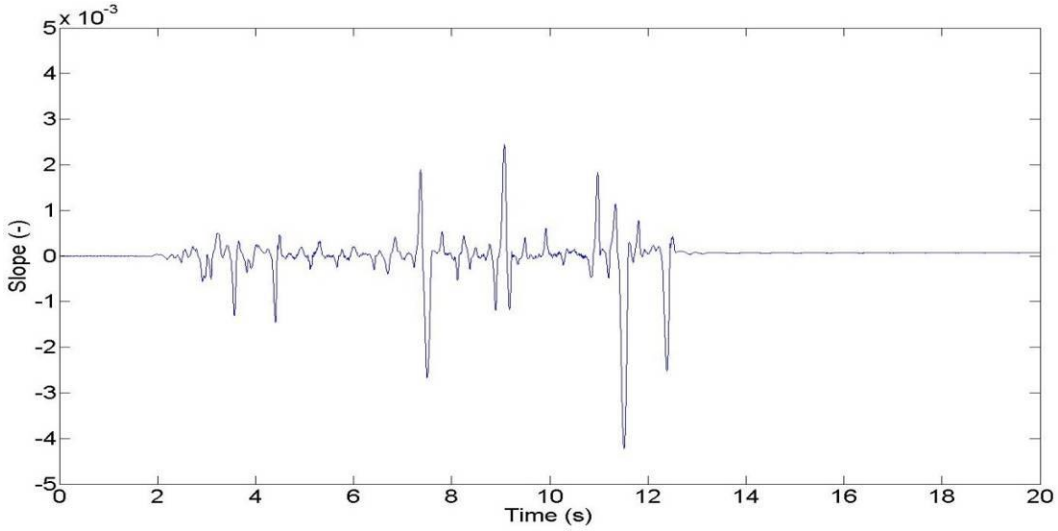

Figure 34 – Base rotation during the seismic test at 0.6878g

As seen on Figure 29, Figure 30 and Figure 31, the mean displacement increases with the acceleration level. However, the displacement increase is not proportional to the acceleration one. Same as the mean displacement, the slope increases in a non-proportional manner when the acceleration level increases. If the acceleration is multiplied by three, the mean maximum slope increases is about twenty times higher. The behaviour is thus clearly non-linear. This is also shown by the values given in Table 16, Figure 35 and Figure 36.

Table 16 – Value of the maximum slope according to the acceleration level

Specimen	*Acceleration level [g]*	*Maximum slope [-]*
Long wall without rubber devices	0.039	$1.99\ 10^{-5}$
	0.238	$1.68\ 10^{-4}$
	0.688	$4.22\ 10^{-3}$
Long wall with rubber devices	0.043	$7.72\ 10^{-6}$
	0.187	$5.24\ 10^{-4}$
	0.639	$8.40\ 10^{-3}$
Short wall without rubber devices	0.041	$2.44\ 10^{-4}$
	0.064	$4.59\ 10^{-4}$
	0.178	$9.70\ 10^{-3}$
Short wall with rubber devices	0.042	$1.30\ 10^{-3}$
	0.061	$2.40\ 10^{-3}$
	0.171	$1.38\ 10^{-2}$

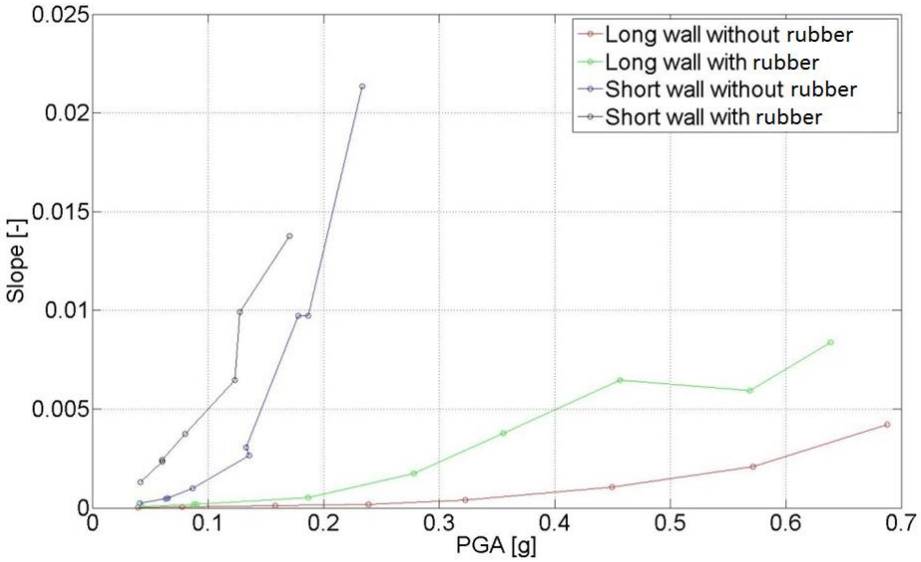

Figure 35 – Evolution of the maximum slope (absolute value) according to the PGA

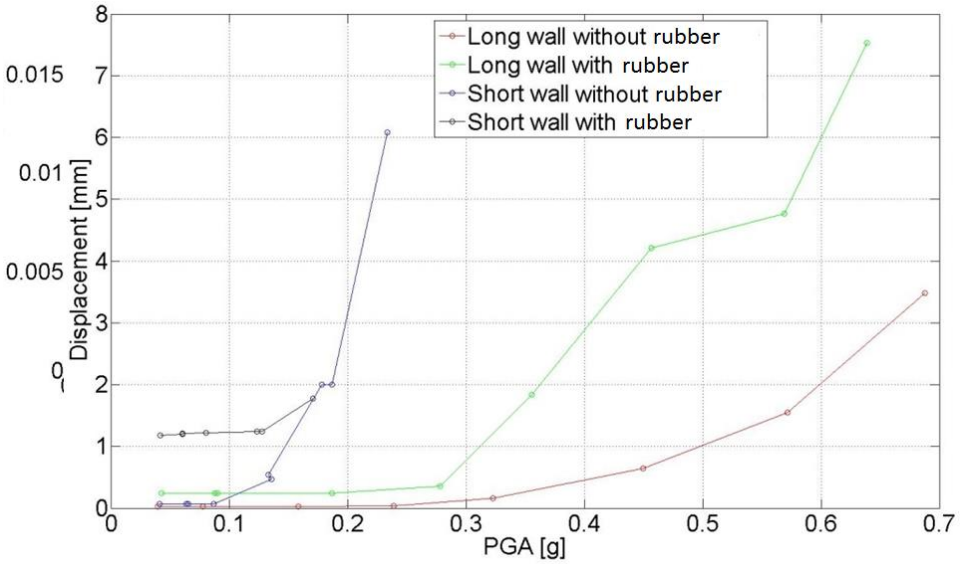

Figure 36 – Evolution of the maximum mean displacement (absolute value) according to the PGA

From the mean vertical displacement and the slope, it is then possible to deduce the contact length, i.e. the length on which the total displacement from combined average uplift and rotation remains negative (conventional positive displacement is in the uplift direction). The time evolution of the compressive length is drawn in terms of percentage of the total length of the wall for three acceleration levels for the long walls (Figure 37 to Figure 42) and for the short ones (Figure 43 to Figure 48) .

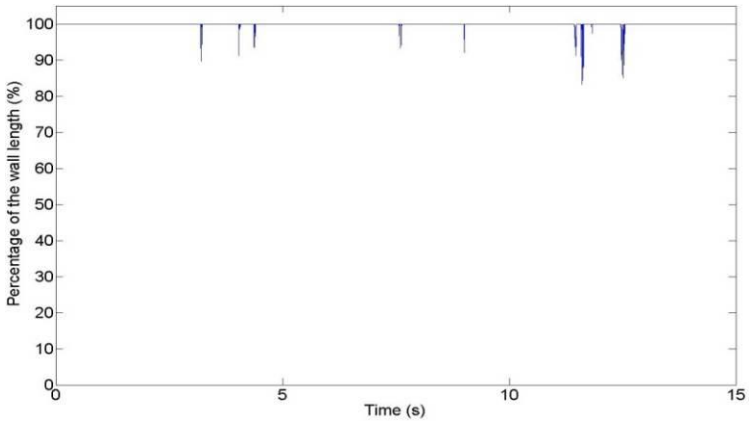

Figure 37 – Time evolution of the compressive length for the long wall without rubber (0.0393g)

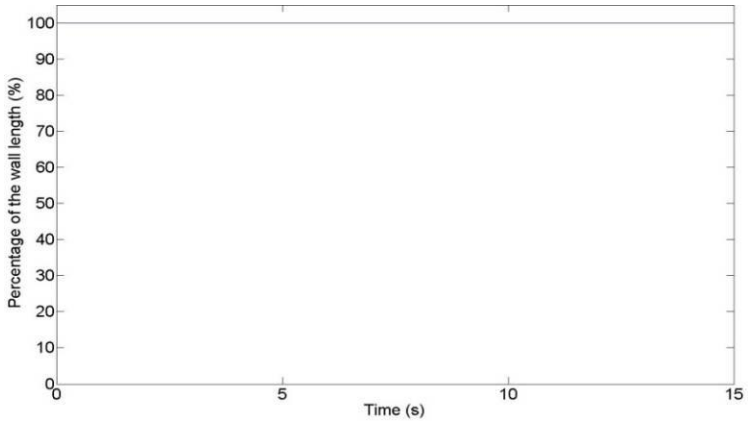

Figure 38 – Time evolution of the compressive length for the long wall with rubber (0.0426g)

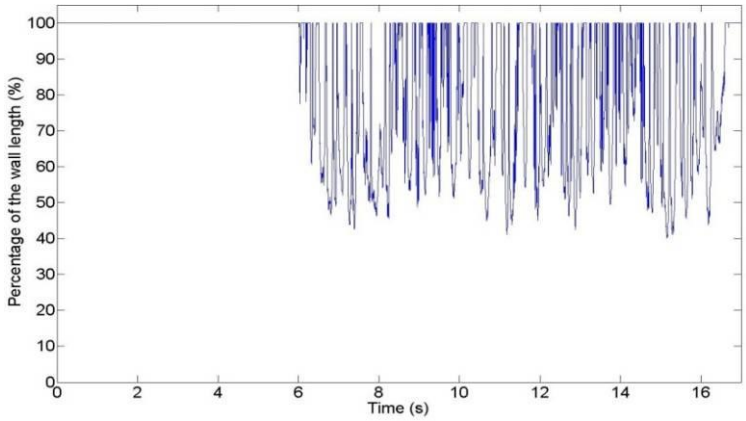

Figure 39 – Time evolution of the compressive length for the long wall without rubber (0.2327g)

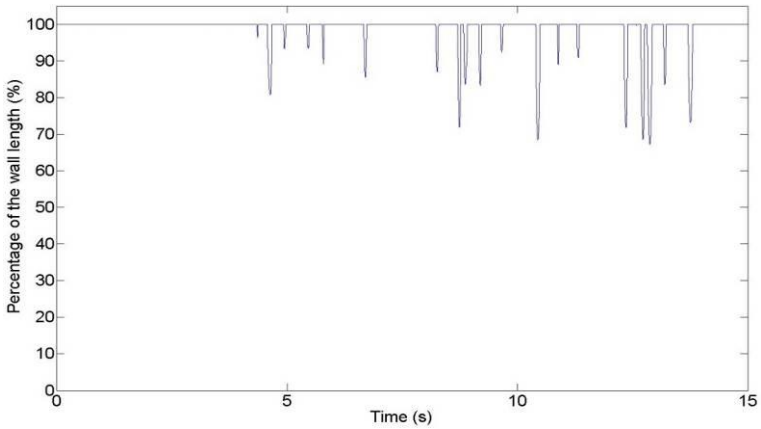

Figure 40 – Time evolution of the compressive length for the long wall with rubber (0.1871g)

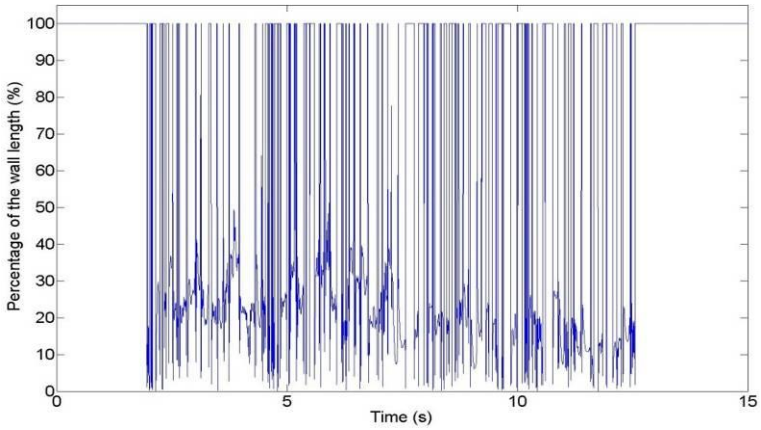

Figure 41 – Time evolution of the compressive length for the long wall without rubber (0.6878g)

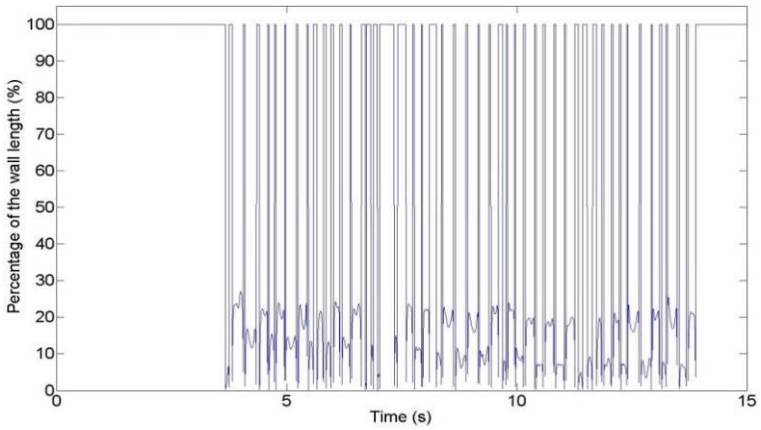

Figure 42 – Time evolution of the compressive length for the long wall with rubber (0.6392g)

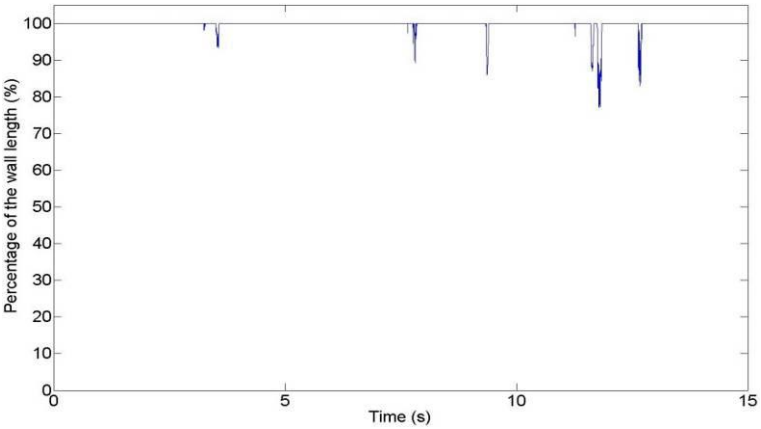

Figure 43 – Time evolution of the compressive length for the short wall without rubber (0.0413g)

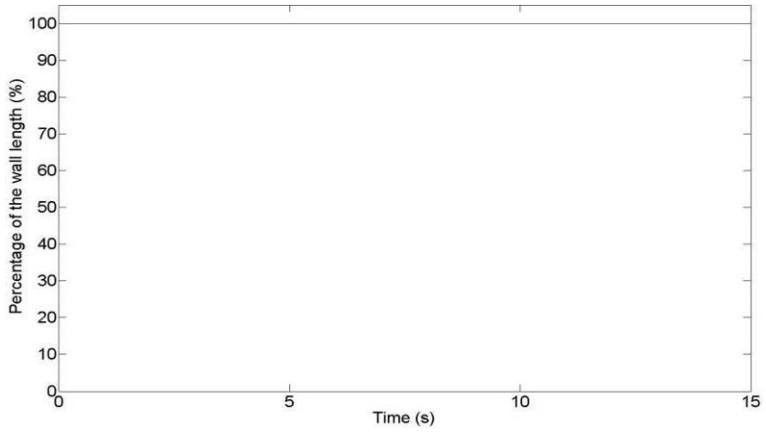

Figure 44 – Time evolution of the compressive length for the short wall with rubber (0.0417g)

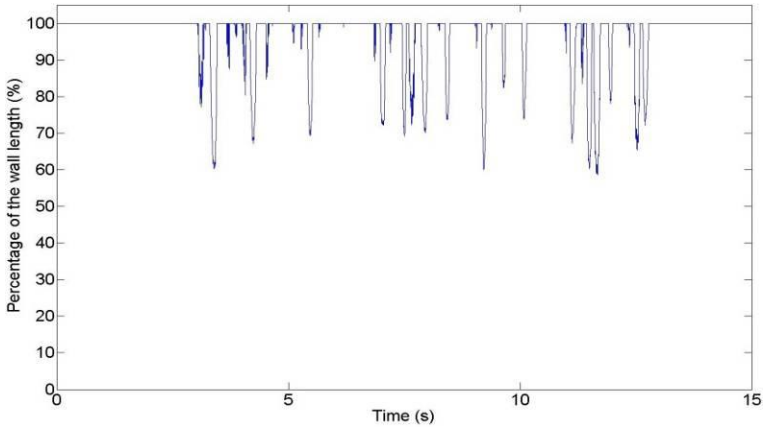

Figure 45 – Time evolution of the compressive length for the short wall without rubber (0.0635g)

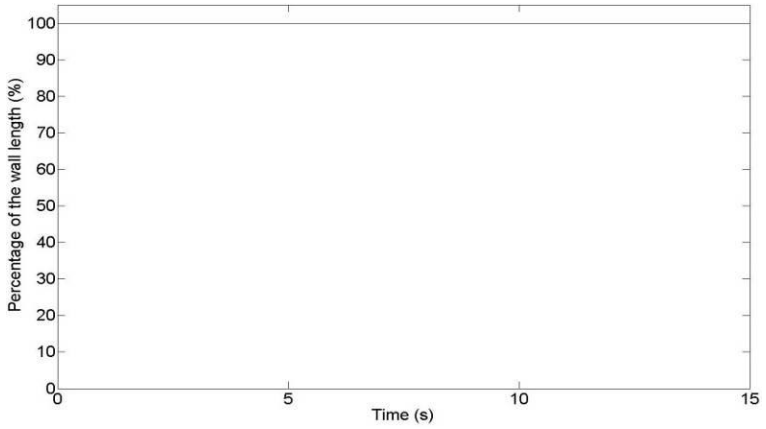

Figure 46 – Time evolution of the compressive length for the short wall with rubber (0.0607g)

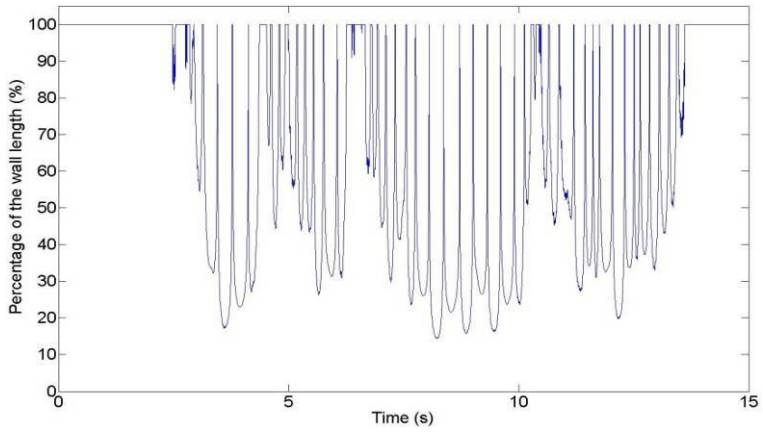

Figure 47 – Time evolution of the compressive length for the short wall without rubber (0.1784g)

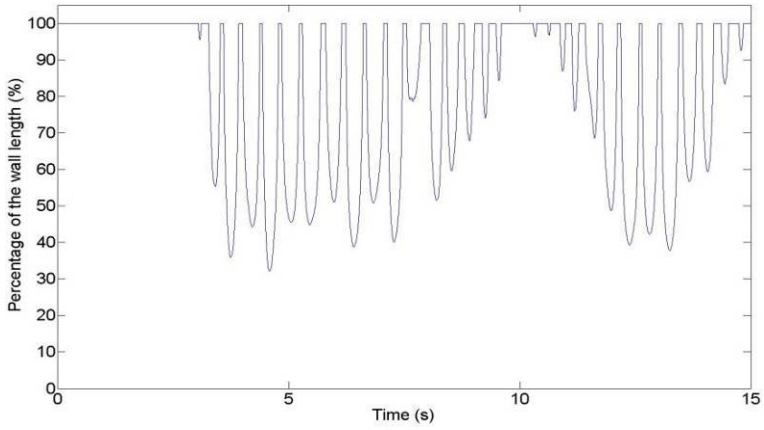

Figure 48 – Time evolution of the compressive length for the short wall with rubber (0.1709g)

From the above figures, it can be observed that:

- The wall behaviour is quite different if acoustic insulation devices are installed. For the same level of PGA, the one-side-uplift is more important in the case of the wall without rubber devices;
- In Figure 41 and Figure 42, the compressive length becomes close to zero for the two long walls (fully developed rocking motion). Nevertheless for this shaking level, the wall without rubber devices spends more time in a position in full contact;
- Conclusions are similar for the short wall, with a rocking appearing for smaller acceleration levels than for long walls.

A full comparison of the results is provided in Table 17 and Figure 49. It is then evidenced that:

- For the same PGA level, it shows that the value of the percentage of compressive length is always higher for long walls. However, the walls are rocking whatever their length, although this

behaviour was not expected for the long walls (a shear failure was predicted by the theoretical models prior to the initiation of the rocking motion);

- At a same acceleration level and for a given wall length, the compressive length is higher in presence of acoustic insulation devices. Nevertheless, these devices lead to higher displacement and rotation at a same PGA level. This is additionally illustrated on Figure 50 and Figure 51 for the maximum acceleration level reached by the long wall (θ_{max} = 4.2 and 8.4 mrad respectively without and with rubber devices);
- The value of the compressive length decreases less than proportionally with the increase of the value of the acceleration of the seismic test.

It is can thus be concluded that rocking is always occurring and that the theoretical prediction of shear failure is over-conservative. Moreover, the presence of the rubber devices makes the behaviour shift from a one-sided rocking (with a contact length approaching zero) to the rocking of a wall resting in almost perfect contact with its elastic foundation.

Table 17 - Minimum value of the compressive length

Specimen	*Acceleration level*	*Compressive length*	
	[g]	*[%]*	*[mm]*
Long wall without rubber devices	0.0393	83.2	1747.2
	02387	41.11	863.31
	06878	0.025	0.525
Long wall with rubber devices	0.0426	100	2100
	0.1871	67.2	1411.2
	0.6392	0.05	1.05
Short wall without rubber devices	0.0413	77.01	554.472
	0.0635	58.7	422.64
	0.1784	14.37	103.464
Short wall with rubber devices	0.0417	100	720
	0.0607	100	720
	0.1709	32.13	231.34

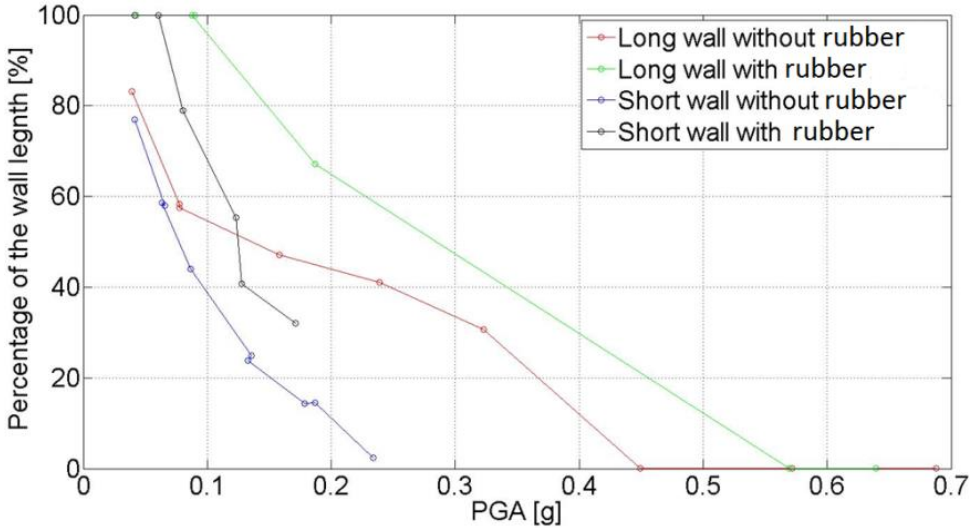

Figure 49 – Compressive length according to the PGA

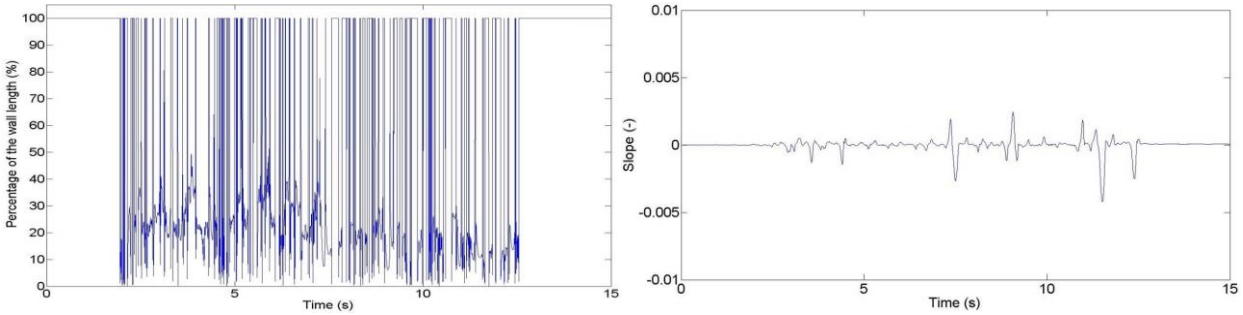

Figure 50 – Compressive length and slope of the long wall without rubber (acceleration level : 0.6878g)

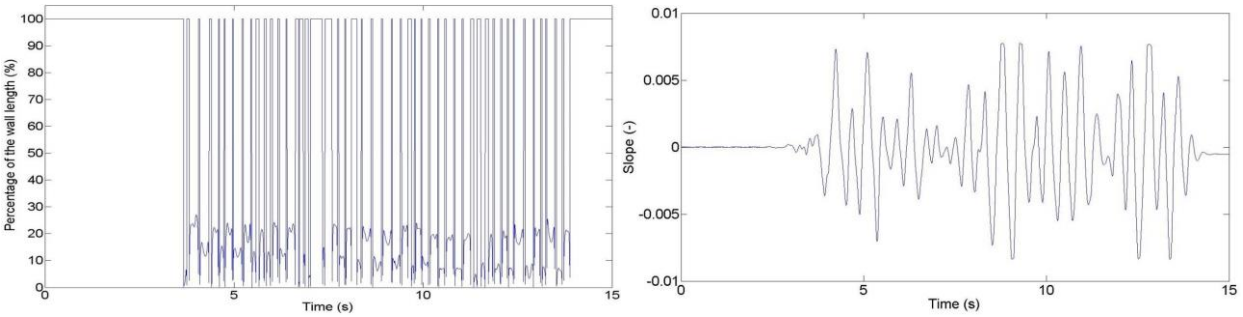

Figure 51 – Compressive length and slope of the long wall with rubber (acceleration level : 0.6392g)

As a final comparison, measured compressive lengths are compared, for the situations without rubber, to reference values obtained with the classical methodology used for the preliminary assessment, but with the measured mass accelerations. Two assumptions are considered regarding the distribution of vertical stresses on the compressive length, i.e. triangular or constant. Therefore, the compressive length is estimated, for the first assumption, by:

$$L_c = \begin{cases} 0 & if\ e \geq L/2 \\ 3.(\frac{L}{2} - e) & if\ e \leq L/2 \wedge e \geq L/6 \\ L & if\ e \leq L/6 \end{cases}$$

And, for the second assumption, by:

$$L_c = \begin{cases} 0 & if\ e \geq L/2 \\ 2.(\frac{L}{2} - e) & if\ e \leq L/2 \wedge e \geq 0 \\ L & if\ e = 0 \end{cases}$$

Where

$$V = Mass\ x\ measured\ \ mass\ acc \qquad M = V.H \qquad e = \frac{M}{N}$$

Table 18 – Compressive length calculated in preliminary assessment (linear stress distribution)

Tested wall	*PGA* [g]	V_{Sd} [N]	*Assessed compressive length* [mm]	[%]	*Measured compressive length* [mm]	[%]
Long wall	0.039	1950	2100.0	100.0	1747.2	83.2
	0.239	13330	1710.4	81.4	990.2	47.2
	0.688	30350	0.0	0.0	0.53	0.02
Short wall	0.041	2555	720.0	100.0	554.5	77.0
	0.064	3510	700.9	97.4	422.6	58.7
	0.178	9245	81.5	11.3	103.5	14.3

Table 19 – Compressive length calculated in preliminary assessment (constant stress distribution)

Tested wall	*PGA* [g]	V_{Sd} [N]	*Assessed compressive length* [mm]	[%]	*Measured compressive length* [mm]	[%]
Long wall	0.039	1950.0	1961.0	93.4	1747.2	83.2
	0.239	13330.0	1140.2	54.3	990.2	47.2
	0.688	30350.0	0.0	0.0	0.53	0.02
Short wall	0.041	2555	536.0	74.5	554.5	77.0
	0.064	3510	467.3	64.9	422.6	58.7
	0.178	9245	54.4	7.6	103.5	14.3

This comparison shows that the theoretical model provides a fairly good estimate of the compressive length, in particular for low to moderate acceleration levels under the assumption of a constant stress distribution, where the relative error between the measurements and the prediction remains below 15 %. It seems also possible to predict the initiation of the transition to pure rocking, for cases where the compressive length tends towards 0. All these issues will be complemented in further comparisons with a theoretical rocking model.

3.5.2 Horizontal displacements of the wall with respect to the support beam

Three sensors are located at the bottom of the wall to measure the horizontal relative displacement between the wall and the support beam. These will be used to better characterize the rocking motion according to the geometrical scheme given in Figure 52 quantified by the following formula.

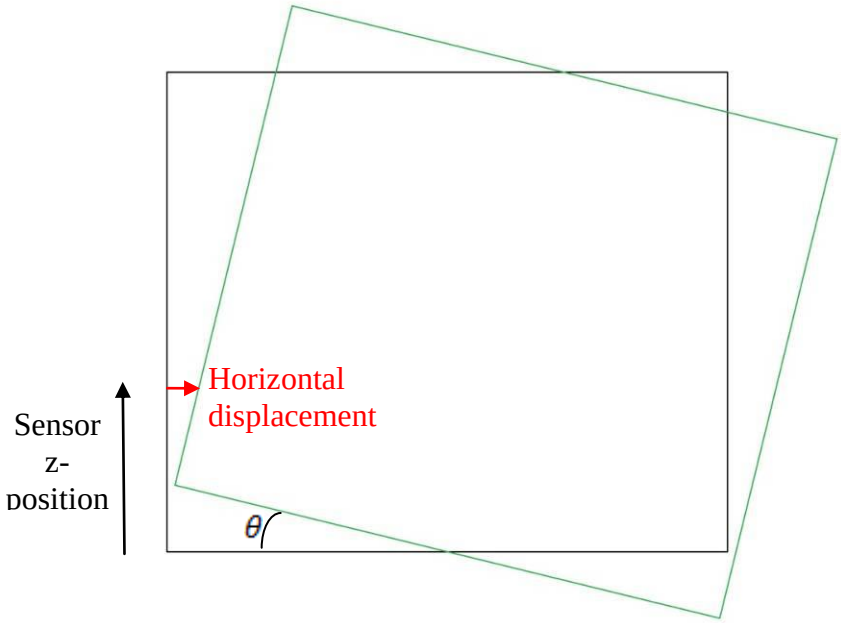

Figure 52 – Sketch of the horizontal displacement involved by the rocking

If θ is the angle characterizing the rocking,

$$\delta_{horizontal} = abs\left(\frac{WallLength}{2}.\tan\theta - z_{sensor}\right).\tan\theta + \frac{WallLength}{2}.(1-\cos\theta)$$

By comparing the calculated values of $\delta_{\text{horizontal}}$ and the horizontal displacement directly measured, it is possible to check if the wall is in pure rocking or if any additional horizontal components of displacement are entering into the game. The time evolution of the measured and calculated horizontal displacement $\delta_{\text{horizontal}}$ is given for the long walls in Figure 53 to Figure 56 and for short walls in Figure 57 to Figure 60. These figures show that both directly and indirectly measured displacements are in good agreement in terms of time evolution and that an additional component is observed in most cases in the amplitude. This is particularly significant for the long wall with rubber device, translating the higher shear deformability contribution of the rubber layer in this situation.

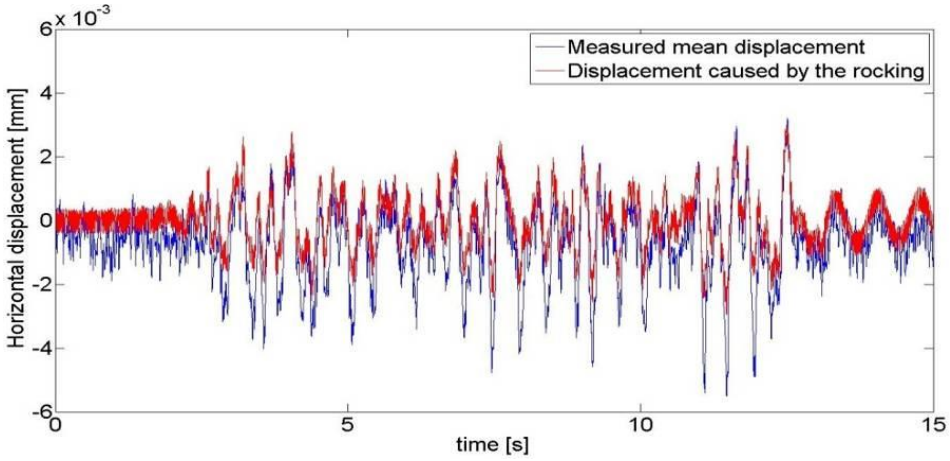

Figure 53 – Time evolution of the horizontal displacement (long wall without rubber – 0.0393g)

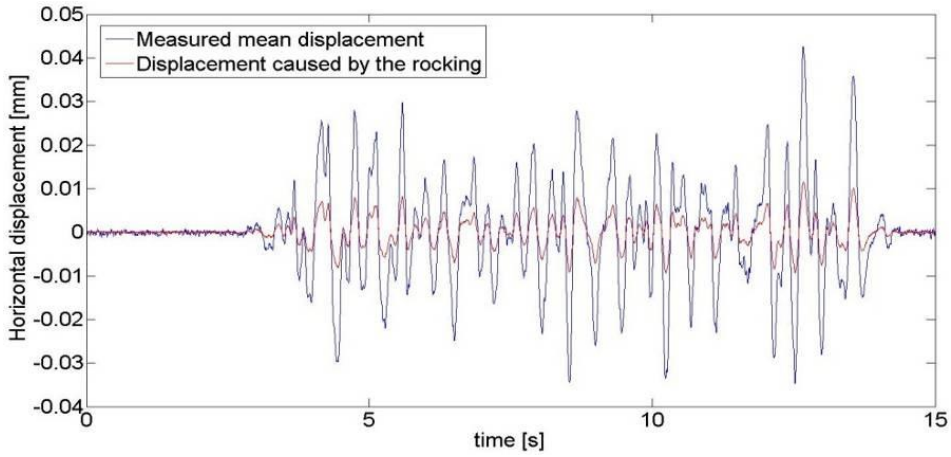

Figure 54– Time evolution of the horizontal displacement (long wall with rubber – 0.0426g)

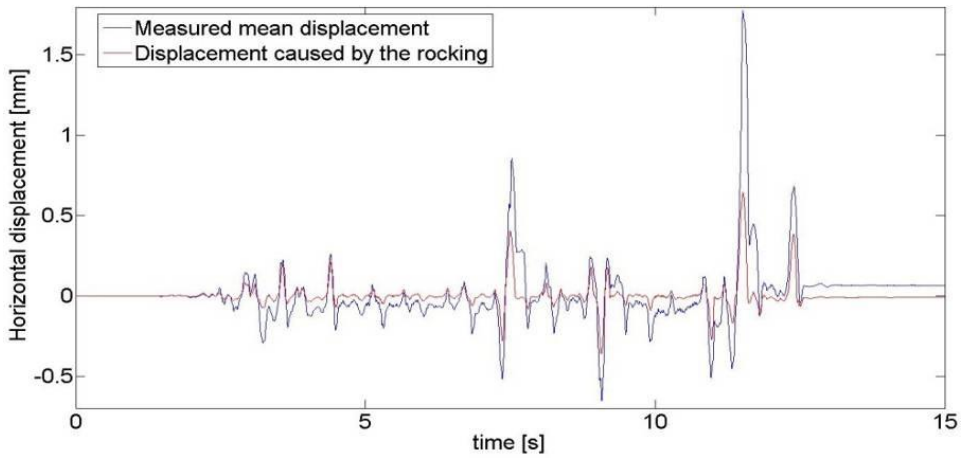

Figure 55– Time evolution of the horizontal displacement (long wall without rubber – 0.6878g)

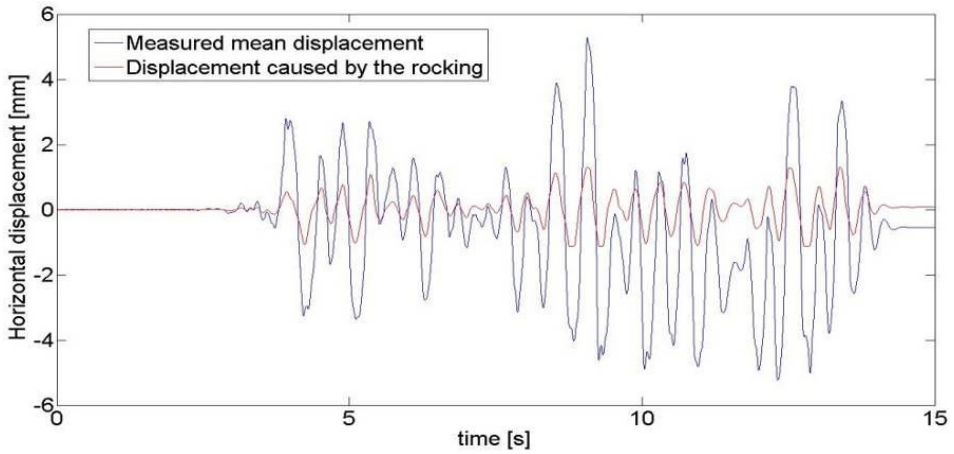

Figure 56– Time evolution of the horizontal displacement (long wall with rubber – 0.6392g)

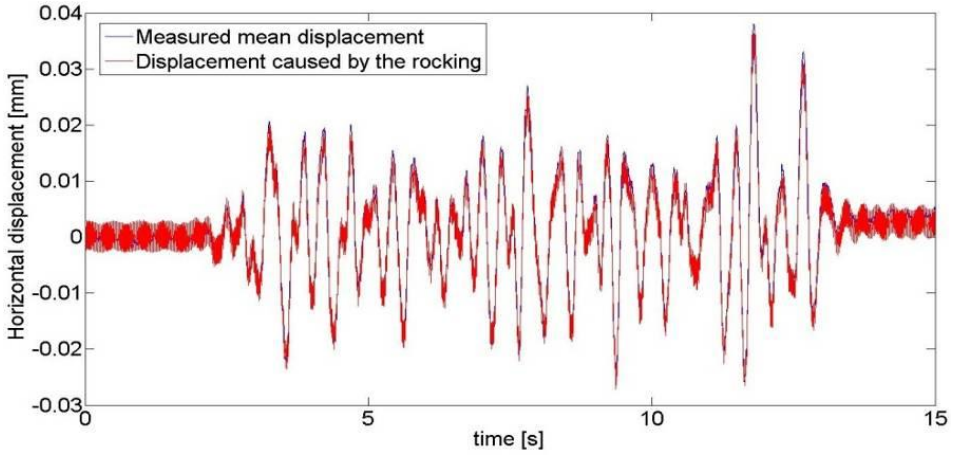

Figure 57 – Time evolution of the horizontal displacement (short wall without rubber – 0.0413g)

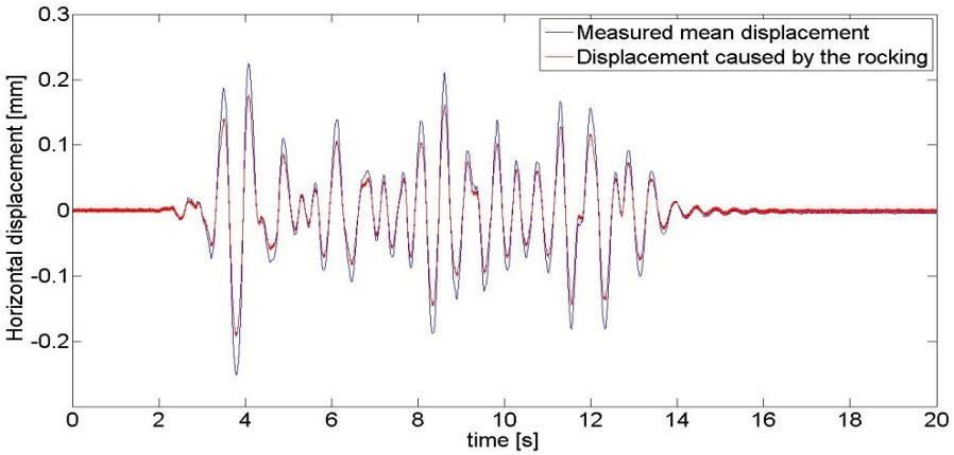

Figure 58 – Time evolution of the horizontal displacement (short wall with rubber – 0.0417g)

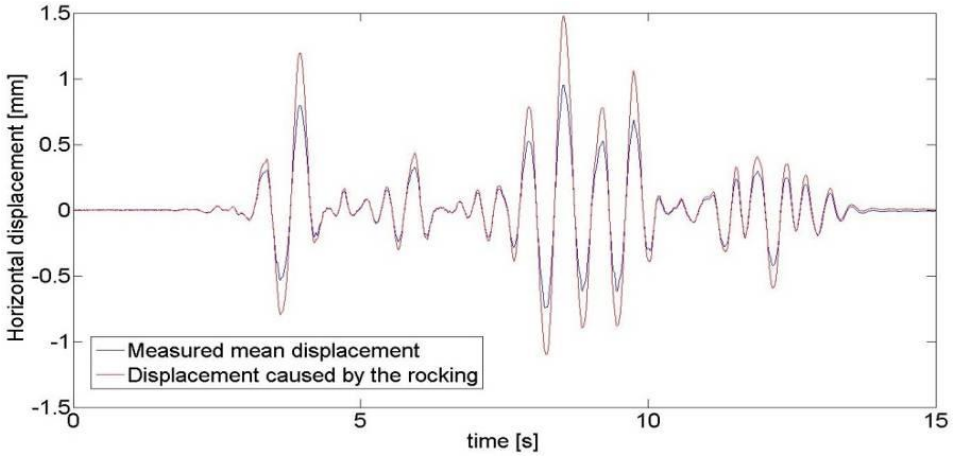

Figure 59 – Time evolution of the horizontal displacement (short wall without rubber – 0.1784g)

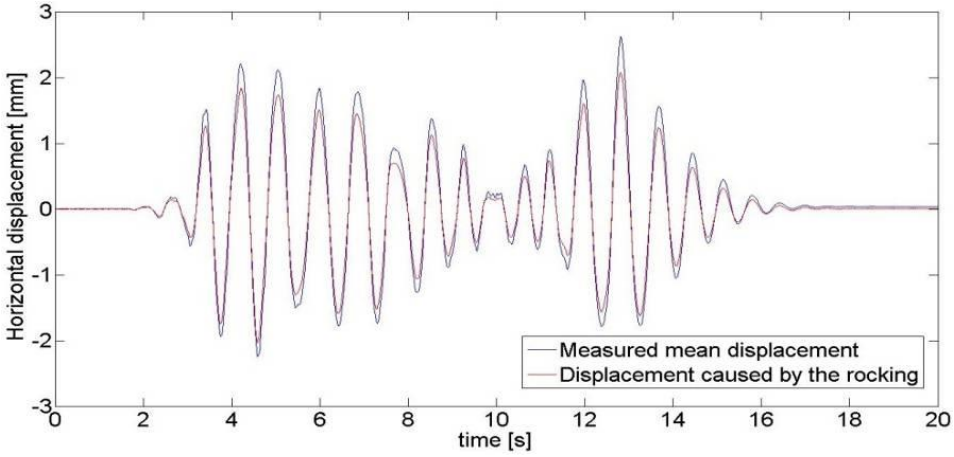

Figure 60 – Time evolution of the horizontal displacement (short wall with rubber – 0.1709g)

3.5.3 Rocking of the mass

A rocking of the additional mass was visually identified for the case of the long wall without rubber device, for all tests at moderate and high intensity. This induces an impact on wall each time the mass comes into perfect contact with the wall, and hence some out-of-plane effects due to rather high slenderness of the wall. This is also evidenced by the comparison of the out-of-plane acceleration for the long wall at moderate intensity, as shown by Figure 61 and Figure 62 for the cases with and without rubber respectively. The out-of-plane acceleration level reached in the first case is about 0.1 g, while it remains limited to 0.02 g in the second situation where the presence if the rubber layer between the wall and the mass is limiting the rocking effect as well as the intensity of the impact.

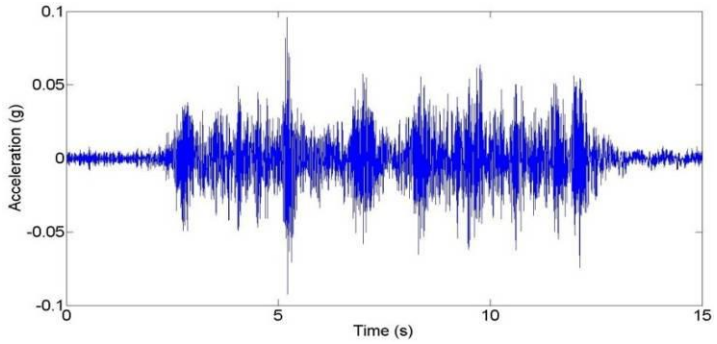

Figure 61 – Time evolution of the Y-direction acceleration (Long wall without rubber – 0.1583g)

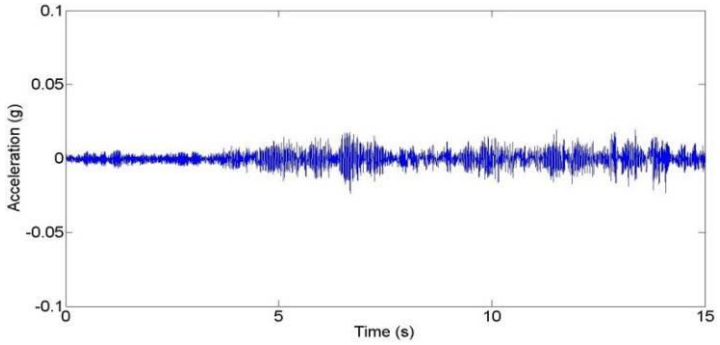

Figure 62 – Time evolution of the Y-direction acceleration (Long wall with rubber – 0.1871g)

A confirmation is obtained from the measurements provided by the sensors 9 and 11 (see Figure 63). They are located on the wall top and measure the relative vertical displacement between the wall and the mass. A contact length between the mass and the wall is derived with the same procedure as for the contact length at the bottom of the wall presented in the previous section.

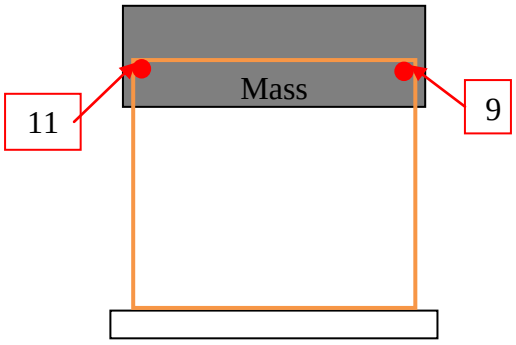

Figure 63 - Position of the sensors 9 and 11

The graph on the left side of Figure 66 clearly evidences the rocking of the mass in the situation without acoustic insulation devices, whereas the graph on the right side only shows a very

limited rocking. In the case of the long wall without rubber devices, the impact is significant because the one-side uplift is important and nothing can absorb the uplift energy when this latter is released. It can thus be concluded that the acoustic insulation devices have a positive effect since they limit both the rocking and the risk of impact, and hence the risk of out-of-plane buckling of the wall.

This phenomenon is not observed for the short wall.

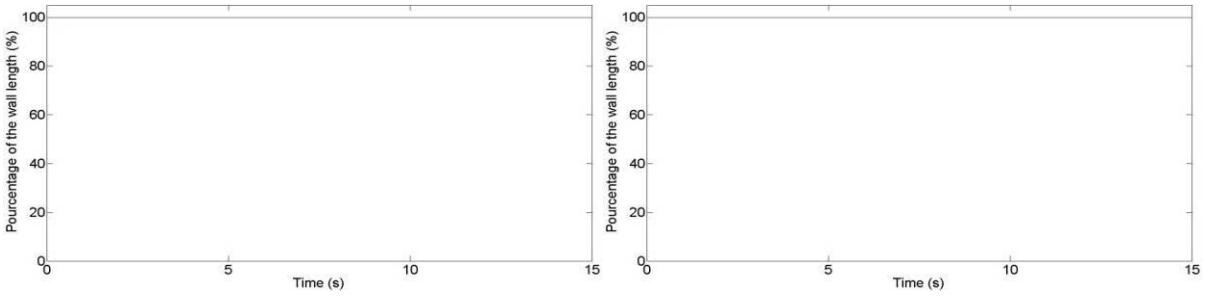

Figure 64 – Compressive length of the mass for the long walls without (left – 0.393g) and with (right – 0.0426g) rubber devices

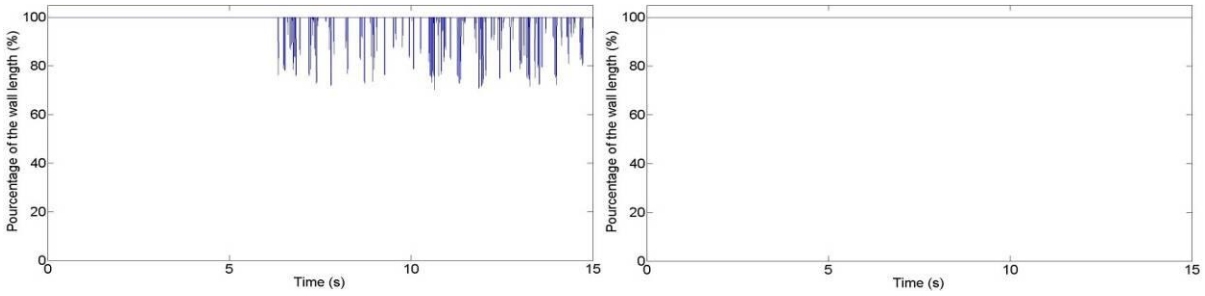

Figure 65– Compressive length of the mass for the long walls without (left – 0.2387g) and with (right – 0.1871g) rubber devices

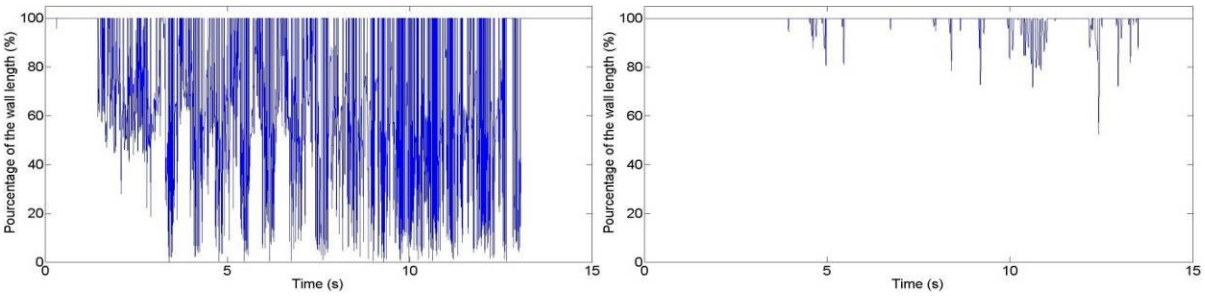

Figure 66 – Compressive length of the mass for the long walls without (left – 0.6878g) and with (right – 0.6392g) rubber devices

3.5.4 Horizontal shear

The objective of the present section is to evaluate the actual shear state of the wall and of the rubber elements if relevant, since the shear effect is expected to be critical point, in particular for the long wall, according to the outcomes of the preliminary theoretical assessment.

3.5.4.1. Horizontal shear in the wall

The shear deformation of the wall is obtained on the base of the "Celesco" devices measuring the elongation/shortening of the diagonal of the walls. Measurements are taken on both faces of the wall and in crossing direction. As a consequence, a pure shear will be translated by identical measurements in both direction, while differential displacements would be the sign of a bending component in the deformation of the system.

From the mean diagonal displacement, it's possible to deduce the horizontal one. Figure 67 explains the geometrical method used to do it. The horizontal displacement is obtained by projecting the diagonal displacement δ_d, measured by a wire between two points, A and B. The average of the displacement measured on both faces is considered for further elaboration.

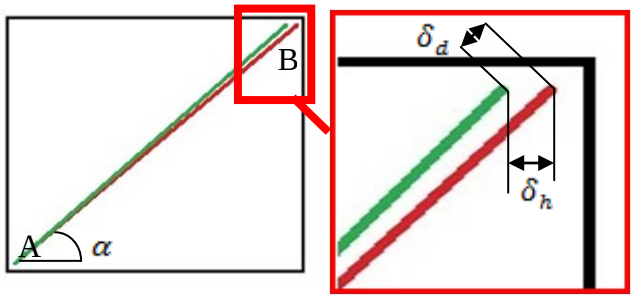

Figure 67 – View of diagonal and horizontal displacements

Assuming the vertical displacement and the variation of the angle α are not significant, the next relation is valid : $\delta_h = \delta_d . \cos\alpha$

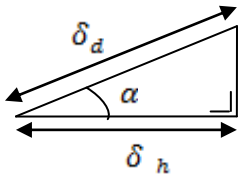

Figure 68 – View of diagonal and horizontal displacements

Once the horizontal displacement is known, the drift can be calculated by referring the height of the wall then the horizontal shear follows.

$$\gamma = \delta_h / height_{wall}$$

$$V = \gamma.G.A'$$

Where - G $[N/mm^2]$ is the shear modulus of the masonry, taken to the 40% of the Young Modulus (Eurocode6, 2004).

- A' $[mm^2]$ is the shear area, taken equal to 5/6 of the area.

3.5.4.1.1. Horizontal shear in the long walls

Figure 69 to Figure 72 show the time evolution of the measured horizontal shear in the long walls during the seismic tests (S1) and (S9) (very low and very high acceleration level) and compare it with a theoretical reference defined as the product of the measured acceleration of the top load by its mass. A same observation can be made for all these figures: some shear is observed (red curves), but the values are significantly below the value obtained on the base of the inertial forces (blue curves).

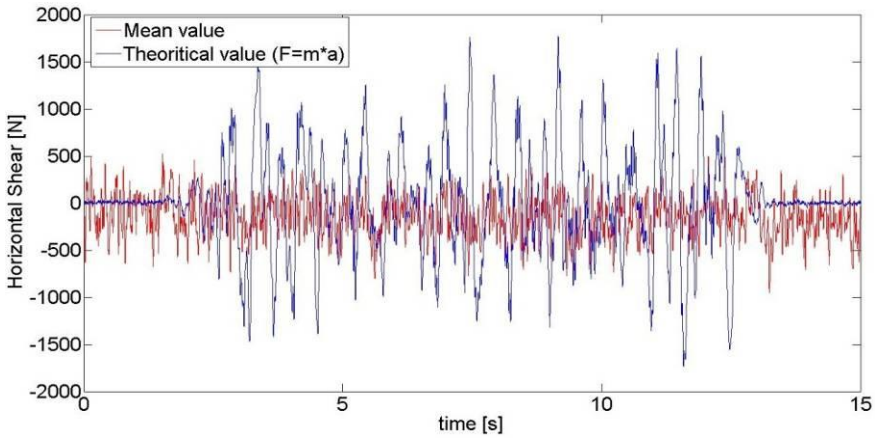

Figure 69 – Time evolution of the horizontal shear (long wall without rubber devices – 0.0393g)

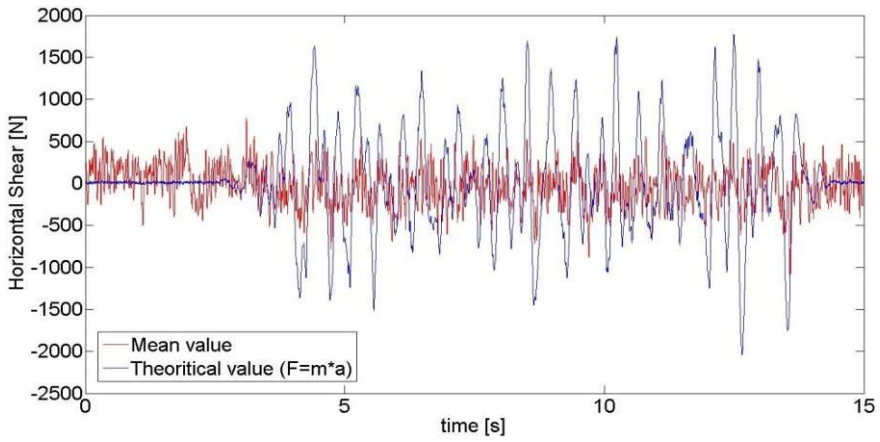

Figure 70 – Time evolution of the horizontal shear (long wall with rubber devices – 0.0426g)

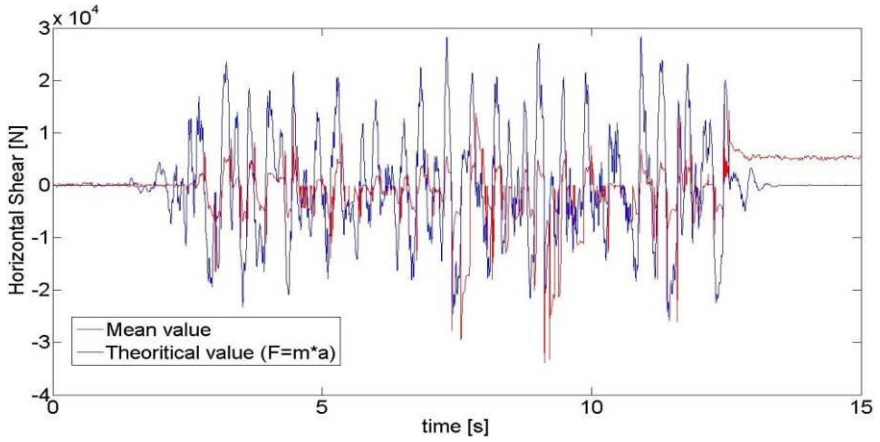

Figure 71 – Time evolution of the horizontal shear (long wall without rubber devices – 0.6878g)

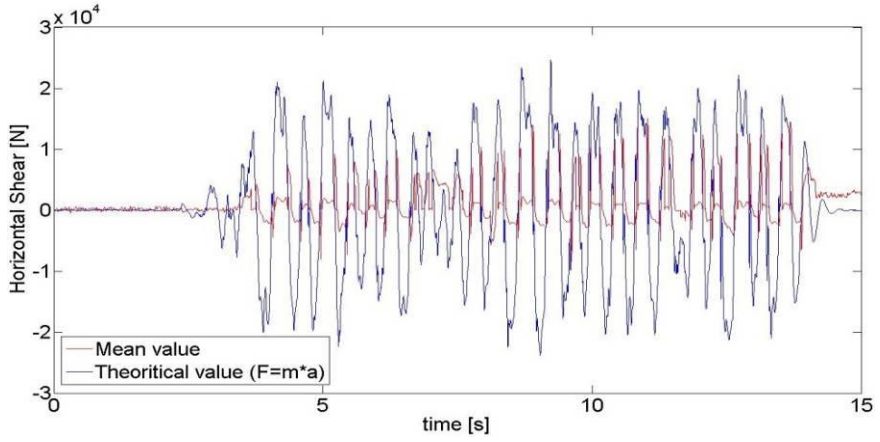

Figure 72 – Time evolution of the horizontal shear (long wall with rubber devices – 0.6392g)

3.5.4.1.2. Horizontal shear in the short walls

Figure 73 to Figure 76 show the same results for the short walls during the seismic test (S1) and (S7). Similar conclusions can be drawn and are even more pronounced than for the long walls.

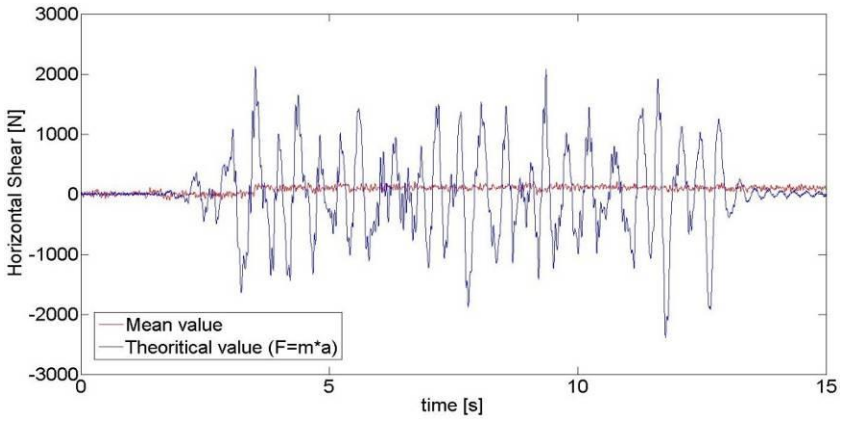

Figure 73 – Time evolution of the horizontal shear (short wall without rubber devices – 0.0413g)

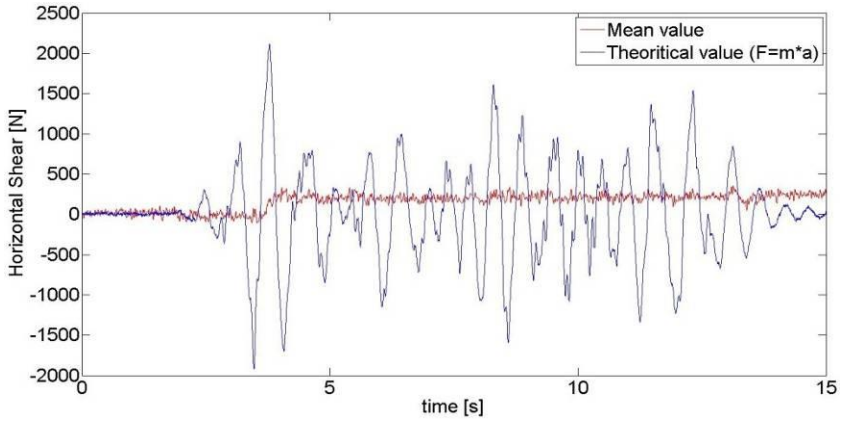

Figure 74 – Time evolution of the horizontal shear (short wall with rubber devices – 0.0417g)

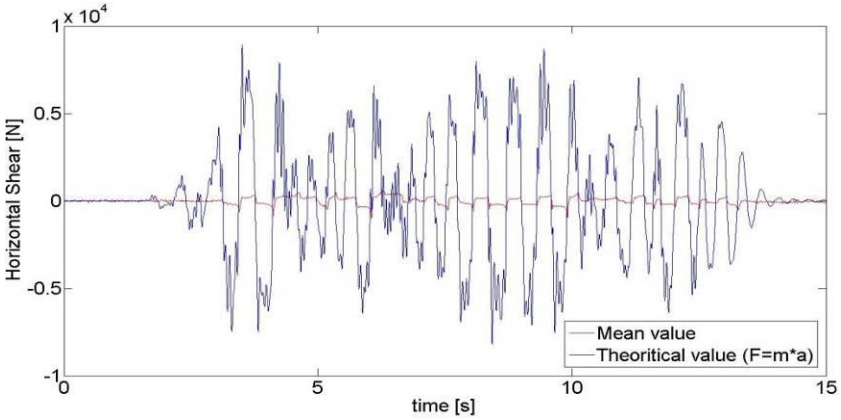

Figure 75 – Time evolution of the horizontal shear (short wall without rubber devices – 0.1784g)

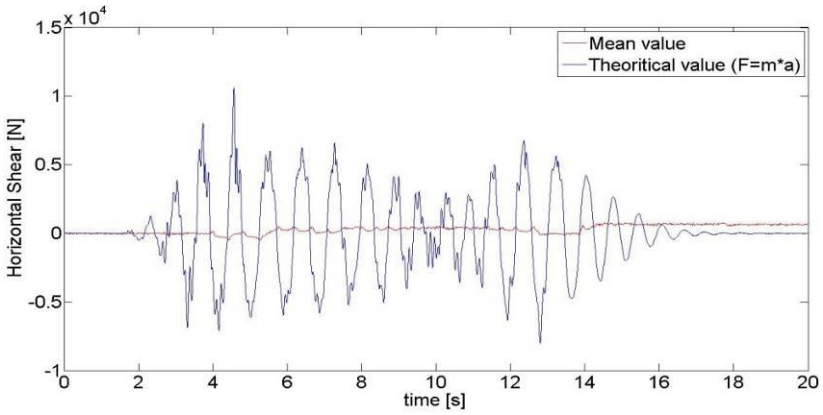

Figure 76 – Time evolution of the horizontal shear (short wall with rubber devices – 0.1709g)

Observations of Figure 69 to Figure 76 show that the load transfer mechanism commonly used to verify the capacity to transfer inertial forces from the top to the ground is certainly not appropriate in the present case. Indeed a significant rocking occurs (in particular for the short wall) and the shear appears to be essentially transferred by the development of a compression diagonal strut (see Figure 77) that is on one hand stiffer and on the other hand more resistant than what is normally considered for the shear verification of masonry (friction shear limited by an upper bound depending on the resistance of units. This aspect will be further investigated in additional processing of the test results.

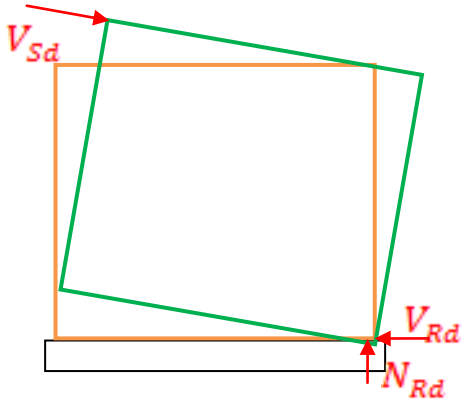

Figure 77 –Illustration of the strut and tie model

3.5.4.2. Horizontal shear in the acoustic insulation devices

Horizontal shear in the rubber layer is directly derived from the measurement of the horizontal relative displacement between respectively the bottom of the wall and the support beam and the

top of the wall and the additional mass, using the shear modulus provided by the producer of the devices.

3.5.4.2.1. Horizontal shear in the bottom rubber layer

Shear in rubber at the bottom of the wall are given in:

- Figure 78, Figure 79 and Figure 80 for the long wall ;
- Figure 81, Figure 82 and Figure 83 for the short wall.

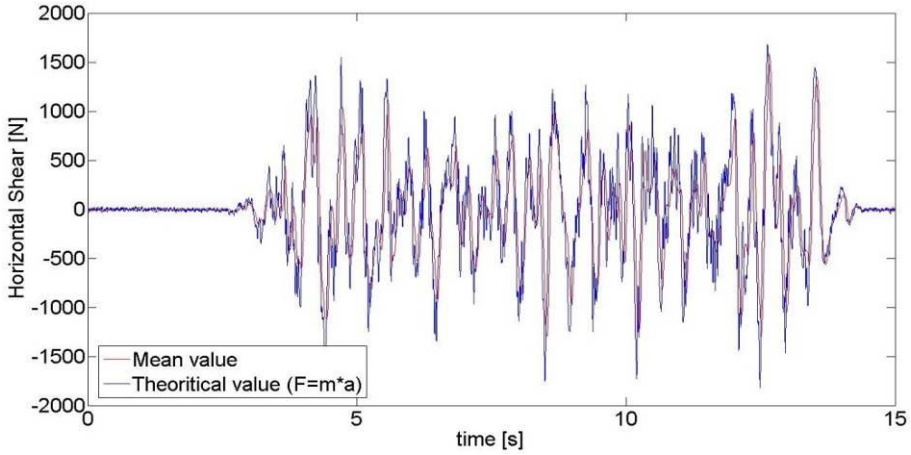

Figure 78 – Time evolution of the horizontal shear (bottom of the long wall – 0.0426g)

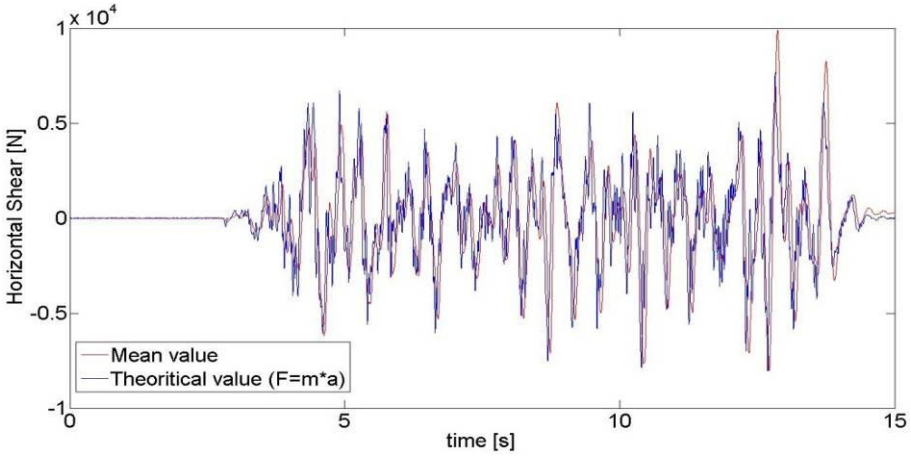

Figure 79 – Time evolution of the horizontal shear (bottom of the long wall – 0.2387g)

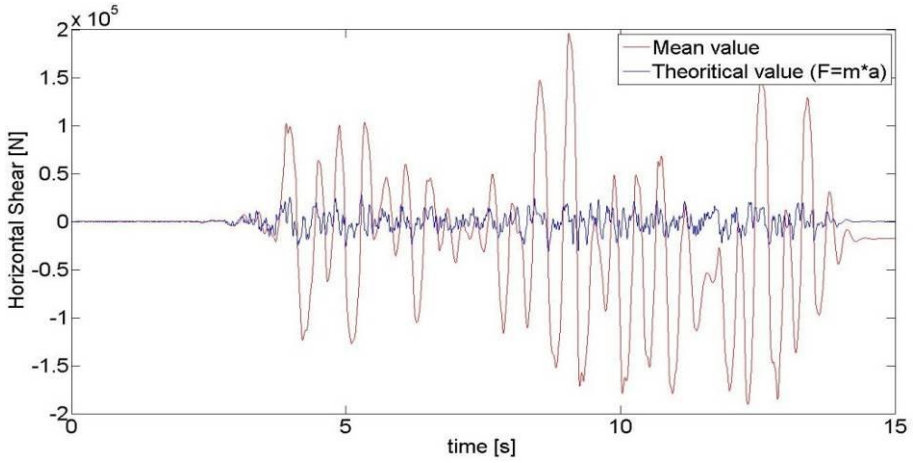

Figure 80 – Time evolution of the horizontal shear (bottom of the long wall – 0.6878g)

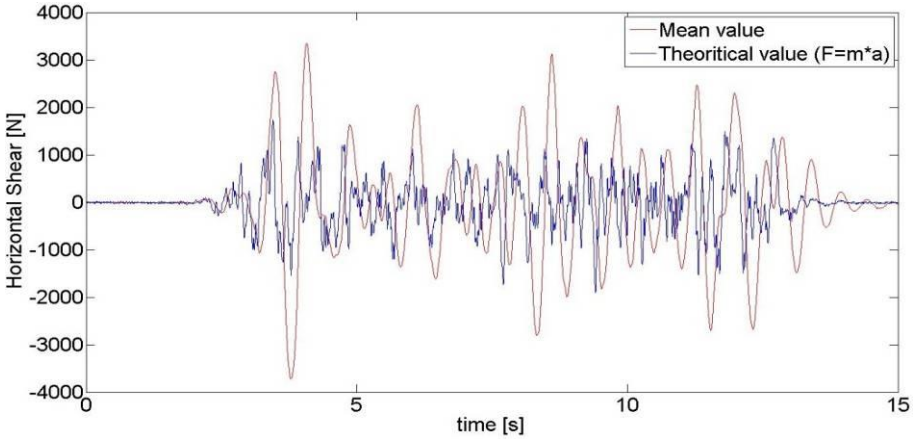

Figure 81 – Time evolution of the horizontal shear (bottom of the short wall – 0.0417g)

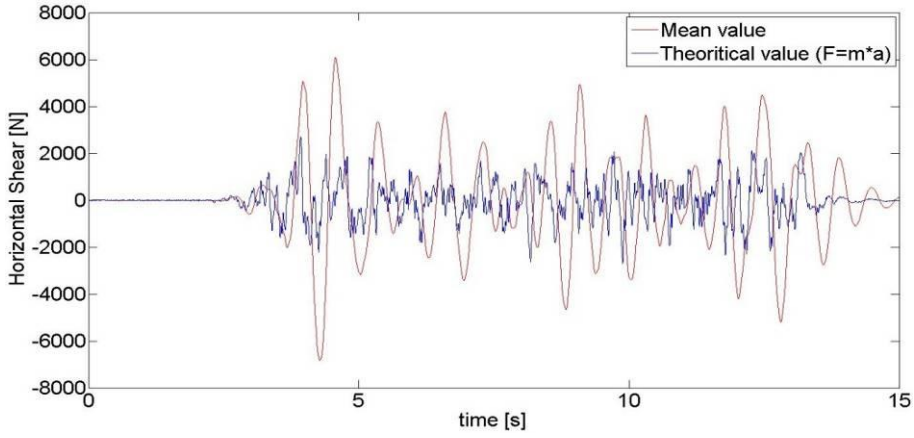

Figure 82 – Time evolution of the horizontal shear (bottom of the short wall – 0.0607g)

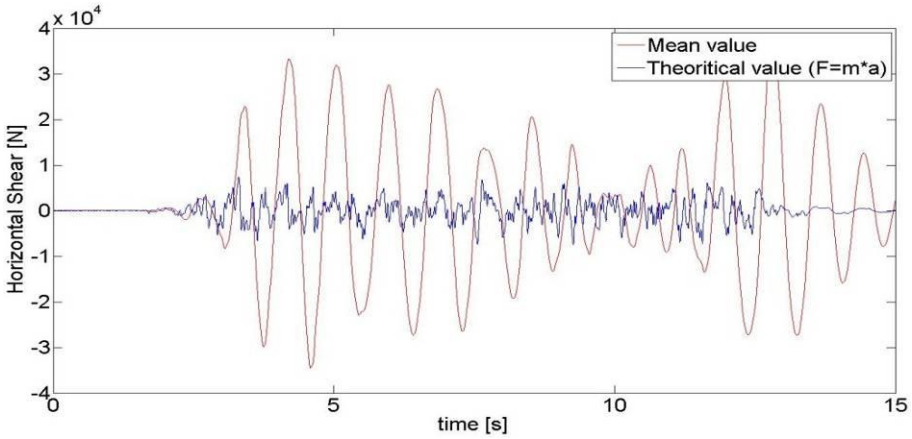

Figure 83 – Time evolution of the horizontal shear (bottom of the short wall – 0.1709g)

For the case of the long wall, results show that the full shear is transferred according to the expected mechanisms since the value of the horizontal shear is equal to the inertial forces except for high acceleration level where the measured shear in rubber exceeds significantly the expected level. This exceeding situation is also observed for the short walls and is more and more pronounced when the rocking increases. The discrepancy is tentatively explained by the fact that, when rocking occurs, the stress and strain state of the rubber is becoming rather complicated and the easy assessment method used to derive the shear from the displacements is certainly too simplified. Advanced model calibration should be used to better understand this strain distribution.

3.5.4.2.2. Horizontal shear in the top rubber layer

Shear in rubber at the bottom of the wall are given in:

- Figure 84, Figure 85 and Figure 86 for the long wall ;
- Figure 87, Figure 88 and Figure 89 for the short wall.

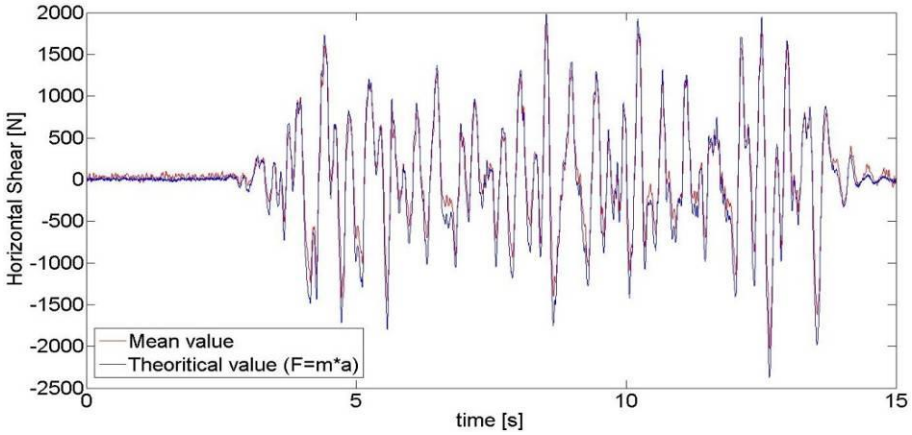

Figure 84 – Time evolution of the horizontal shear (top of the long wall – 0.0426g)

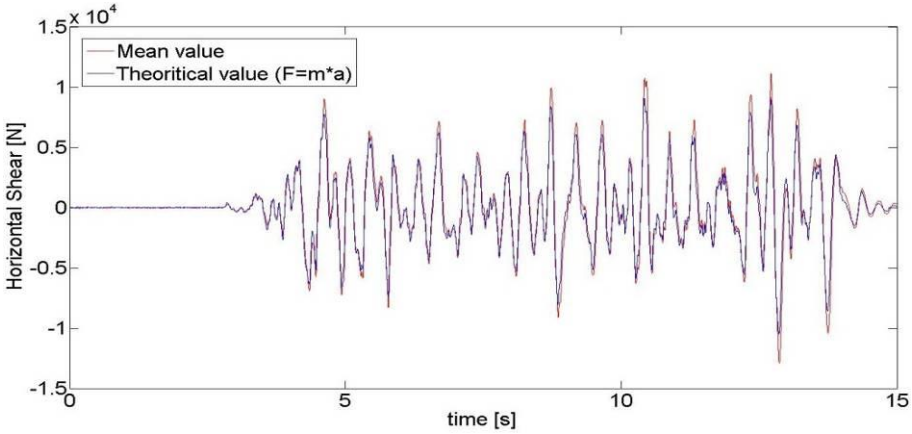

Figure 85 – Time evolution of the horizontal shear (top of the long wall – 0.1871g)

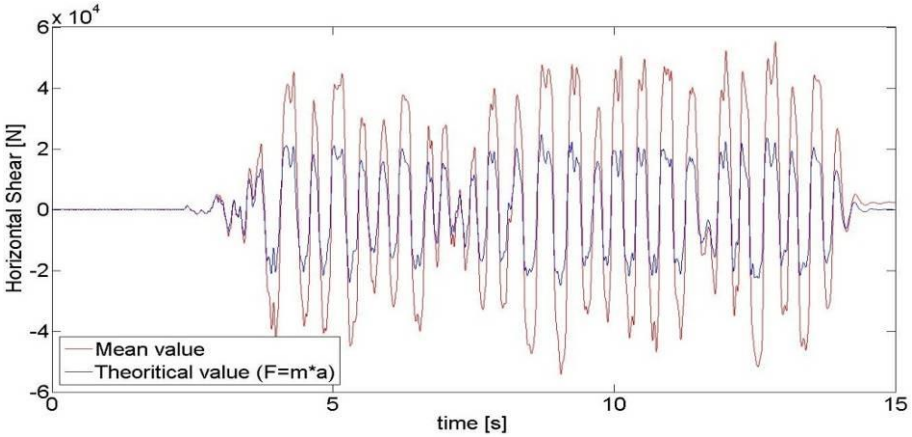

Figure 86 – Time evolution of the horizontal shear (top of the long wall – 0.6392g)

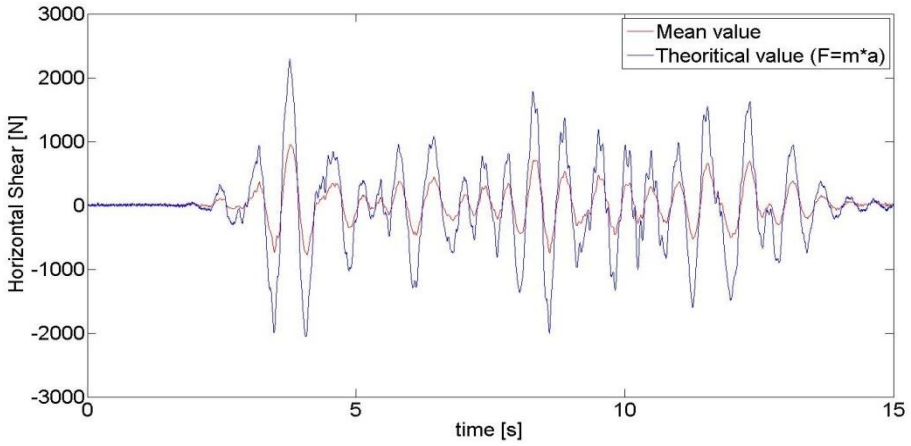

Figure 87 – Time evolution of the horizontal shear (top of the short wall – 0.0417g)

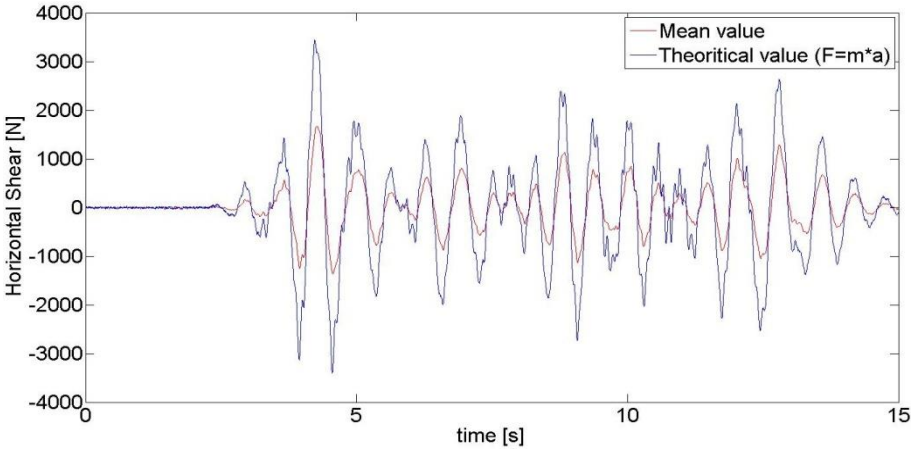

Figure 88 – Time evolution of the horizontal shear (top of the short wall – 0.0607g)

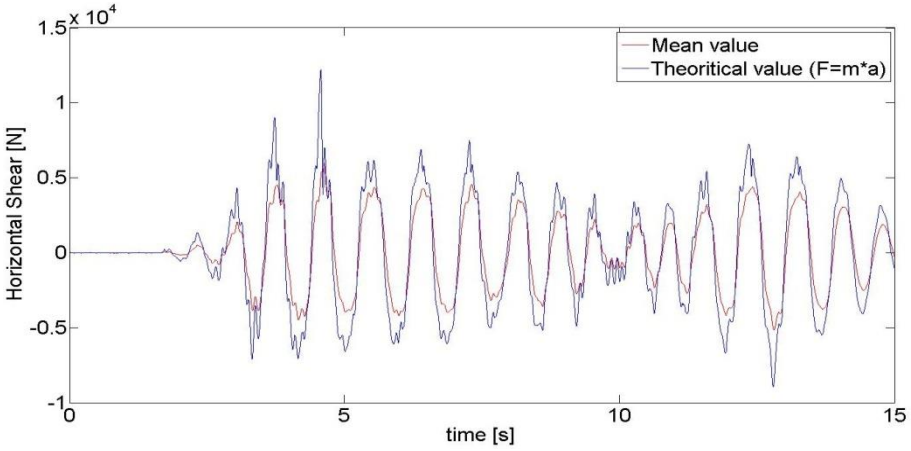

Figure 89 – Time evolution of the horizontal shear (top of the short wall – 0.1709g)

Consistency of results between measured shear and inertial forces is much better for what regards the behaviour of the top rubber layer. This may be explained by the more limited rocking motion of the top mass, leading to a more homogeneous distribution of the compression stress in the top layer.

For the case of the short wall, the estimated shear is smaller than expected. This is tentatively justified by the dependency of the shear modulus to the compression state. The average compression in the rubber is higher for the short wall than for the long one and the resulting shear modulus should normally be increased, yielding higher shear stress for a same deformation. In the present case, a factor of 1.5 applied on the shear modulus seems to allow reaching a good agreement, but this value should be confirmed by additional characterization of the acoustic rubber mats.

4 Second test series – Design of specimens and preliminary assessment

4.1 GEOMETRY OF THE SPECIMENS

Overall geometry of the specimens have been defined based on a set of considerations like dimensions and payload of the shake table, standard size of a door and additional constructive requirements from Eurocodes 6 and 8. It follows:

For both shear walls (walls in the plan of the frame) and flanges (walls perpendicular to the frame): Length = 0.74m / Width = 0.138m / Height =1.8m

For the L-shaped piers, the connection on the shear walls and the flange is realized in a standard way on one side (alternation of units) while both walls are simply fabricated separately then connected by a glued joint all over the height for the other pier. Detailed geometry of the specimens is given from Figure 90 up to Figure 93. The lintel is a classical full RC beam fabricated in purpose for these tests and connected with the walls by a standard mortar layer. Characteristics of the masonry can be found in section 2.3.1.

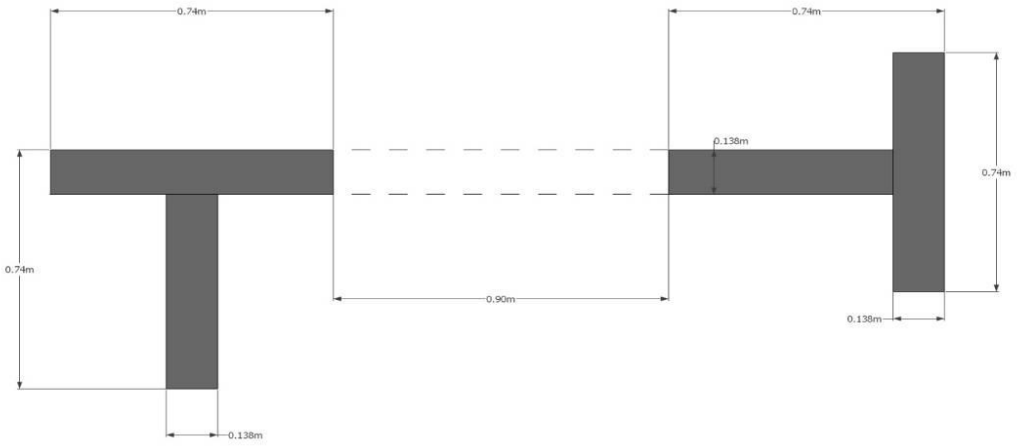

Figure 90 – Geometry of the first specimen (plan view)

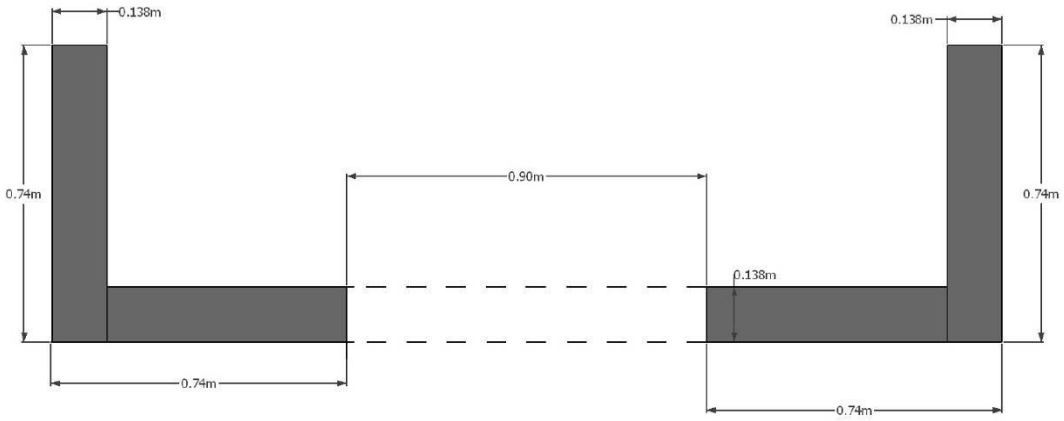

Figure 91– Geometry of the second specimen (plan view)

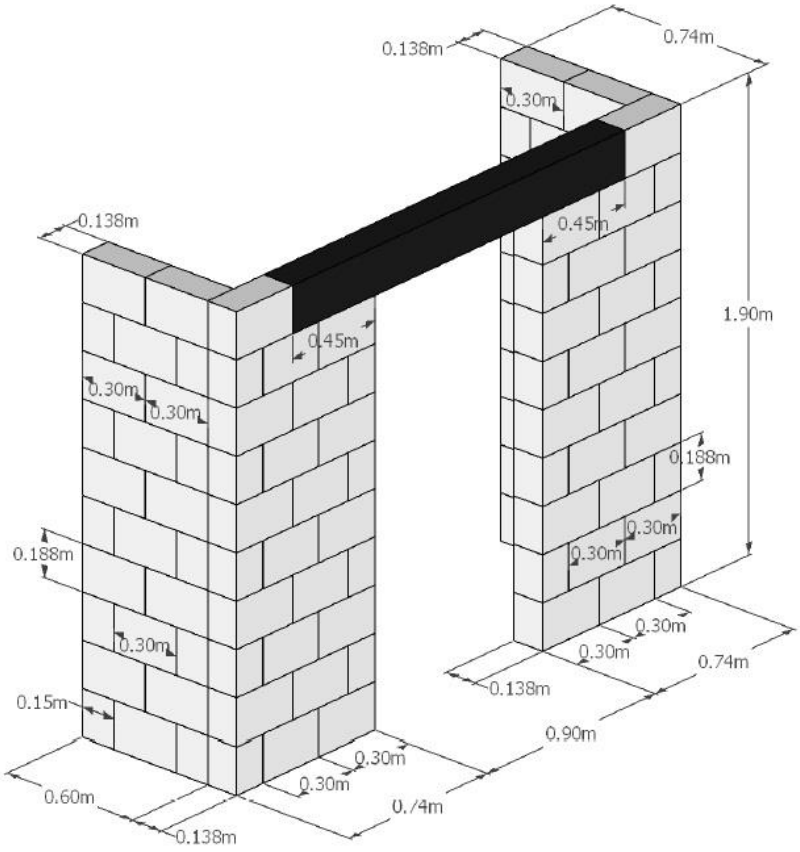

Figure 92 – Geometry of the first specimen (3D view)

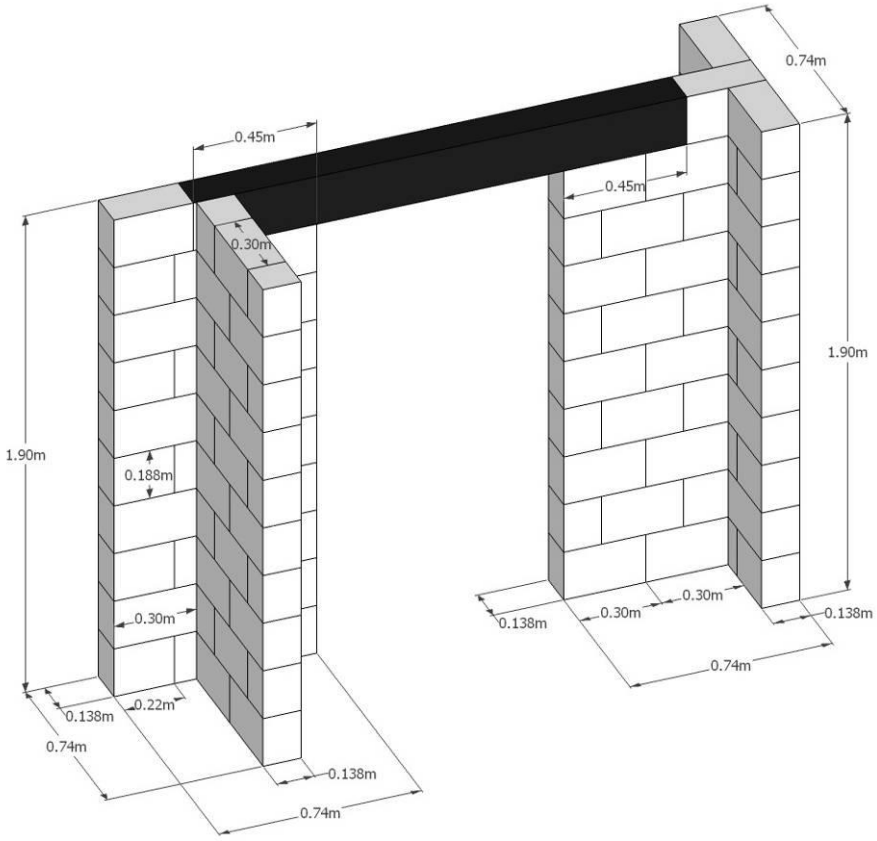

Figure 93 – Geometry of the second specimen (3D view)

4.2 GRAVITY LOADING

One of the objective of this testing campaign is to allow a comparison of flanged walls (L and T) when all elements are under compression or when only part of them are acting as gravity load-bearing elements. It is therefore necessary to implement a loading system flexible enough for these different options. It is therefore chosen to load the system with a concrete slabs on which the additional masses will be located and to develop some interface elements between the top of the wall and the slab that can be easily removed. These interface steel elements are shown at Figure 94.

A U-shaped piece is chosen to avoid the risk of out-of-wall sliding. A piece of expanded metal sheet is also welded on the inside of the U and steel plates are welded perpendicular to the longitudinal axis of the U-shaped piece. The expanded metal panel increases the friction between the device and the top of the wall, while the steel plates will connect it to the RC slab through appropriately designed slots. Additional steel masses are then placed on the RC slab for total of 5

tons. The resulting compression level of the walls is given in Table 20. The values of compression level fall within the usual range of compressive stress of masonry walls. Note that, for safety reasons, the additional masses are hung from the crane throughout the duration of the tests.

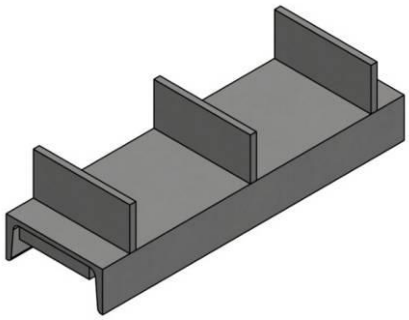

Figure 94 – Steel part

Table 20 - Compression level of different loading cases

	Loaded wall	*Compression level*
Frame with T-shaped walls	Shear wall Flange Both	0.245MPa 0.245MPa 0.135 MPa
Frame with L-shaped walls	Shear wall Flange Both	0.245MPa 0.245MPa 0.135 MPa

4.3 PRELIMINARY ASSESSMENT OF THE SPECIMENS

A preliminary assessment of the specimens is carried out to estimate the acceleration likely to lead to the collapse of the structure.

4.3.1 Geometrical characteristics

The masonry frame is composed of two piers, each of them comprising two perpendicular walls coupled by a lintel. Geometrical properties of these piers are derived hereunder. The considered reference system is given in Figure 95 and Figure 96, with the origin of axes marked by the green dot.

Table 21 and

Table 22 detail the final geometrical characteristics in X and Y directions. The effective length of the wall perpendicular to the stress direction and contributing to the second moment of area of the pier is calculated according to the Eurocode 6 recommendations. It is also assumed that the total shear area is limited to the shear area of the wall oriented in the same direction as the seismic action.

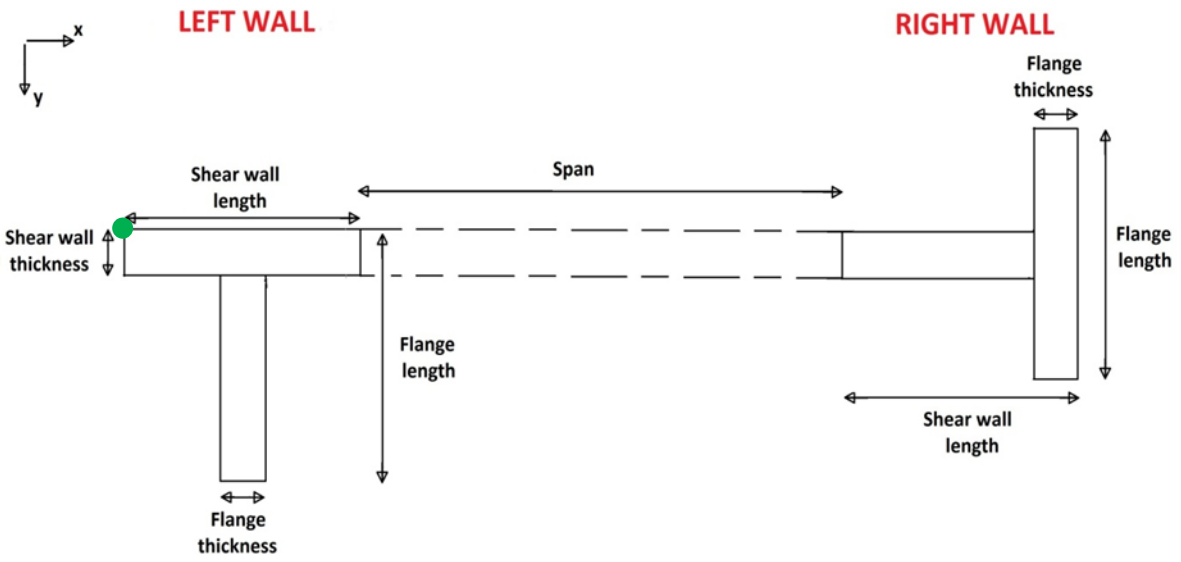

Figure 95 – Sketch of the specimen with T-shaped walls

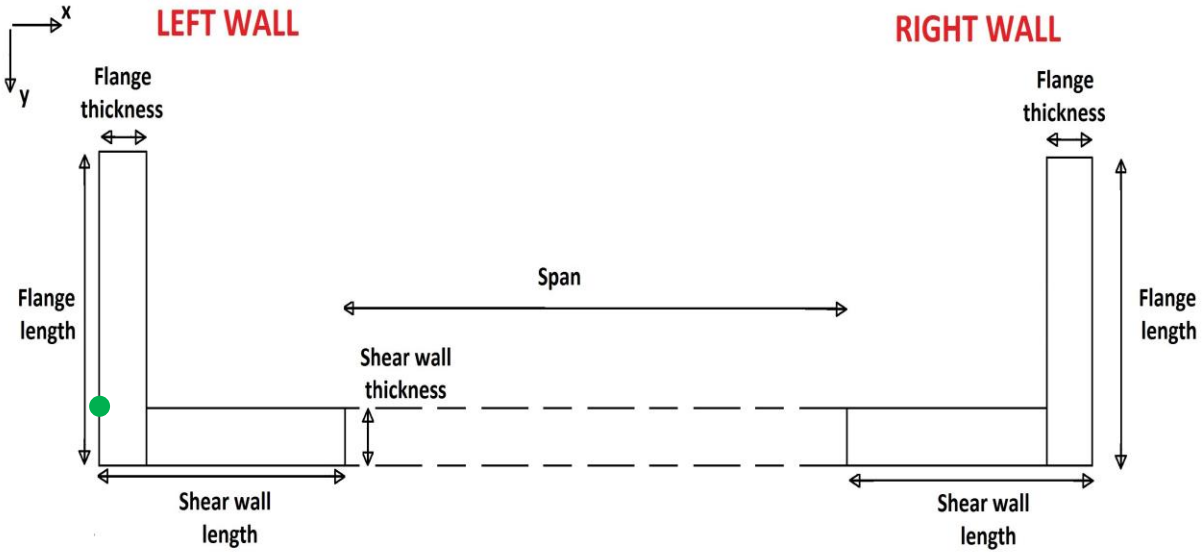

Figure 96– Sketch of the specimen with L-shaped walls

Table 21 – Mechanical characteristics of the specimen – X direction

Specimen	*With T-shaped walls*		*With L-shaped walls*	
Wall	*Left*	*Right*	*Left*	*Right*
Effective length of the flange	0.498 m	0.740 m	0.498 m	0.498 m
Gravity centre of				
shear wall :	0.370 m	1.941 m	0.370 m	1.941 m
flange :	0.370 m	2.311 m	0.069 m	2.311 m
all :	0.370 m	2.145 m	0.272 m	2.109 m
Area of				
shear wall :	0.1021 m²	0.0831 m²	0.1021 m²	0.0497 m²
flange :	0.0497 m²	0.1021 m²	0.0497 m²	0.1021 m²
all :	0.1518 m²	0.1852 m²	0.1518 m²	0.1518 m²
Inertia I	0.004739 m^4	0.008943 m^4	0.007767 m^4	0.007767 m^4
Shear area A_{eff}	0.1021 m²	0.1021 m²	0.1021 m²	0.1021 m²

Table 22 – Mechanical characteristics of the specimen – Y direction

Specimen	*With T-shaped walls*		*With L-shaped walls*	
Wall	*Left*	*Right*	*Left*	*Right*
Effective length of the shear wall	0.740 m	0.498 m	0.498 m	0.498 m
Gravity centre of				
shear wall :	0.069 m	0.069 m	0.069 m	0.069 m
flange :	0.439 m	0.069 m	-0.301 m	0.050 m
all :	0.235 m	0.069 m	-0.134 m	-0.134 m
Area of				
shear wall :	0.1021 m²	0.0497 m²	0.0687 m²	0.0497 m²
flange :	0.0831 m²	0.1021 m²	0.0831 m²	0.1021 m²
all :	0.1852 m²	0.1518 m²	0.1518 m²	0.1518 m²
Inertia I	0.008943 m^4	0.004739 m^4	0.007767 m^4	0.007767 m^4
Shear area A_{eff}	0.1021 m²	0.1021 m²	0.1021 m²	0.1021 m²

Wall stiffness is then derived, based on the following assumptions:

- To take into account the effect of cracking under seismic action, elastic modulus is taken equal to half of its value under normal conditions (i.e. a value of $E = 500\ f_k$ is used);
- The shear modulus G is taken equal to 0.4 E according to Eurocode 6;
- Three different options are considered regarding the support conditions of the top of the pier.

Consequently, the pier stiffness is given by:

$$K = \frac{1}{\frac{H^3}{\alpha EI} + \frac{H}{GA'}}$$

Where α is a parameter depending on the support conditions;

H is the height of the level.

The resulting values of stiffness are given in Table 23.

Table 23 – Stiffness of the walls [N/m]

Specimen	*With T-shaped walls*		*With L-shaped walls*	
Wall	*Left*	*Right*	*Left*	*Right*
X-direction				
Built-in $\alpha = 12$	13,270,856.0	19,771,365.6	18,246,458.1	18,246,458.1
Simply supported $\alpha = 6$	7,808,878.0	12,737,298.6	11,499,076.6	11,499,076.6
Free $\alpha = 3$	4,283,170.1	442,006.9	6,610,250.3	6,610,250.3
Y-direction				
Built-in $\alpha = 12$	19,771,365.6	13,270,856.0	18,246,458.1	18,246,458.1
Simply supported $\alpha = 6$	12,737,298.6	7,808,878.0	11,499,076.6	11,499,076.6
Free $\alpha = 3$	7,442,006.9	4,283,170.1	6,610,250.3	6,610,250.3

A last interesting characteristic of the piers is the position of their rigidity (or shear) centre, necessary to estimate the torsional effects. The torsional stress is indeed directly proportional to the distance between the gravity centre and the rigidity centre. The shear centre of a L-shaped or T-shaped section being located as shown in Figure 97, the resulting position of the rigidity centre are given in Table 24 with respect to the chosen reference axes,.

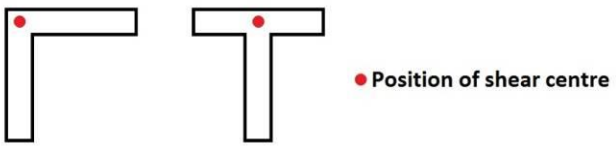

Figure 97 – Position of shear centre

Table 24 – Position of the rigidity centre

Specimen	*With T-shaped walls*		*With L-shaped walls*	
	X-direction	*Y-direction*	*X-direction*	*Y-direction*
Rigidity centre				
Left wall :	0.370 m	0.069 m	0.069 m	0.069 m
Right wall :	2.311 m	0.069 m	2.311 m	0.069 m
Frame :	1.042 m	0.069 m	1.190 m	0.069 m

4.3.2 Estimation of the maximum acceleration – X-direction

Estimation of the maximum acceleration is carried out using a static pushover method applied on an equivalent frame model of the structure. The N2-method is used to estimate the maximum sustainable acceleration. Due to the unsymmetrical geometry of the specimen, equivalent static loading is applied in both positive and negative direction. Torsional effects are taken into account and different connection conditions of the lintel are considered. The results are given in Table 25 and
Table 26 respectively for the T and L-shaped piers.

Table 25 – Results of the preliminary assessment (T-shaped walls, x-axis horizontal shear)

Support conditions of the lintel	*Loading case*	*Horizontal shear [N]*	*Acceleration [g]*
Left and right built-in	Shear wall	13745	0.939
	Flange	4148	0.795
	Both	8912	0.857
Left and right simply supported	Shear wall	10808	0.780
	Flange	3527	0.640
	Both	6797	0.763

Table 26 – Results of the preliminary assessment (L-shaped walls, x-axis horizontal shear)

Support conditions of the lintel	*Loading case*	*Horizontal shear [N]*	*Acceleration [g]*
Left and right built-in	Shear wall	13795	1.200
	Flange	8220	0.752
	Both	9610	0.997
Left and right simply supported	Shear wall	10850	0.854
	Flange	7120	0.654
	Both	8430	0.829

4.3.3 Estimation of the maximum acceleration – Y-direction

In case of an earthquake occuring in the Y-direction, the frame-model is no more valid since collapse happens now as soon as one of the piers reaches its own limit state. The total horizontal shear is thus shared between the two walls according to their bending stiffness, the position of the specimen shear centre and the position of the gravity centre of each wall (see Figure 98 and Figure 99 and accompanying equations). Assessment is then done as for the X-direction analysis, with the specimens verified for overturning, shear, torsion and local crushing. The final results are given in Table 27 and
Table 28.

$$x_{Shearcentre,frame} = \frac{x_{Shearcentre,leftwall} I_{y,leftwall} + x_{Shearcentre,rightwall} I_{y,rightwall}}{I_{y,leftwall} + I_{y,rightwall}}$$

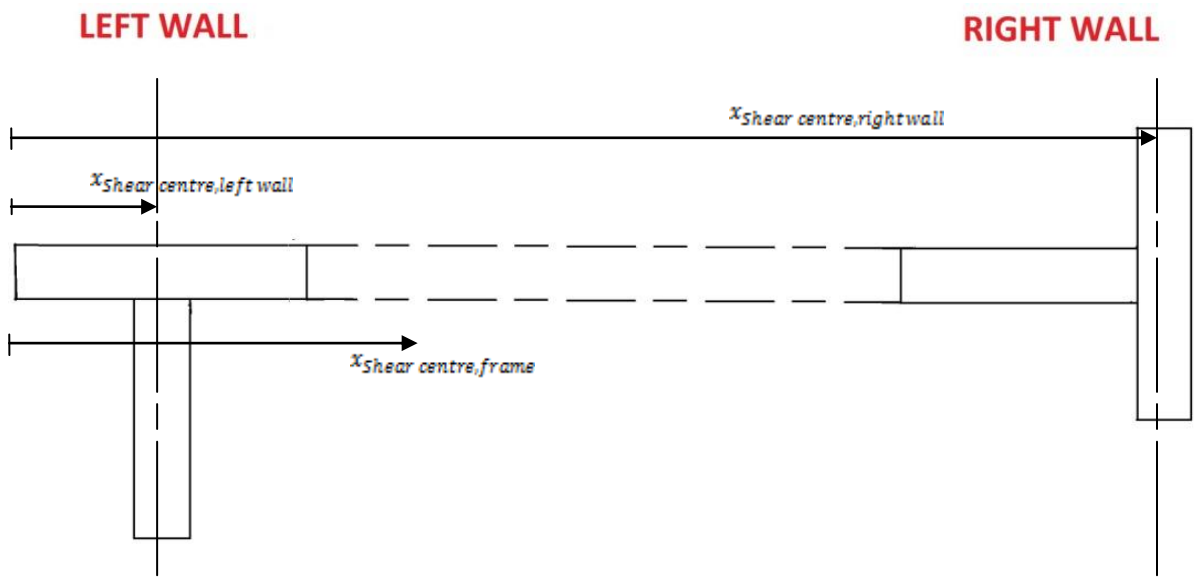

Figure 98 - Global shear centre (example with the T-shaped walls)

$$V_{Left} = -V.\frac{x_{Shearcentre,frame} - x_{rightwall}}{x_{leftwall} + x_{rightwall}}$$

$$V_{Right} = V.\frac{x_{Shearcentre,frame} + x_{leftwall}}{x_{leftwall} + x_{rightwall}}$$

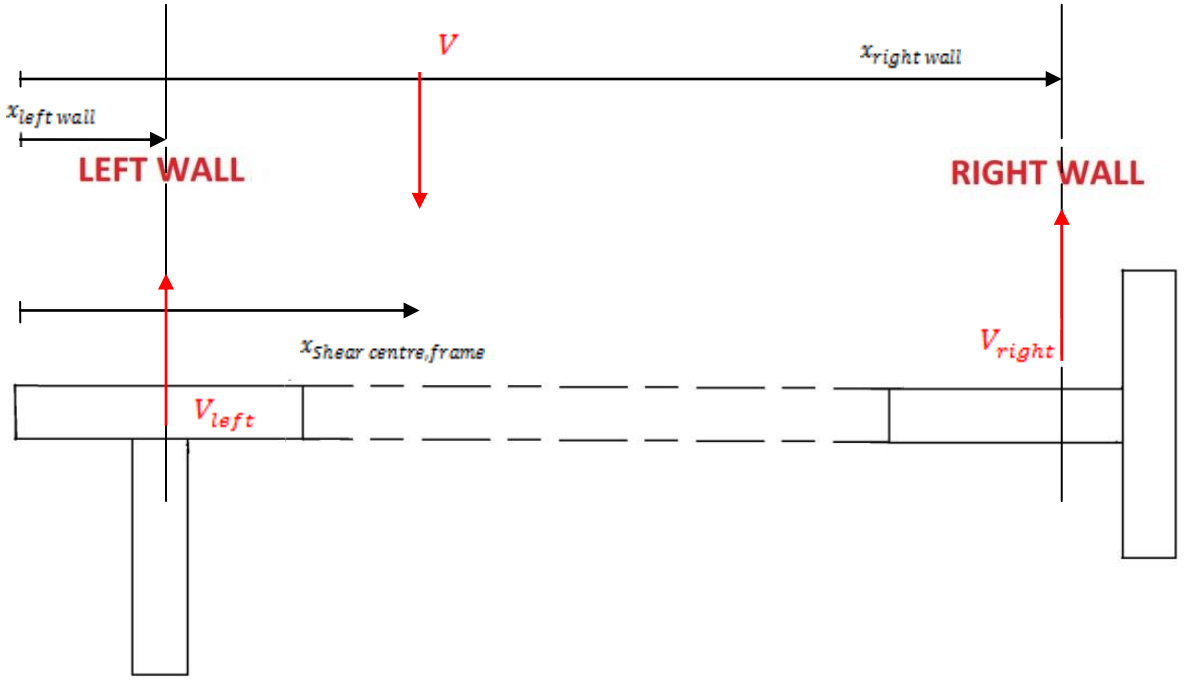

Figure 99 - Calculation of the shear stress (example with the T-shaped walls)

Table 27 – Results of the preliminary assessment (T-shaped walls, y-axis horizontal shear)

Support conditions of the walls	*Loading case*	*Horizontal shear [N]*	*Acceleration [g]*
Top wall free	Shear wall	1548	0.013
	Flange	6800	0.055
	Both	5652	0.046

Table 28 – Results of the preliminary assessment (L-shaped walls, y-axis horizontal shear)

Supported conditions of the walls	*Loading case*	*Horizontal shear [N]*	*Acceleration [g]*
Top wall free	Shear wall	7632	0.057
	Flange	10960	0.081
	Both	8516	0.063

4.3.4 Comparison with a specimen without flanges

As a matter of comparison, a similar assessment procedure is also carried out without taking into account the perpendicular walls. So the studied configuration studied is a specimen with two simple piers made of 0.74 m long walls separated by an opening. The frame behaviour is still

considered. Obviously, the comparison is mainly relevant for the case of earthquake acting in the X-direction. The results are given in Table 29. The comparison shows a beneficial contribution of 6% resp. 26% for T and L configurations.

Table 29 - Results for a simple frame (earthquake in X-direction)

Compressive load [kg]	Compression Level [MPa]	V_{Sd} [N]	$a_{g,frame}$ [g]	$a_{g,T\text{-}shaped}$ [g]	$a_{g,L\text{-}shaped}$ [g]
5000	0.245	11450	0.884	0.939	1.199

4.3.5 Comparison with a simple solid wall

A final comparison is carried out to compare the influence of an opening. The analysis is also done for a simple wall of the same cumulative length, i.e. the preliminary assessment methodology is applied to a 1.5 m long solid wall. The analysis provides the following outcomes, which is by far less than what is obtained considering the frame effect.

Table 30 - Results for a simple wall

Length [m]	Compressive load [kg]	Compression Level [MPa]	VSd [N]	a_g [g]	Stiffness K [N/m]	Period T [s]
1.5	5000	0.242	20350	0.148	$77.003\ 10^6$	0.089

4.4 CONSTRUCTIVE ASPECTS

As it was made for the first test series, the specimens are built on steel beams as foundations appropriately designed for an easy and safe handling of the specimens. As it can be seen in Figure 100 and Figure 101, the supporting system is composed of three pieces of steel profiles bolted together.

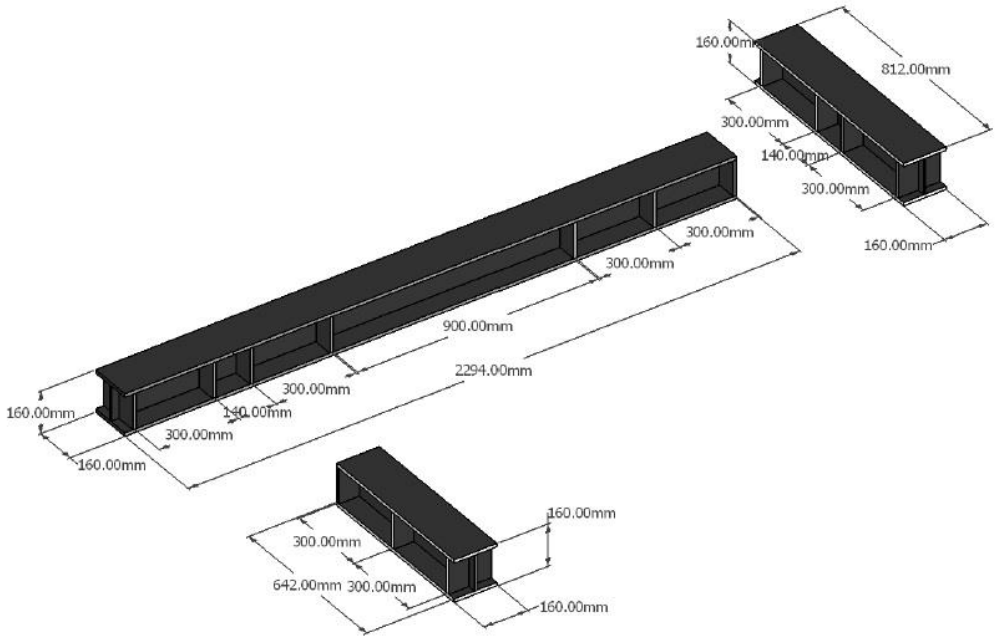

Figure 100 – 3D view of the support beams (T-shaped walls)

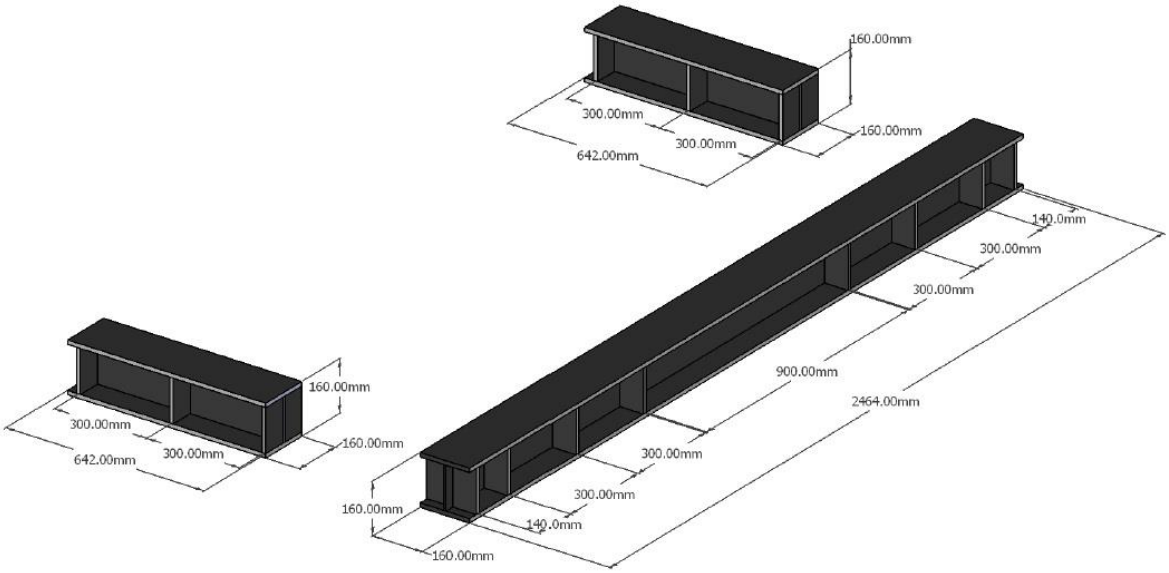

Figure 101 – 3D view of the support beams (L-shaped walls)

4.5 INSTRUMENTATION

Location of the measurement devices are given in the following figures (the legend is similar as the one used for single walls, as given in section 2.5).

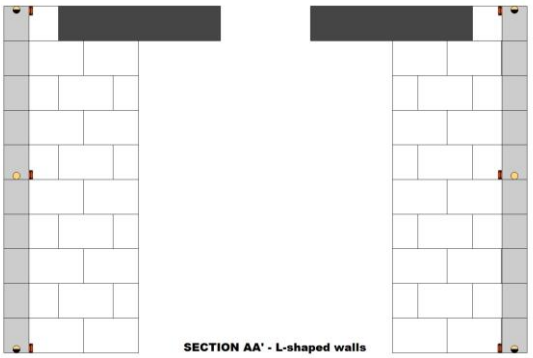

SECTION AA' - L-shaped walls

SECTION BB' - L-shaped walls

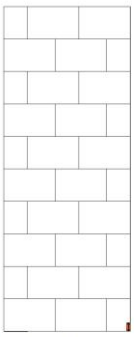

SECTION CC' - L-shaped walls

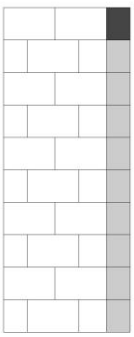

SECTION DD' - L-shaped walls

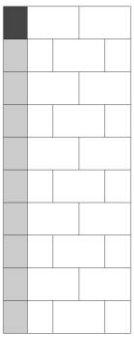

SECTION EE' - L-shaped walls

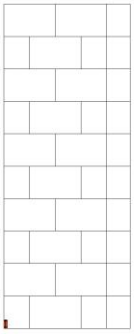

SECTION FF' - L-shaped walls

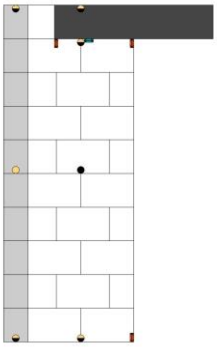

SECTION AA' - T-shaped walls

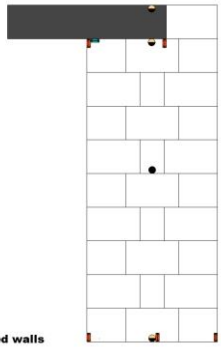

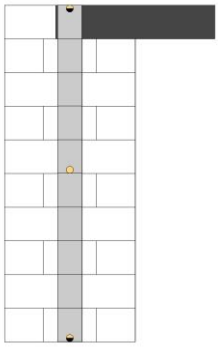

SECTION BB' - T-shaped walls

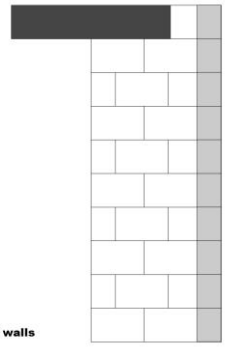

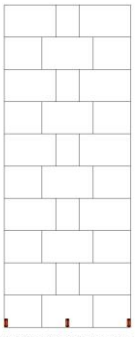

SECTION CC' - T-shaped walls

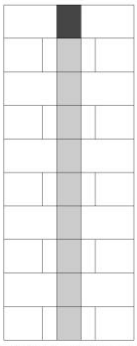

SECTION DD' - T-shaped walls

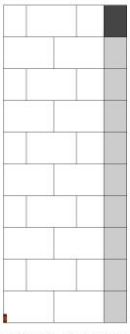

SECTION EE' - T-shaped walls

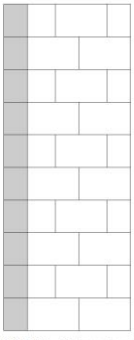

SECTION FF' - T-shaped walls

The instrumentation layouts also include Imetrum Video-Gauge Vision System (VS). Fourteen targets are located on the specimen and the slab (Figure 102 and Figure 103) and their horizontal and vertical displacements are recorded.

Figure 102 - View of the targets (T-shaped walls) for the Imetrum Video-Gauge Vision System (VS).

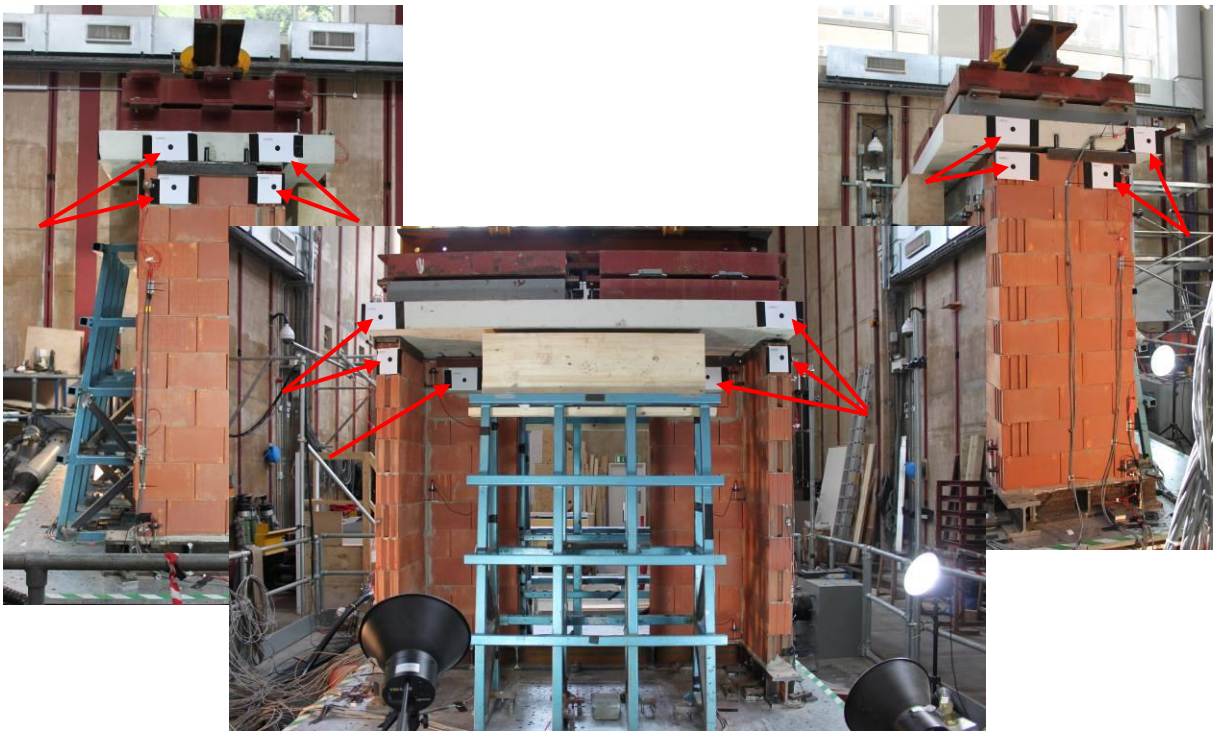

Figure 103 - View of the targets (L-shaped walls) for the Imetrum Video-Gauge Vision System (VS).

5 Second test series - Results

5.1 SET-UP OF THE SPECIMENTS

Figure 104 - Figure 105 (T-shaped piers) and Figure 106 (L-shaped piers) illustrate the set-up of the specimens. They are positioned so that the plan of the main frame is oriented in the Y-direction according to the reference system of the laboratory.

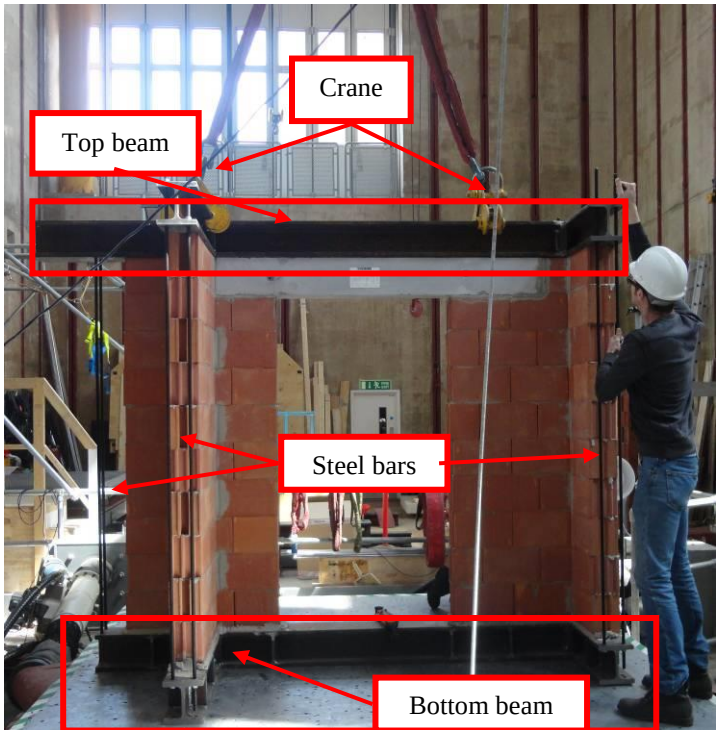

Figure 104 – Set up of the T-shaped walls

Figure 105 – View from the mezzanine (T-shaped walls)

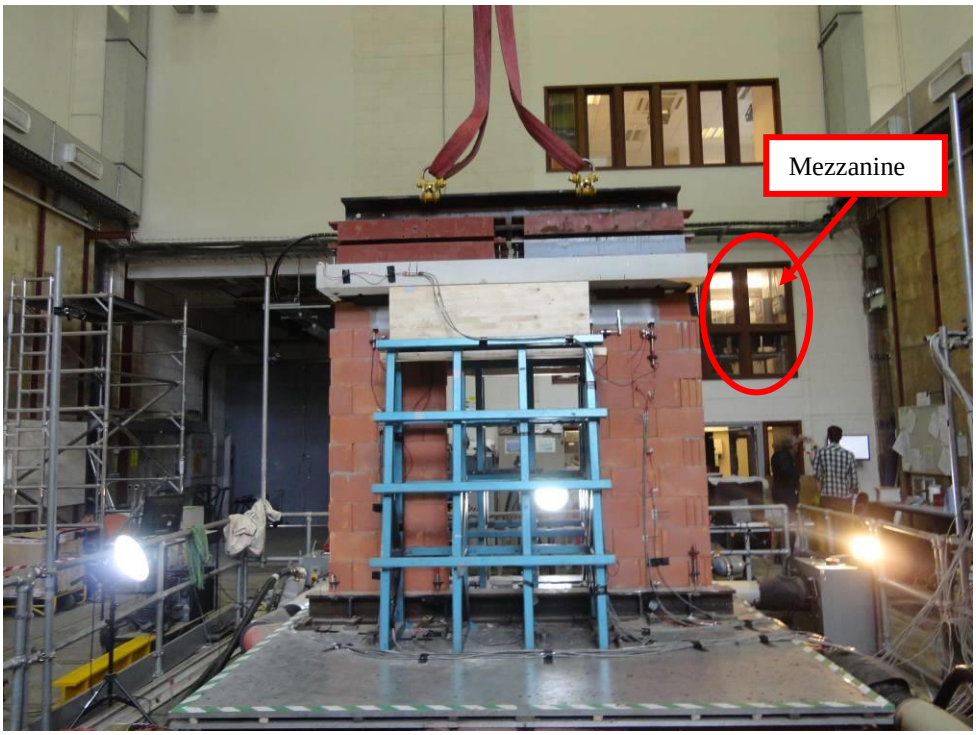

Figure 106 – View of the L-shaped walls specimen

5.2 TEST SEQUENCES

Test sequence is given in Table 31 and Table 32 for the T-shaped and the L-shaped systems respectively. As for the first test series, this one includes white noise identification tests at the very beginning of the process to characterize the initial state of the specimen and after each seismic test to characterize the degradation effects. Identification tests are performed in the X and Y directions. Regarding the seismic tests, 100% corresponds to the PGA of the reference waveform sent to the table (i.e. 0.485g).

Table 31 – Testing sequence for the T-shaped walls

Test No.	*Type of test*	*Direction*	*%*	*PGA [g]*
	Loading on shear walls and flanges			
1	Noise (N1)	X	/	/
2	Noise (N2)	Y	/	/
3	Seismic (S1)	Y	16	≈ 0.08
4	Noise (N3)	X	/	/
5	Noise (N4)	Y	/	/
6	Seismic (S2)	Y	32	≈ 0.16
7	Noise (N5)	X	/	/
8	Noise (N6)	Y	/	/
9	Seismic (S3)	Y	64	≈ 0.32
10	Noise (N7)	X	/	/
11	Noise (N8)	Y	/	/
12	Seismic (S4)	X	10	≈ 0.05
13	Noise (N9)	X	/	/
14	Noise (N10)	Y	/	/
15	Seismic (S5)	X	20	≈ 0.1
16	Noise (N11)	X	/	/
17	Noise (N12)	Y	/	/
18	Seismic (S6)	X	40	≈ 0.2
19	Noise (N13)	X	/	/
20	Noise (N14)	Y	/	/
21	Seismic (S7)	X	60	≈ 0.4
22	Noise (N15)	X	/	/
23	Noise (N16)	Y	/	/
24	Seismic (S8)	Y	96	≈ 0.45

25	Noise (N17)	X	/	/
26	Noise (N18)	Y	/	/

Table 32 – Sequence of tests for the L-shaped walls

Test No.	Type of test	Direction	%	PGA [g]
	Loading on shear walls and flanges			
1	Noise (N1)	X	/	/
2	Noise (N2)	Y	/	/
3	Seismic (S1)	Y	16	≈ 0.08
4	Noise (N3)	X	/	/
5	Noise (N4)	Y	/	/
6	Seismic (S2)	X	10	≈ 0.05
7	Noise (N5)	X	/	/
8	Noise (N6)	Y	/	/
9	Seismic (S3)	Y	32	≈ 0.16
10	Noise (N7)	X	/	/
11	Noise (N8)	Y	/	/
12	Seismic (S4)	X	20	≈ 0.10
13	Noise (N9)	X	/	/
14	Noise (N10)	Y	/	/
15	Seismic (S5)	Y	48	≈ 0.24
16	Noise (N11)	X	/	/
17	Noise (N12)	Y	/	/
18	Seismic (S6)	X	30	≈ 0.15
19	Noise (N13)	X	/	/
20	Noise (N14)	Y	/	/
21	Seismic (S7)	Y	64	≈ 0.32
22	Noise (N15)	X	/	/
23	Noise (N16)	Y	/	/
24	Seismic (S8)	X	40	≈ 0.20
25	Noise (N17)	X	/	/
26	Noise (N18)	Y	/	/
	Loading on flanges only			
27	Noise (N19)	X	/	/
28	Noise (N20)	Y	/	/
29	Seismic (S9)	Y	16	≈ 0.08
30	Noise (N21)	X	/	/

31	Noise (N22)	Y	/	/
32	Seismic (S10)	X	10	≈ 0.05
33	Noise (N23)	X	/	/
34	Noise (N24)	Y	/	/
35	Seismic (S11)	Y	20	≈ 0.10
36	Noise (N25)	X	/	/
37	Noise (N26)	Y	/	/
38	Seismic (S12)	X	20	≈ 0.10
39	Noise (N27)	X	/	/
40	Noise (N28)	Y	/	/
41	Seismic (S13)	Y	30	≈ 0.15
42	Noise (N29)	X	/	/
43	Noise (N30)	Y	/	/
44	Seismic (S14)	X	30	≈ 0.15
45	Noise (N31)	X	/	/
46	Noise (N32)	Y	/	/
47	Seismic (S15)	Y	40	≈ 0.20
48	Noise (N33)	X	/	/
49	Noise (N34)	Y	/	/
50	Seismic (S16)	X	40	≈ 0.20
51	Noise (N35)	X	/	/
52	Noise (N36)	Y	/	/
53	Seismic (S17)	Y	50	≈ 0.25

5.3 ACCELERATION MEASURED AT THE TABLE

Values of the PGA given in Table 31 and Table 32 are target theoretical values. As for the simple walls of the first test series, the weight of the specimens has however an influence on the real PGA. Effectively measured accelerations are given in Table 33. It shows also that, due to the rather large mass and significant in-plane stiffness irregularities of the specimens, the control system could not succeed in imposing a perfectly unidirectional motion to the table. A parasite transverse effect with intensity between 10 and 30 % of the main acceleration is observed. This is however not felt as significantly disturbing the general conclusions of the test campaign and will be properly included in the post-processing and model calibration. Note also that

measurements devices most likely experienced some troubles for tests S3, S5 and S7 of the L-shaped specimens, seen the abnormally low level of the measured acceleration.

Table 33 – Acceleration experimented on the table

Test	T-shaped walls				L-shaped walls			
	Target PGA [g]		Measured PGA [g]		Target PGA [g]		Measured PGA [g]	
	X-direct.	Y-direct.	X-direct	Y-direct.	X-direct.	Y-direct.	X-direct.	Y-direct.
S1	0	0.078	0.007	0.069	0	0.078	0.006	0.062
S2	0	0.155	0.018	0.146	0.049	0	0.038	0.001
S3	0	0.310	0.001	0.279	0	0.155	0.015	0.004
S4	0.049	0	0.038	0.005	0.097	0	0.087	0.001
S5	0.097	0	0.083	0.008	0	0.233	0.036	0.006
S6	0.194	0	0.176	0.025	0.146	0	0.135	0.001
S7	0.291	0	0.276	0.057	0	0.310	0.077	0.007
S8	0	0.466	0.107	0.465	0.194	0	0.180	0.001
S9	/	/	/	/	0	0.078	0.011	0.061
S10	/	/	/	/	0.049	0	0.039	0.001
S11	/	/	/	/	0	0.097	0.14	0.077
S12	/	/	/	/	0.097	0	0.080	0.018
S13	/	/	/	/	0	0.146	0.026	0.133
S14	/	/	/	/	0.146	0	0.125	0.035
S15	/	/	/	/	0	0.194	0.039	0.195
S16	/	/	/	/	0.194	0	0.170	0.037
S17	/	/	/	/	0	0.243	0.058	0.197

5.4 OBSERVATIONS AND COMMENTS OF THE TESTS

5.4.1 Specimens with T-shaped walls

The specimen with T-shaped walls was tested under one gravity load case only, with the slab resting on both shear wall and flanges.

Preliminary remark

Due to some approximations in the execution of the slots realised in the slab to ensure its connection with the walls through the interface steel pieces, a rather significant eccentricity of

the centre of mass of the slab with respect to the shear centre of the walls (Figure 107) was induced. This eccentricity was much higher than foreseen at the preliminary design stage:

Left wall: $e_x \approx 0.15m$ $ey \approx 0.10m$

Right wall: $e_x \approx 0.03m$ $ey \approx 0.00m$

This higher eccentricity induced unforeseen torsion effects both at global (resulting in additional bending effects in the piers) and local level (resulting in local torsion of the piers). These effect, although considered in the preliminary assessment, were significantly underestimated by the prediction. These torsional effects should be reconsidered in the final model calibration.

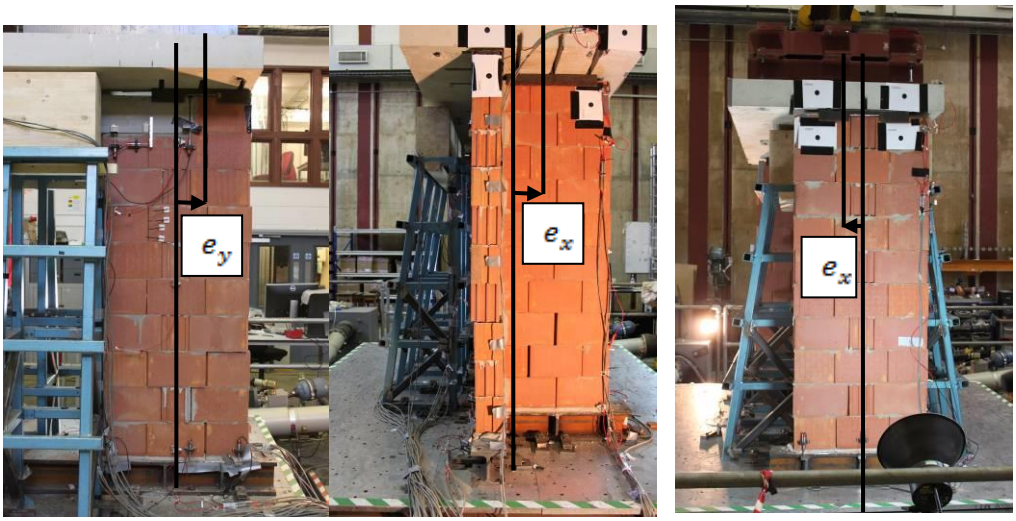

Figure 107 – Eccentricity of the load

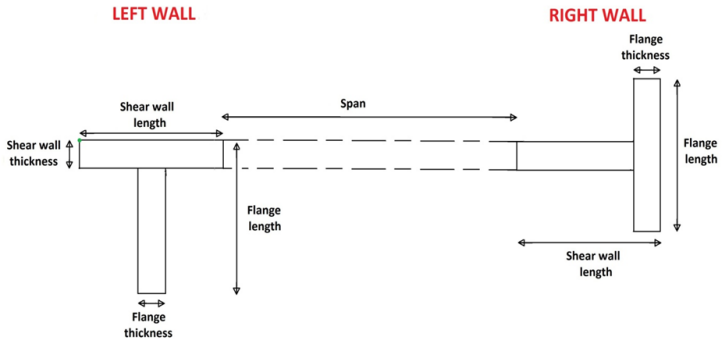

Figure 108 – Left and right walls

Observations

The first important observed phenomenon deals with the behaviour of the lintel. As soon as the second seismic test, some cracks appeared at the mortar interface between the lintel and the wall. The cracks were vertical and horizontal. It means that the lintel was actually completely disconnected from the wall and free to rotate. An appropriate modelling should thus consider the lintel as hinged on each end. Moreover, during the last seismic test, the lintel lifted up from the wall.

Figure 109 –Cracks at the interface between lintel and the walls

The second observed phenomenon is a significant rocking of the piers.

The third relevant observed phenomenon is an important torsion of the piers, in particular of the left pier. As already commented above, this torsion effect is due to two main causes. The first one is the overall non-symmetrical configuration. Indeed, the two piers are characterized by very different bending stiffness. The left pier is thus overstressed in comparison to the right one. The second cause is the additional eccentricity of the slab commented before. This high level of combined bending and torsion in the left pier resulted in a rather significant level of damage for table accelerations lower that foreseen. As illustrated in Figure 110, several units of this pier switched and some joints opened. Many cracks were also observed. At the contrary, only limited and very localized cracking was observed in the right pier, for which the torsional effects were obviously more limited, as shown in Figure 112.

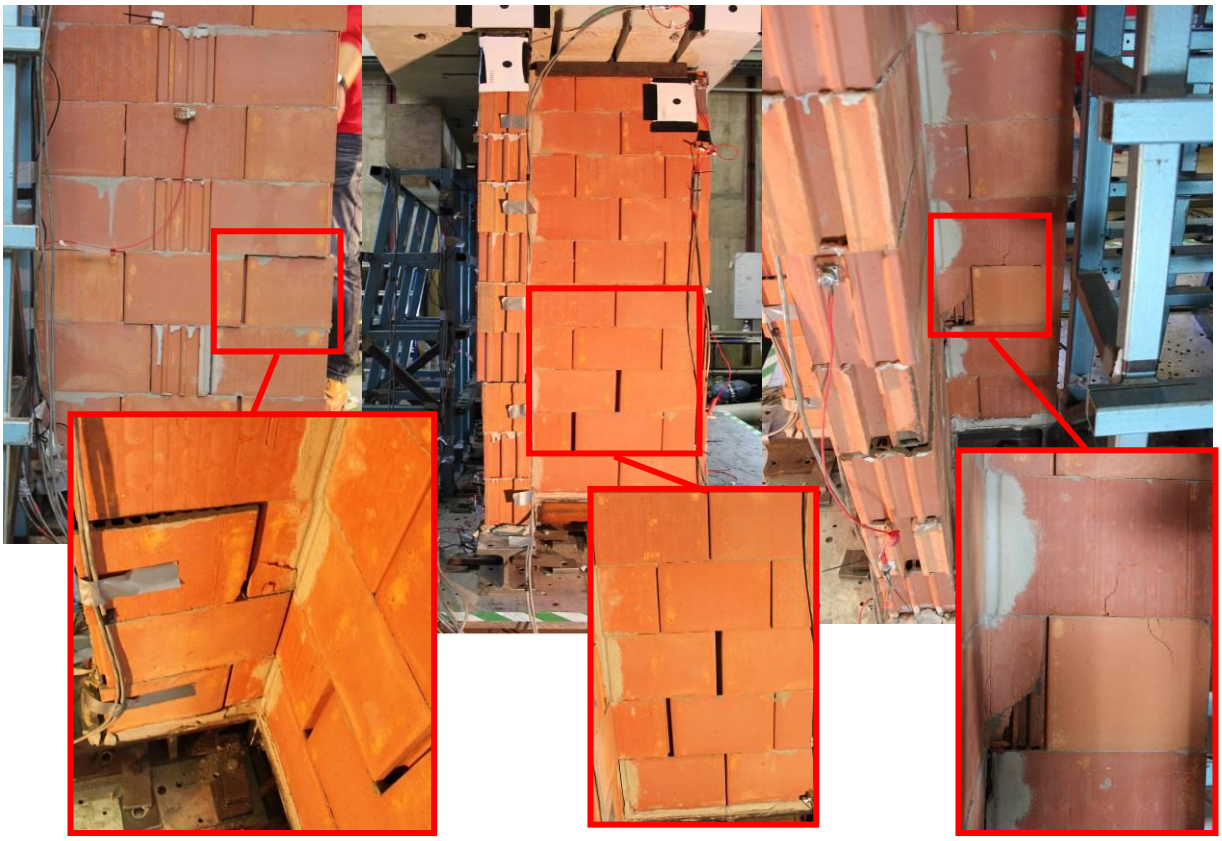

Figure 110 –Collapse of the “left” wall

Figure 111 –Cracks in the right” wall

Testing was finally limited to one single gravity load case because of the large damages induced in the left pier by the torsional effects.

5.4.2 Specimens with L-shaped walls

The specimen with L-shaped walls has been tested under two loading cases. First the shear walls and the flanges were both gravity loaded. Then the mass was only supported by the flanges, similarly to what can happen for one-directional spanning floors.

Contrary to the situation faced with the T-shaped pier specimens, the alignment of the slots and steel elements was better realized. Associated with a more limited natural in-plan irregularity of the system, it lead to a situation where the torsional effects became less critical (see Figure 112).

Figure 112 - Position of the slab (L-shaped walls)

First gravity load case

For this first load case, two main effects were observed.

On one hand, the specimen behaviour exhibited again a significant rocking. As the input acceleration level increased,

On the other hand, some vertical and horizontal cracks at the lintel-wall interfaced appeared similarly as for the T-specimen. However this cracking developed more progressively. The crack state after the seismic test S6 is shown in Figure 113. After this test S6, cracks were actually only observed at the interface of the lintel with the left pier. No visible cracks were identified on the right pier.

For this first gravity load case, seismic level have been limited to a reasonable intensity level in order to allow a second gravity load case to be carried out on a specimen with limited damages.

Figure 113 - Cracks near the lintel (after S6)

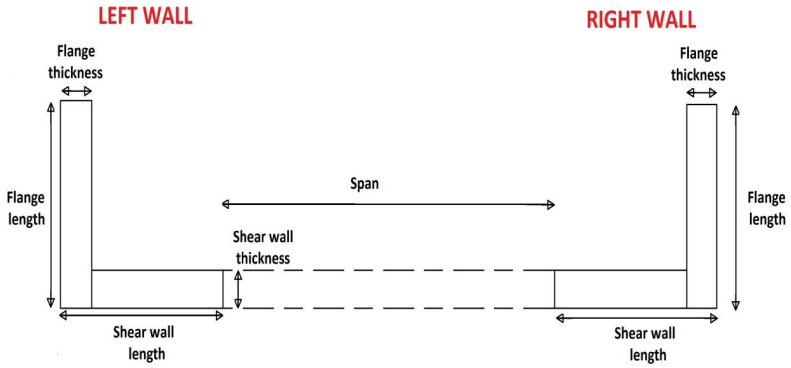

Figure 114 – Left and right walls

Second gravity load case

From the previous observations, it comes out that the specimen at the starting of the second phase of testing was already partially damaged, specifically at the connection of the lintel with the right pier.

During the seismic tests with the new positioning of the slabs, the main observations dealt with:

- A rocking of the wall, with amplitude much more pronounced than for the first case;
- An intensification of the cracking at the interface lintel-pier;
- A final collapse of the right pier by rupture of the vertical connection line between the main wall and the perpendicular flange.

The cracks at the interface of the lintel with the right pier are illustrated on Figure 115. This confirms once more that the most relevant assumption is a hinged connection between lintel and walls.

Figure 115 - Cracks near the lintel (after S17)

Figure 117 illustrates the final state of the specimen with L-shaped walls, with a rupture of the vertical connection line. This failure occurred in the pier where the connection was executed in a classical manner, namely with alternated units. At the contrary for the other pier, where the connection was ensured by a continuous glued joint, no significant damage was observed.

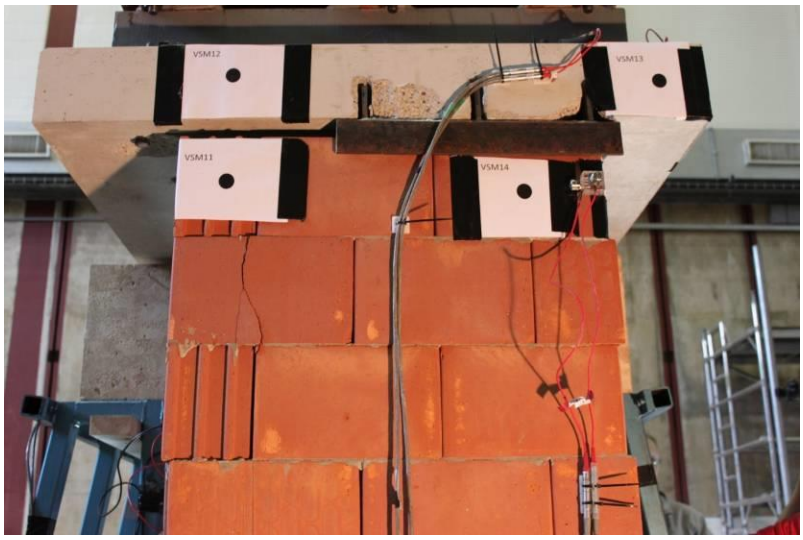

Figure 116 – Collapse of the « right » wall

6 Conclusions and perspectives

This report has presented a general overview of the shake table tests carried out at EQUALS Laboratory (University of Bristol) in the frame of the SERIES project (sub-project 'MAID', TA user group 5 led by University of Liège) and aiming at the characterization of the seismic behaviour of modern clay masonry structural elements, including the effect of soundproofing rubber devices and the contribution of the walls perpendicular to the direction of the earthquake action.

The test campaign comprised two stages. During the first one, four single walls with different aspect ratio and including or not soundproofing elements have been tested, while the second stage consisted in testing two substructures made of two masonry piers with L or T cross-section and coupled by reinforced concrete lintel and slab. Different ways of introducing the gravity load into the system prior to the seismic testing were also taken into consideration.

At the time of issuing the present report, the elaboration of the test results of the first stage is completed and first conclusions can be drawn:

- A significant rocking motion is observed for all specimens for the highest acceleration levels, even for cases where the theoretical assessment is predicting a shear failure prior to the initiation of rocking. This seems to be due to a poor estimate of the actual shear failure mechanism by the current code provisions, in cases where the shear effect is induced by dynamic actions such as earthquakes.

- Theoretical models succeed in predicting the length of the contact zone between the wall and its foundation, and consequently in estimating the seismic intensity from which the system is shifting from a cantilever-like behaviour to a dynamic rocking motion, namely when the contact length becomes a point-like contact. In classical verification procedures, this situation of zero-length contact zone is considered as the limit state associated with the in-plane overturning of the wall. The present tests have however shown that a stable rocking phenomenon may occur for acceleration levels up to 3 times the theoretical overturning level.

- Dynamic identifications carried out after seismic shakes with increasing intensity have evidence a progressive degradation of the system, translated into a reduction of its first natural frequency and an increase of its damping ratio. This degradation is mainly localized at the interface of the wall with its foundation and associated with in-plane bending or rocking effects. Degradation is more pronounced for longer walls due to a higher impact energy released when the wall is coming back to a vertical straight position. For the longer wall, important out-of-plane accelerations are identified as associated with such impacts and are the sign of a sensitivity of the system to out-of-plane buckling. This impact effect and consequent system degradation are less pronounced for the shorter walls.

- Acoustic rubber elements have a favourable effect on the degradation in the sense that they soften the impact during rocking. However they induce a much higher deformability of the system.

- Prediction of the system flexibility by the methods proposed in Eurocode 6 and 8 is rather poor. In particular, the estimates of the elastic compression and shear modulus seem to be not suitable for clay masonry with vertical open joints.

- A significant effect of the compression level and of the possibly non homogeneous distribution of compressive stresses in the acoustic layers is observed. These rubber elements are indeed characterized by a non-linear elastic behaviour and a strong coupling between their compressive (influencing thus the overall bending properties of the structural system) and shear mechanical properties.

The second testing phase on sub-structure is for the time being only post-processed in a qualitative manner. However, the observations already available are opening interesting further exploitation of the results in terms of:

- Rocking behaviour of masonry structural elements with perpendicular flange contributions and various gravity loading patterns;
- Torsional effects at local and global level;
- Support conditions of the lintels and slabs;
- Failure of the vertical connection of intersecting walls.

The test results elaborated during this experimental campaign open the door to interesting perspectives, some of them already under way:

- A comprehensive quantitative exploitation of the results of the second phase;

- The development and calibration of theoretical and numerical models adequately representing the behaviour of the wall elements, with a particular focus on the mechanical properties such as the compression and shear modulus, and the ability to predict properly the rocking behaviour;

- A combination of the outcomes of the two experimental phases by appropriate modelling in order to study the influence of the acoustic layers in a full structural context;

- Complementary investigations on the behaviour of the connections between perpendicular walls and on their capacity in transferring the longitudinal shear associated with the overall bending of the entire structural element, as well as on the torsional behaviour of masonry walls, in particular in the case of piers constituted as an assembly of walls.

References

Cerfontaine, B. (2010). *Development of a software for automatical application of masonry part Eurocode 8 in Belgium.* Liège.

Dietz, M. (2012). *TEST METHOD STATEMENT - TA5/TMS - Seismic behaviour of L- and T-shaped unreinforced masonry shear xalls indluding acoustic insulation devices.* Bristol: University of Bristol - Departement of Civil Engineering - Earthquake Engineering Research Centre.

Eurocode6. (2004). *Eurocode 6 : Design of the masonry structures - Part 1-1 : Common rules for reinforced and unreinforce masonry structures.*

Eurocode8. (2004). *Eurocode 8 : Design of structures for earthquake resistance - Part 1 : General rules, seismic actions and rules for buildings.*

Eurocode8*. (2004). *EurcoCode8 : Annex B(Informative) : ”Determination of the target displacement for nonlinear static (pushover) analysis.*

Grigoletto, S. (2006). *Etude du comportement sismique de structures à comportement non continu.* Liège.

Hervé Degee & Laurentiu Lascar. (2011). *Cyclic shear behaviour of clay masonry walls – Part 1 : walls including acoustic devices or with a door opening.* Liege.

Hervé Degee & Larentiu Lascar. (2011). *Cyclic shear behaviour of clay masonry walls – Part 2 : Cyclic shear test on prefabricated clay masonry walls with T-shaped.* Liege.

Jaspart, J.-P. (2010). *Constructions métalliques et en béton II - Partim constructions métalliques - "Chapitre 9 : Elements d’assemblage".* Liege.

K.Beyer, A.Abo-El-Ezz & A.Dazio. (2010). *Quasi-static cyclic trsts on different types of masonry spandrels.* Zürich.

Oropeza Ancieta, M. (2011). *Fragility Functions for Seismic Risk in Regions with Moderate Seismicity.* Lausanne.

Serge Cescotto & Charles Massonet. (2001). *Mécanique des matériaux.* Bruxelles: De Boeck.

Stuerz. (2009, 02 10). *ESECMaSE - Enhanced Safety and Efficient Construction of Masonry Structures in Europe*. Retrieved May 2012, from ESECMaSE: http://www.esecmase.org

Tomazevic, M. (1999). *Earthquake-Resistant Design of Masonry Buildings.* London: Imperial College Press.